U.PORTO

FEUP FACULDADE DE ENGENHARIA UNIVERSIDADE DO PORTO

NUMERICAL SIMULATION AND OPTIMIZATION OF AN OVERTOPPING BASED WAVE ENERGY CONVERTER

HENRIQUE DANIEL MACEDO RIOS DOS SANTOS

Dissertação submetida para satisfação parcial dos requisitos do grau de

MESTRE EM ENGENHARIA CIVIL – ESPECIALIZAÇÃO EM HIDRÁULICA

_____

Orientador: Professor Doutor Paulo Rosa Santos

_____

Coorientador: Professor Doutor Francisco Taveira Pinto

_____

Coorientador: Engenheiro Tiago Morais

MARÇO DE 2015

MESTRADO INTEGRADO EM ENGENHARIA CIVIL 2014/2015

DEPARTAMENTO DE ENGENHARIA CIVIL

Tel. +351-22-508 1901

Fax +351-22-508 1446

✉ miec@fe.up.pt

Editado por

FACULDADE DE ENGENHARIA DA UNIVERSIDADE DO PORTO

Rua Dr. Roberto Frias

4200-465 PORTO

Portugal

Tel. +351-22-508 1400

Fax +351-22-508 1440

✉ feup@fe.up.pt

http://www.fe.up.pt

I have not failed. I've just found 10.000 ways that won't work.

Thomas A. Edison

ACKNOWLEDGMENT

First and foremost, I would like to thank my supervisor, Professor Paulo Rosa Santos, for the orientation and knowledge transmitted. I also would like to thank the generously invaluable assistance during the last six months, the encouragement and the dedication provided, without which the dissertation would be no more than a mere dream.

I would like to express my gratitude to my co-supervisors, Professor Francisco Taveira Pinto, and Eng. Tiago Morais for the effort to help the development of the work.

I would like to thank Jens Peter Kofoed, who provided the numerical model WOPSim v3.11 used in the optimization of the SSG geometry, and Javier López Lara who enable the application of IHFOAM to analyze the interaction between waves and the SSG structure.

I would like to gratefully acknowledge my parents who always supported me and promoted the best environment for my studies and development as a person, student and future professional.

At last, but not the least, I cannot forget my friends with whom I spend the last years in the course, the experienced camaraderie, and the incentive provided.

ABSTRACT

The consumption of energy has been increasing throughout the years, particularly the electric energy. Due to the negative impacts associated with the use of nonrenewable energy resources, the interest in the production of electric energy using renewable sources experienced a significant growth. In the course of this work, the ocean energy resources are briefly characterized, particularly the wave energy.

Several technologies are currently available to harvest wave energy. In order to take advantage of the energy associated to the wave run-up and overtopping, the Sea-wave Slot-cone Generator (SSG) was idealized. This wave energy converter (WEC) captures the water that overtops the structure in elevated reservoirs. The stored water has potential energy that, when returned to the maritime environment, is converted in electricity by special low-head turbines.

This thesis focuses in the numerical simulation and optimization of a SSG device and gives continuity to the experimental work carried out by Oliveira (2014). The numerical model WOPSim v3.11 (Meinert *et al.*, 2008) was used to optimize the SSG geometry having into account typical conditions from the Portuguese west coast. The optimization study was carried out for an installation in the North breakwater of Foz do Douro, Porto, Portugal, having into account existing local conditions (water depth, wave climate, tidal range). WOPSim was applied to simulate the sea states and to calculate the hydraulic efficiency of the device, as well as to estimate the electric energy produced. The starting point was the work carried out by Oliveira (2014), and the study resulted in a new geometry with a better hydraulic performance.

Finally, a Computational Fluid Dynamics numerical code (IHFOAM, developed at IH Cantabria), was applied to study the interaction between the incident waves and the SSG structure, and its hydraulic performance. The numerical simulations reproduced the conditions tested in the physical model study carried out by Oliveira (2014), in the Hydraulic Laboratory of FEUP – Faculty of Engineering of the University of Porto, Portugal. The numerical results obtained were then compared qualitatively with the experimental ones, in order to validate the numerical approach followed. Further studies will attempt to numerically analyze new test conditions, minimizing the need of additional physical model tests.

KEYWORDS: Wave energy, Overtopping, SSG, WOPSim, IHFOAM.

SUMMARY IN PORTUGUESE

Ao longo dos anos, o consumo de energia tem vindo a aumentar, particularmente de energia eléctrica. O interesse pela produção de energia eléctrica através de fontes renováveis tem crescido devido aos efeitos negativos associados à utilização de fontes não renováveis. No decurso deste trabalho serão apresentadas as tecnologias disponíveis para o aproveitamento da energia marítima, com especial destaque para a energia das ondas.

Com o intuito de aproveitar a energia associada ao galgamento de estruturas costeiras, foi idealizado um dispositivo chamado *Sea-wave Slot-cone Generator* (SSG), entre outros também apresentados na tese, que captura em reservatórios elevados a água do mar. Essa água, armazenada num nível superior ao do mar, apresenta energia potencial e, quando devolvida ao meio marítimo, passa por turbinas hidráulicas que convertem essa energia em electricidade.

Nesta dissertação, a geometria do SSG foi otimizada através de simulações realizadas com o *software* WOPSim para condições de agitação marítima típicas da costa portuguesa. Este estudo teve assim por base as condições locais correspondentes a uma instalação no molhe Norte da Foz do Douro, Porto, Portugal. O WOPSim foi utilizado, não apenas para a simulação dos estados de mar e cálculo da eficiência hidráulica do dispositivo para as várias condições estudadas, mas também para estimar a energia eléctrica produzida. O trabalho desenvolvido por Oliveira (2014) foi utilizado como ponto de partida, sendo, no entanto, proposta uma nova geometria para a estrutura, com melhor comportamento hidráulico.

O modelo IHFOAM (código numérico CDF – *Computational Fluid Dynamics*) foi também utilizado para estudar a interação da agitação marítima com o dispositivo SSG e o seu desempenho hidráulico. Nesta segunda parte do trabalho foram simuladas ondas de características similares às utilizadas no modelo físico desenvolvido por Oliveira (2014) e testado no tanque de ondas do Laboratório de Hidráulica da Faculdade de Engenharia da Universidade do Porto. Os resultados numéricos foram, depois, comparados qualitativamente com os obtidos por Oliveira (2014), com o intuito de validar a abordagem numérica seguida. Estudos posteriores procurarão simular numericamente novas condições de teste, minimizando assim a necessidade de recorrer a testes experimentais.

PALAVRAS-CHAVE: Energia das ondas, Galgamento, SSG, WOPSim, IHFOAM.

CONTEXT

CONTENTS OF FIGURES

CONTENTS OF TABLES

NOMENCLATURE

SMALL LATIN LETTERS

a	wave amplitude
c	Courant number
c_i	empirical coefficients
d	water depth
d_r	draft
f	freespace, distance between the crest and the water surface inside the reservoir
g	gravity acceleration
h	water depth at the toe of the structure
k	wave number
k_p	peak wave number
n	spreading index
p	pressure
p_w	random number
q	average overtopping discharge per unit width
$q_{ov,j}$	total overtopping flow rate to the j-reservoir
s_0	wave steepness
v	velocity
w	water head
z_i	vertical boundary of the i-reservoir

CAPITAL LATIN LETTERS

A	non-linear regression analysis constant
B	non-linear regression analysis constant
C	velocity of wave propagation or wave celerity or non-linear regression analysis constant
C_0	velocity of wave propagation on deep waters
C_{g0}	velocity of wave groups in deep waters
C_{gs}	velocity of wave groups in shallow waters
D	direction of the generic Fourier component
D_0	mean wave direction
$\bar{E}$	kinetic energy per unit length
H	wave height

$\bar{H}$	mean wave height
HD	horizontal distance
H_{max}	maximum wave height
$H_{m,0}$	incident significant wave height
H_{rms}	root-mean-square wave height
H_s	significant wave height
$H_{1/n}$	average wave height of the largest 1/n
L	wavelength or reservoir length
$L_{m-1,0}$	deep water wave length
L_0	wavelength in deep waters
P_{crest}	total power over the crest
P_{in}	total power stored in the reservoirs
P_{ov}	probability that a wave does not overtop the reservoir crest
P_{turb}	total mean power production
P_{wave}	mean wave power per unit of width
Q	dimensionless overtopping discharge
$Q_{in,j}$	total overtopping flow rate to the j-reservoir
Q_{over}	overtopping flow
Q_{res}	flow that enters in the reservoir
Q_{turb}	flow in the reservoir
$Q_{upper,over}$	spillage from the above reservoir
R	dimensionless crest level
$R_{c,i}$	freeboard of i-reservoir
$R_{u,2\%}$	wave run-up height exceeded by 2% of incoming waves
S	spreading function
T	wave period or average zero-crossing wave period
$\bar{T}$	mean wave period
T_c	wave crest period
T_e	energy period
T_p	peak wave period
T_r	record length
W	reservoir width

ACRONYMS

CFD	Computational Fluid Dynamics
CFL	Courant-Friedrichs-Lewy
DNS	Direct Numerical Simulations
EEZ	Exclusive Economic Zone
EU	European Union
FEUP	Faculty of Engineering of the University of Porto
MST	Multi-Stage Turbine
MWL	Mean Water Level
LES	Large Eddy Simulation
RAS	Reynolds Average Stress
RANS	Reynolds Average Navier-Stokes
SSG	Sea-wave Slot-cone Generator
SWL	Sea Water Level
VOF	Volume of Fluid
WEC	Wave Energy Converter
WOPSim	Wave Overtopping Power Simulation

GREEK LETTERS

α	seaward slop steepness
α_m	optimal slope angle
β	angle of wave attack
γ_b	influence factor for a berm
γ_f	influence factor for roughness elements on a slope
γ_h	influence factor for shallow foreshore
γ_r	influence factor for roughness elements on a slope
γ_β	influence factor for oblique wave attack
Δt	time-step
Δx	cell size
η	water free surface elevation
η_{in}	overtopping hydraulic efficiency
η_{res}	hydraulic efficiency of the reservoir
η_{turb}	efficiency of the turbines

λ_{dr}	slope angle parameter
λ_s	correlation parameter
λ_α	slope angle parameter
$\xi_{m-1,0}$	breaker parameter
ρ	density of sea water

1
INTRODUCTION

1.1. CONTEXT

The use of renewable energies has been being promoted throughout the last decades due to diminishing fossil fuel reserves, global warming, environmental pollution, security in energy supply as well as volatility of oil prices in international markets. One of the most promising clean energy sources is the ocean wave energy (Cruz, 2008). Gunn and Stock-Williams (2012) estimated the mean wave power resource available worldwide in 2.11 ± 0.05 TW, corresponding to around 18 500 TWh/year. This potential energy production from ocean waves is of the same order of magnitude of the world's electricity consumption (Cruz, 2008).

This huge potential of untapped energy justifies the efforts in the development of technologies for harvesting power from waves, which corresponds to the transport of energy by ocean surface waves. Therefore, technologies have evolved and have been diversified in order to develop Wave Energy Converters (WECs), capable of converting wave power into electric energy through a wide range of working principles, each one being more suitable for certain application conditions.

The Sea-wave Slot-cone Generator (SSG) is an overtopping based wave energy converter (WEC) that is being developed by the company WAVEnergy AS (Stavanger, Norway). The structure of this WEC consists of a number of reservoirs one in the top of each other (above the mean water level) that store temporary the water of incident waves. Low-head multi-stage hydraulic turbines are then used to convert the potential energy of the stored water into electric power.

The SSG technology has been extensively studied in the last ten years mostly in Aalborg University, Denmark. The first experimental studies on the hydraulic performance of this WEC were carried out in 2005 (*e.g.* Kofoed, 2005a, Kofoed, 2005b). These studies were followed by others that intended to address the nature and magnitude of wave loadings (Margheritini *et al.*, 2008, Margheritini *et al.*, 2009) to optimize the WEC geometry and mode of operation for specific locations (*e.g.* Kvitsøy in Denmark, Swakopmund in Namibia and Sines in Portugal), as well as to analyze technical problems and economical risks related to the integration of SSG in tradition coastal and harbor structures. In parallel, the Technic University of Munich developed a new turbine concept design to increase the efficiency of energy conversion from the reservoirs of the SSG.

A pilot project was planned for Kvitsøy, Norway, in order to validate and verify the experimental and numerical models results from previous works, but the structure was never implemented. Since then, several works were carried out in order to improve the SSG performance and take better advantage of wave power (Margheritini *et al.*, 2009, Vicinanza *et al.*, 2012, among others).

Based on the conclusions of previous studies, Oliveira (2014) developed a new SSG geometry that was tested under the action of wave conditions typical of the Portuguese west coast. The most important improvement was the introduction of waves focusing elements (named reflectors) in the device, with the aim of increasing the amount of wave energy absorbed and therefore the performance of SSG technology. Nevertheless, this work left open the study of the performance for different sea water levels (important for installation sites with a large tidal range) and, additional opening angles of the wave focusing elements, the numerical simulation of the device, the analysis of wave loadings and the structural behavior of the SSG components, as well as a comprehensive study on the economic feasibility and reliability, including installation and maintenance cost, and financial risk analysis.

1.2. THESIS STRUCTURE

This thesis is organized in five chapters and two appendices. The present chapter provides an overview of the subject and describes the main goals of the study. The second chapter explains how important the electric energy is nowadays and how it is possible to generate it using the available renewable, carbon-free power. It also introduces the characteristics of ocean tides and waves, and presents different technologies that are currently available to take advantage of wave run-up and overtopping to produce electricity. The Sea-wave Slot-cone Generator is presented in more detail.

The third chapter not only summarizes the significance of numerical modelling for the development and optimization of wave energy conversion technologies, but it also describes and provides the theoretical basis of the numerical models WOPSim (v3.11) and IHFOAM (v2.1.1) that are applied in chapter four in the study of the SSG. Hence, chapter four deals with the application of those numerical models to simplified problems and to the thesis case-study (SSG), the validation of the numerical models with results of existing physical model tests, but it also presents and critically analyses the results of all the numerical simulations carried out. The last chapter summarizes the main conclusions of this work and identifies paths for future developments.

In short, the present thesis gives continuity to the work developed by Oliveira (2014), proposes alternative optimized SSG geometry applicable to conditions typical of the Portuguese west coast (in terms of water depths, tidal range and sea wave characteristics), presents estimates of the energy produced using numerical tools (WOPSim, v3.11) and develops a numerical study on the performance and behavior of the SSG using a sophisticated Computational Fluid Dynamics (CFD) numerical model (IHFOAM v2.1.1), based on the 3D Reynolds-Average Navier-Stokes (RANS) equations for two incompressible phases using a finite volume discretization and the Volume Of Fluid method (VOF). The roadmap of this work is presented on the flowchart of Figure 1.

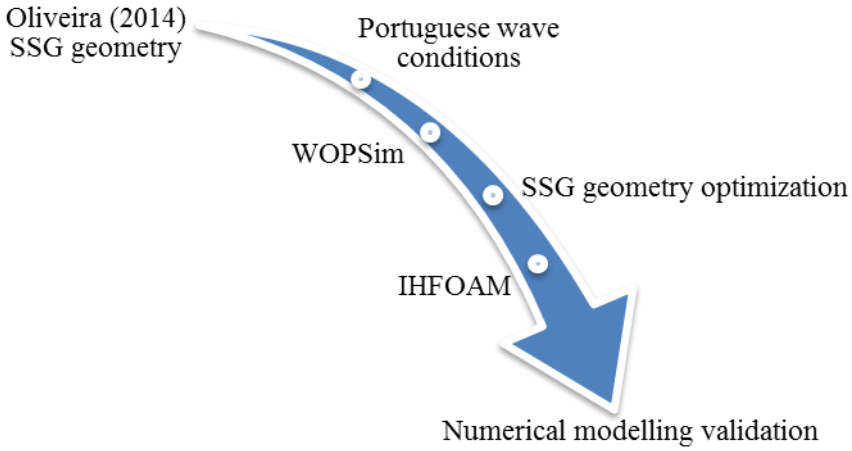

Figure 1 - Flowchart of work steps

2
STATE OF ART

2.1. INTRODUCTION

This chapter briefly describes the ocean resources and discusses the importance of renewable energies in a context of increasing energy consumption and growing concerns with environmental pollution, global warming, among others. The technologies presently available to harvest wave energy are classified and briefly described. Overtopping based wave energy converters are presented in more detail.

Because this dissertation deals with the development of a SSG device, it must have in consideration all the factors that affect its overall performance. The wave characteristics and the tide amplitude present a relatively high range of variation in the Portuguese west coast along the year, and have a significant influence on the SSG design and performance.

In this context, the most important maritime environmental actions are the ocean waves, but tides and currents cannot be neglected. Currents may be created by the movement of water caused by the rotation of the Earth, the Coriolis Effect, the wind, density differences, among others. Tides can be seen as a "long wave" with a period of almost twelve hours as a consequence of the position of the Sun and the Moon. The salinity and the thermic gradients are also important ocean energy resources. It is also possible to use ocean space to exploit solar and wind energy through the installation of solar panels or wind turbines, respectively.

2.2. RENEWABLE VERSUS NON-RENEWABLE ENERGIES

With the Industrial Revolution, it was necessary to obtain large amounts of energy. The efforts to find alternative ways of generating energy from other energy sources led to the discovery of fossil fuels. Fossil fuels (*e.g.* oil, coal and natural gas) are named non-renewable energies because their speed of consumption is much higher than its natural restoration, and therefore they will cease to exist over time. Therefore, it was and it is still necessary to produce electric energy from other sources: the solution is to use renewable energies sources. These are called "renewable" because they do not exhaust ever in a human scale due to the natural replenishing.

In addition, renewable energies started to be used instead of fossil fuels because the consumption of the last ones has negative impacts on Earth, such as, the increase of its temperature, thaw of glaciers and the rise of mean water level, contamination of air and soil, pollution of water, among others. Another consequence is the economic effect in the countries' economic balance, since many of them have to import fossil fuels. Nevertheless, on the other hand, the introduction of non-conventional

renewable energies in the global energetic mix may have repercussions in the cost of the electricity, due to the higher level cost of the energy produced from those resources.

In order to reduce the negative impacts associated to the use of non-renewable energies, the European Union (EU) defined targets for the share of renewable energies in each state-member for 2030. One of the mandatory goals is to produce, at least, 27% of the overall energy consumption using renewable sources (European-Council, 2014). The main sources of renewable energy are solar, wind, hydraulic, ocean, biomass, biofuel, and geothermal. This work will focus on ocean renewable energy, in particular wave energy.

2.3. ELECTRIC ENERGY CONSUMPTION

The consumption of energy in the world is growing every year, particularly the electric energy share. From 2000 to 2013, the annual electric energy consumption in the world raised almost 7 000 TWh, being Asia the main responsible for this significant increase (Figure 2).

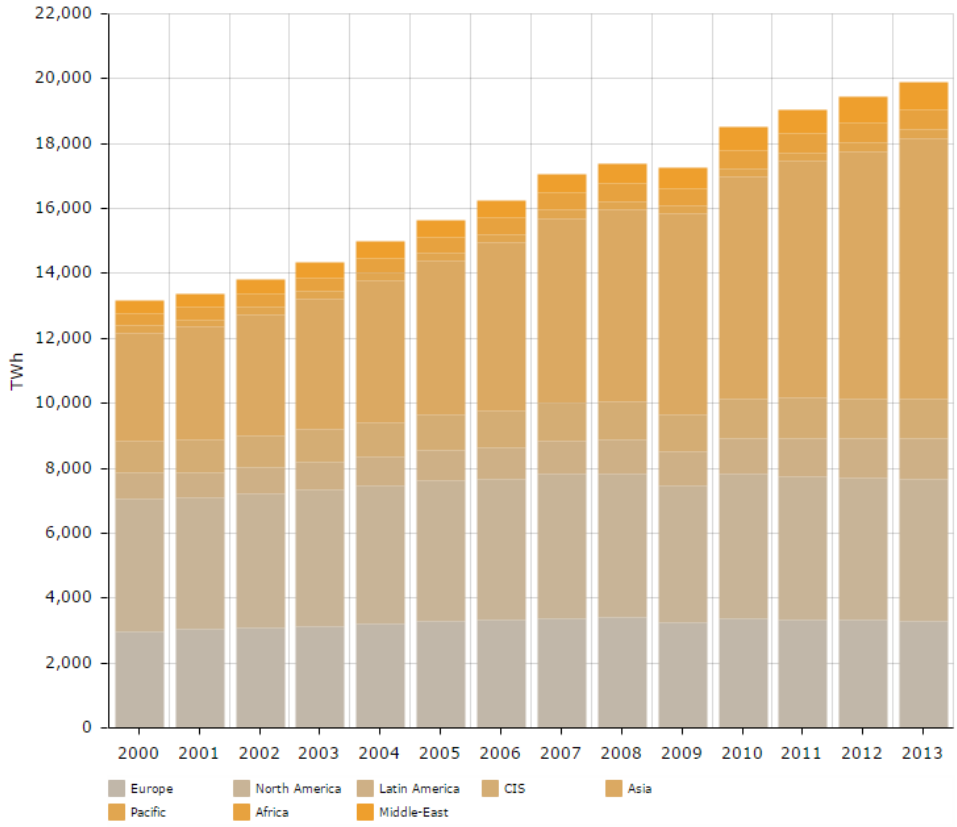

Figure 2 - Electricity domestic consumption around the world between 2000 and 2013 [1]

In Portugal the evolution was slightly different. The energy consumption increased until 2006, when 49 TWh were consumed. Nevertheless, after that year, the electricity consumption remained nearly constant, between 48 and 51 TWh (48 TWh consumed in 2013). Figure 3 presents the evolution of the domestic electric energy consumption in Portugal between 2000 and 2013, *i.e.* power plants, industry, transport and the residential and tertiary sectors of the energy consumption.

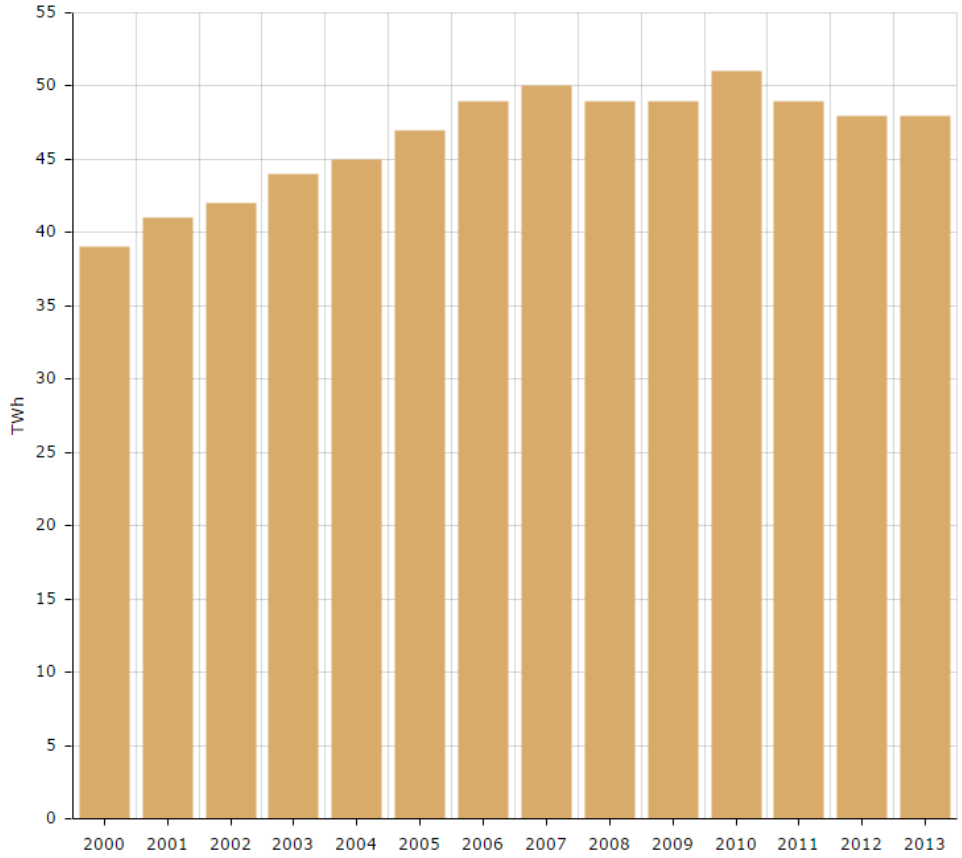

Figure 3 - Electric energy consumed in Portugal between 2000 and 2013 [1]

The annual mean incident wave power on the ocean-facing coastlines around the world (but neglecting some small islands and the poles) is estimated in 2.11 ± 0.05 TW. Estimates for Europe and Portugal are 270 ± 20 and 15 ± 2 GW, respectively (Gunn and Stock-Williams, 2012). These figures correspond to theoretical energy productions of around 18 500, 2 360 and 130 TWh/year for the planet, Europe and Portugal, respectively (Figures 2 to 6). However, not all the wave resource can be converted in electric energy. In fact, constrains of different natures will limit the installation of wave energy converters in specific location all over the word. On the other hand, only part of the wave energy available in a certain place can be used, due to the losses in the wave energy conversion processes (wave-to-wire losses).

Despite the global electricity consumption is not well distributed around the world, the annual mean wave resource is better allocated, as it is possible to compare in Figure 4 (Gunn and Stock-Williams, 2012).

Electric energy production in Portugal along the years presents some variations, probably due to the fact that Portugal depends a lot on the production of electric energy by renewable sources. According to Enerdata year book[1], Portugal produced 52 TWh of energy in 2013 (Figure 5), however only 48 TWh was consumed (3 TWh were sold).

[1] https://yearbook.enerdata.net/

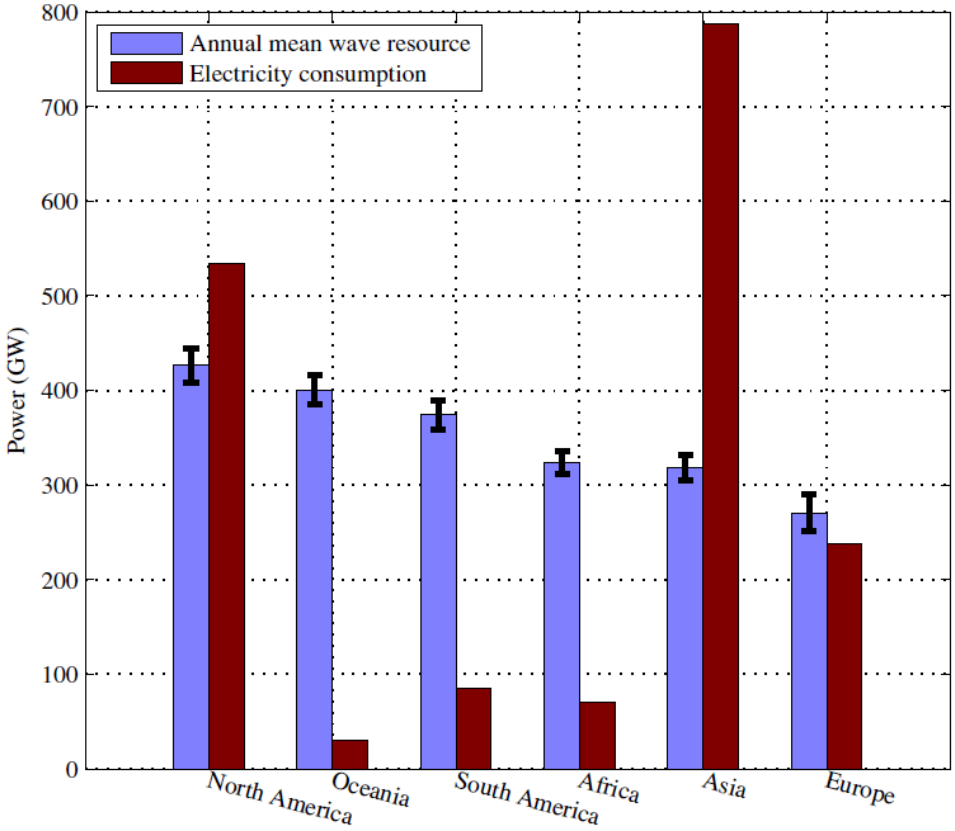

Figure 4 - Annual mean wave resource vs Electricity consumption (Gunn and Stock-Williams, 2012)

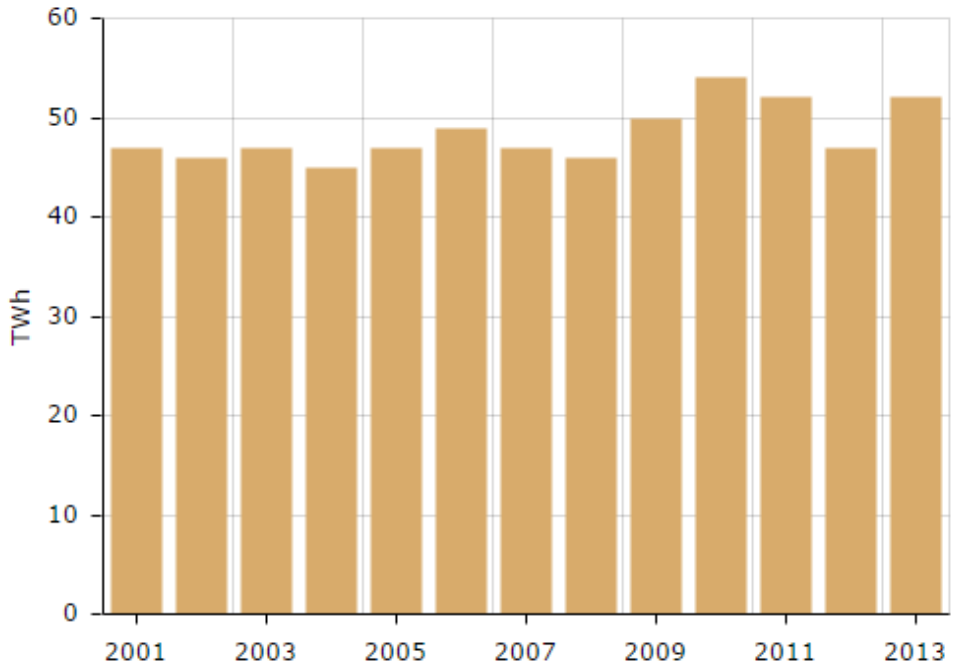

Figure 5 - Electric energy produced in Portugal between 2001 and 2013 [1]

Portugal electricity production from renewable sources was 62.5% of electricity production (Figure 6). Despite Portugal already is in the path to fulfill the target pointed by EU, there is the objective of all the energy production came from renewable sources, like ocean energy, particularly from waves.

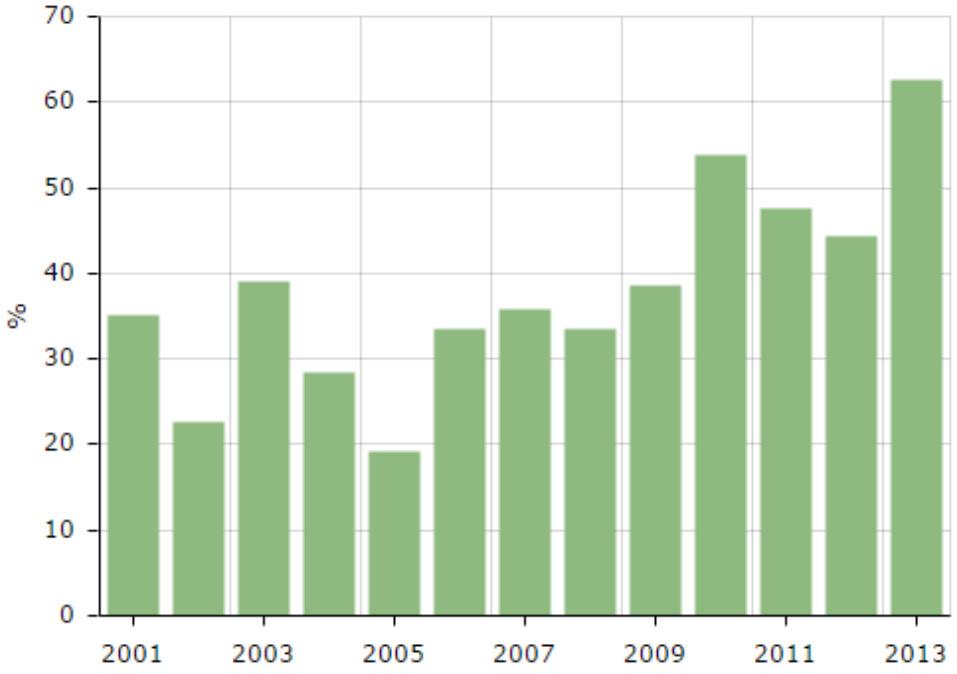

Figure 6 - Percentage of electric energy produced from renewable energies in Portugal between 2001 and 2013 [1]

2.4. OCEAN RESOURCES

2.4.1. INTRODUCTION

Since the last century, several technologies were developed to harness ocean energy and transfer it to electric energy. The ocean energy resources available are: waves, tides, currents, salinity gradient and thermal gradient. Nevertheless, solar and wind power can also be converted inland. In these cases, a location on the ocean surface is used to harness renewable energy, rather than taking advantage of a specific ocean energy source. In addition, oceans may also be used to produce biomass for biodiesel production.

The oceans have a huge amount of energy, are close to many concentrated populations worldwide, and present the potential of providing a substantial amount of renewable energy. The contribution of each energy resource is presented in Table 1 (adapted from OTEO, 2014).

Table 1 - Estimated global ocean energy resources (OTEO, 2014)

Form of Ocean Energy	Estimated Global Resources (TWh/year)
Waves	80 000
Tide Amplitude	300
Tide Currents	800
Thermal Gradient	10 000
Salinity Gradient	2 000

2.4.2. CHARACTERIZATION

The possible electricity generation from waves in the planet ranges from 8 000 to 80 000 TWh/year (IEA-OES[2]). At present, there are several technologies capable of harnessing wave power and convert it into electric energy. In the Portuguese EEZ (Exclusive Economic Zone), the amount of energy that may potentially be extracted from ocean waves is estimated in about 10 TWh/year, which corresponds approximately to 20% of the electric energy consumption (OTEO, 2012). Figure 7 shows the variation of available wave power (kW/m) around the world.

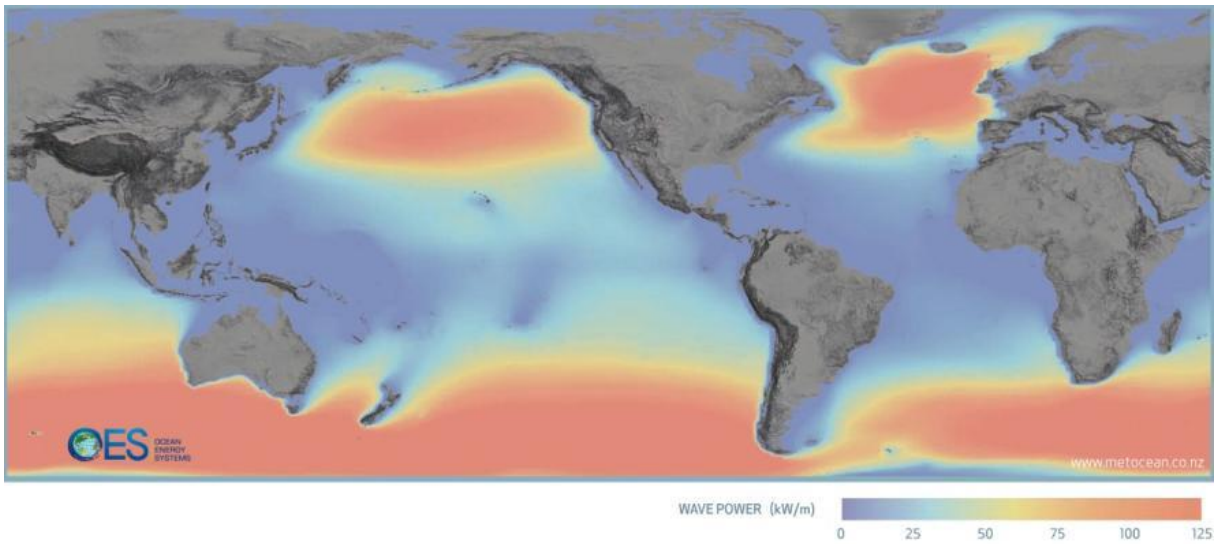

Figure 7 – Mean wave energy flux (OTEO, 2012)

The tidal energy comprises the resource available either in tide currents or related to the tide amplitude variation. The first one may provide more than 800 TWh/year and the second one more than 300 TWh/year (IEA-OES). Semi diurnal tide amplitude variation (the most globally common) is presented in Figure 8 (OTEO, 2012).

[2] http://pt21.ru/docs/pdf/28_e.pdf

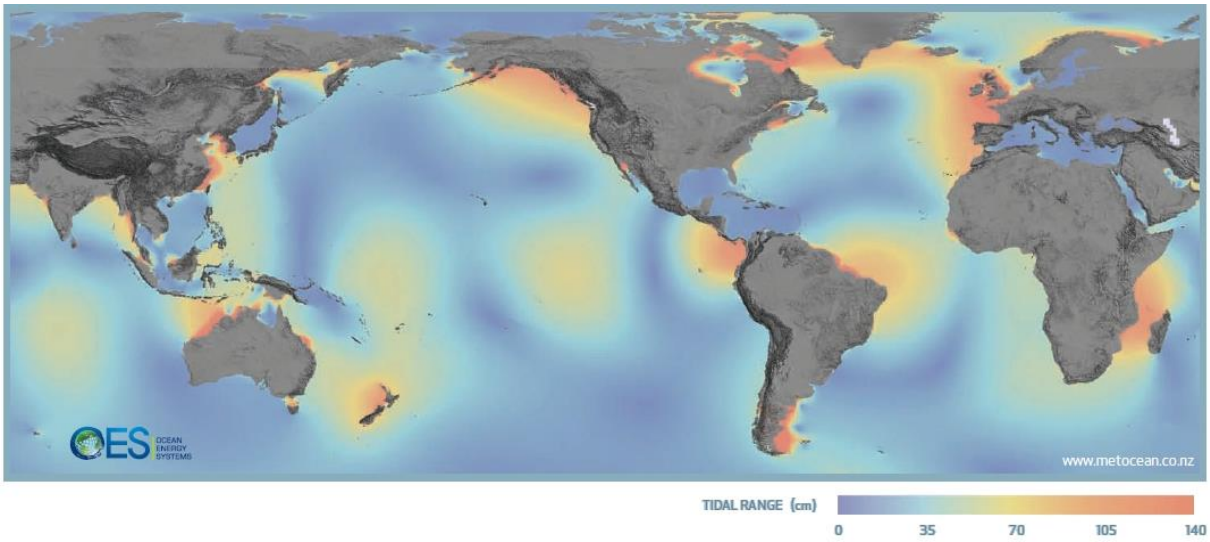

Figure 8 - Tide amplitude variation (OTEO, 2012)

Wind power can be used for electric energy production, either onshore or offshore. An offshore wind turbine with a diameter of 126 m can produce up to 7.5 MW of electric energy. This technology is still under development and it is expected that in 2020 turbine rotors will have diameters of 252 m and a rated power of up to 20 MW. The energy production of a single turbine is not significant as these units are usually installed in group, in wind farms, to increase overall energy production (OTEO, 2012). Figure 9 presents the available energy resource from offshore wind in Europe.

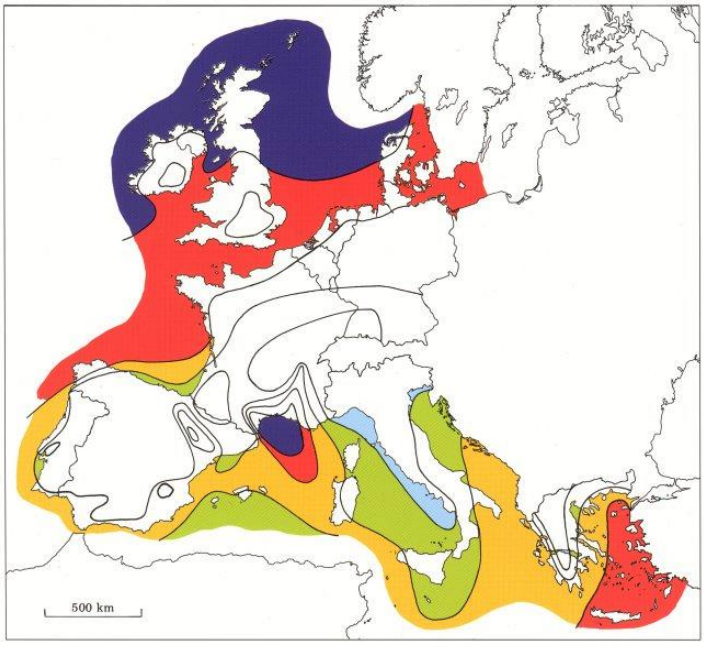

Wind resources over open sea (more than 10 km offshore) for five standard heights

	10 m		25 m		50 m		100 m		200 m	
	$m\,s^{-1}$	Wm^{-2}	$m\,s^{-1}$	Wm^{-2}	$m\,s^{-1}$	Wm^{-2}	$m\,s^{-1}$	Wm^{-2}	$m\,s^{-1}$	Wm^{-2}
	> 8.0	> 600	> 8.5	> 700	> 9.0	> 800	> 10.0	> 1100	> 11.0	> 1500
	7.0-8.0	350-600	7.5-8.5	450-700	8.0-9.0	600-800	8.5-10.0	650-1100	9.5-11.0	900-1500
	6.0-7.0	250-300	6.5-7.5	300-450	7.0-8.0	400-600	7.5- 8.5	450- 650	8.0- 9.5	600- 900
	4.5-6.0	100-250	5.0-6.5	150-300	5.5-7.0	200-400	6.0- 7.5	250- 450	6.5- 8.0	300- 600
	< 4.5	< 100	< 5.0	< 150	< 5.5	< 200	< 6.0	< 250	< 6.5	< 300

Figure 9 - Available energy resource from offshore wind (OTEO, 2014)

Solar energy may also be collected onshore or offshore. Figure 10 presents the worldwide yearly mean solar irradiance. Geographically, Portugal is situated in a latitude in which the solar irradiance rounds 200 W/m^2, against almost 300 W/m^2 registered in equatorial regions (OTEO, 2012).

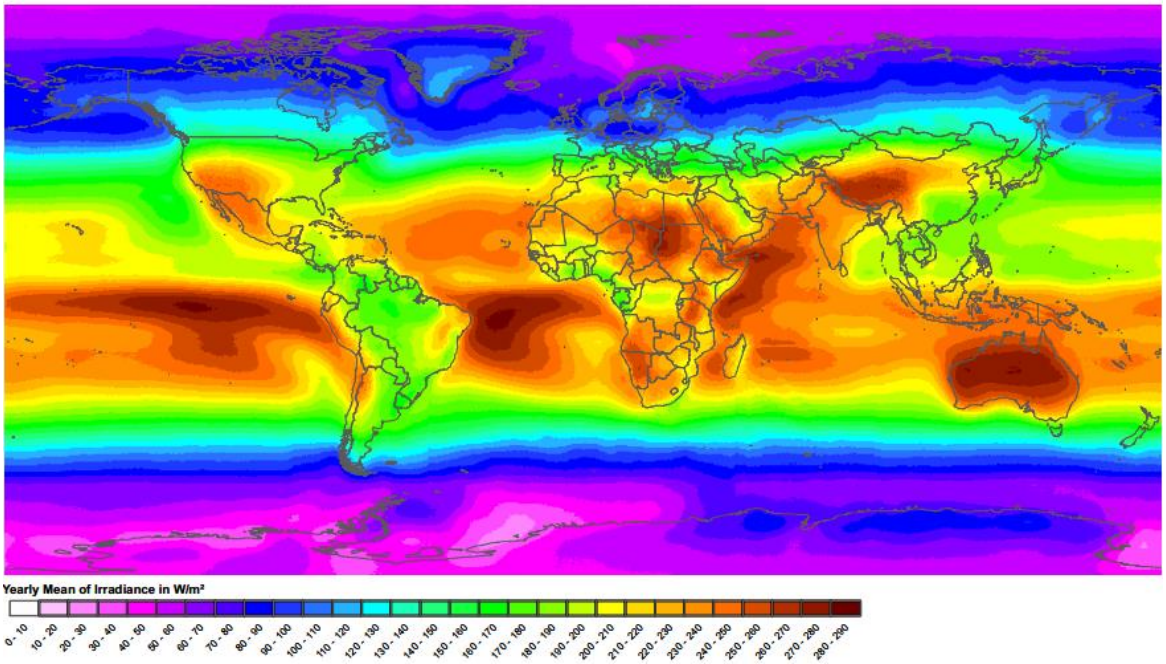

Figure 10 - Yearly mean of solar irradiance (OTEO, 2014)

The ocean thermal energy gradient consists in a difference of temperature of at least 20ºC between the warmer water on the ocean surface and the cooler water in higher water depths (OTEO, 2012). IEA-OES estimates that around 10 000 TWh/year are available in the oceans in the form of thermal energy. Figure 11 presents temperature differences for a depth range of 20 - 1 000 m.

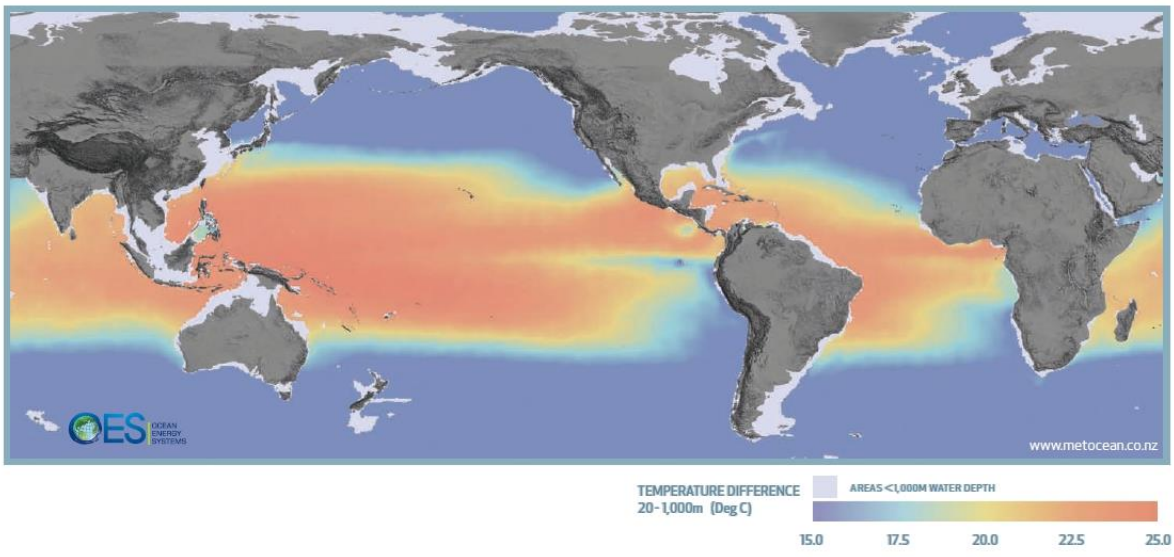

Figure 11 - Temperature difference in the depth range 20 - 1000 m (OTEO, 2014)

The salinity gradient power (or Osmotic power) is the energy available from the difference in the salt concentration between sea water (salt water) and river water (fresh water). Energy conversion relies on osmosis with ion specific semipermeable membranes. Technologies are applied where fresh water meets with salt water and take advantage of the internal energy difference (OTEO, 2012). Figure 12 presents the salinity gradient distribution on Earth.

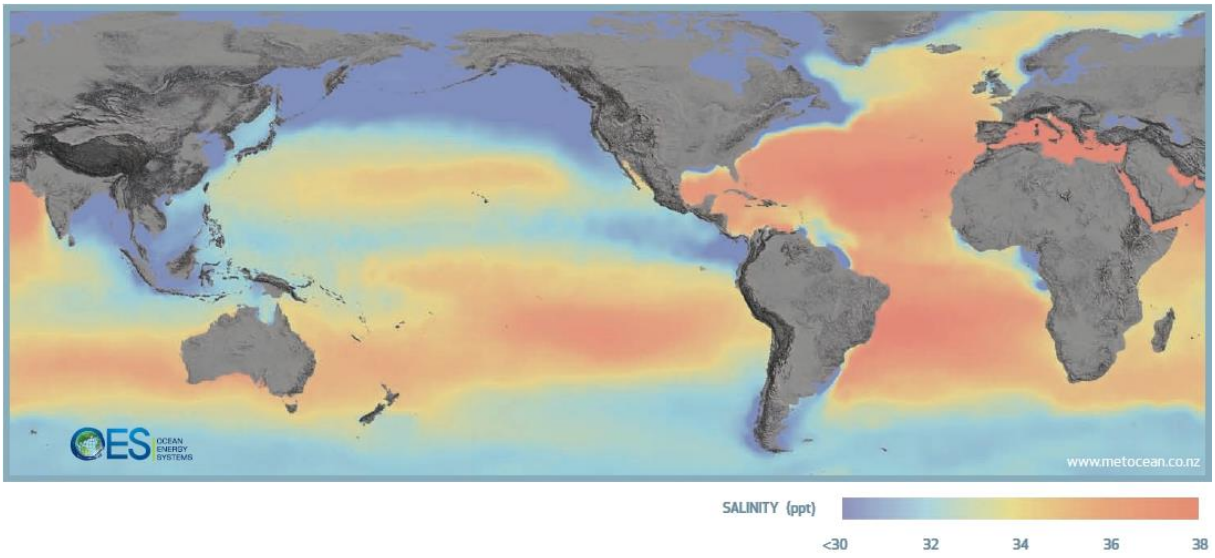

Figure 12 - Salinity gradient distribution (OTEO, 2014)

The importance of seaweeds as an energetic resource depends on its value in relation to traditional biomass sources and its correlation with solar irradiation distribution worldwide. Seaweeds are used to produce biofuel. The EU intends that, by 2020, 10% of the energy used on transportation became from biofuel (OTEO, 2012). Figure 13 presents a technology developed by OMEGA System[3] for biofuel production from seaweeds.

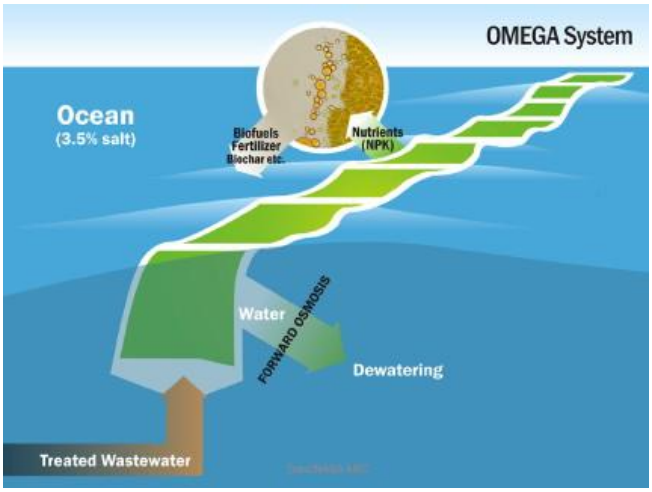

Figure 13 - OMEGA System for biofuel production from seaweeds (OTEO, 2014)

[3] http://www.nasa.gov/centers/ames/research/OMEGA/#.VNSX8NKsVZ4

2.5. MARITIME ENVIRONMENT

2.5.1 INTRODUCTION

In order to take advantage of all ocean potential it is required to have a comprehensive understanding of its resources. Therefore, along the years, several studies have been conducted with that purpose. In what concerns wave energy harvesting, it is of paramount importance the characterization of the wave energy resource, wave hind casting, as well as the estimation of the energy that could be produced by a wave energy converter deployed in any location.

As mentioned earlier, waves and tides may significantly affect the performance of a SSG wave energy converter. For that reason, hereafter, waves and tides are described in more detail, namely in what concerns their origins and characteristics, defining parameters, and influence on the SSG performance. With that knowledge it is possible to take a better advantage of the SSG potential, having in mind its optimization in terms of energy production for the local conditions of the case-study considered in this thesis.

2.5.2. TIDES

Tides are defined by the cyclic motion of water on the oceans. They are a consequence of the combination of the attractive forces from Moon and Sun upon the rotating Earth. They are called of equilibrium tides (Kamphuis, 2010).

If we consider a layer of water around the Earth, the mass of water that is more close to the Moon is pulled and, as a result, the water level rise (high tide or high water). Figure 14 represents the forces' direction caused by Moon (Nathaniel-Bowditch, 2002). The closest local to the Moon is called of sublunar point and the opposite local on the Earth is the antipode. The halfway point between sublunar point and antipode (on the line of the water layer) experience null tractive forces. Therefore, the height of the tide is lower on those locations (low tide or low water). The same actions occur with Sun effect; however, results have lower values. For each component is called of equilibrium tide (Nathaniel-Bowditch, 2002).

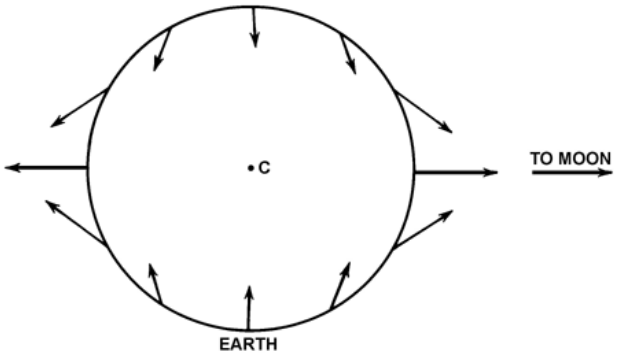

Figure 14 – Forces caused by Moon (Nathaniel-Bowditch, 2002)

When the Moon and the Sun are aligned, tides are higher than the average. However, at moon quarters, the forces from Moon and Sun are perpendicular and the equilibrium tides subtract to each other, tides will be lower than the average. The first ones are called spring tides (Figure 15a) and the

last ones are neap tides (Figure 15b). The period of the tide combination of both Astros is 12.42 hours (Kamphuis, 2010).

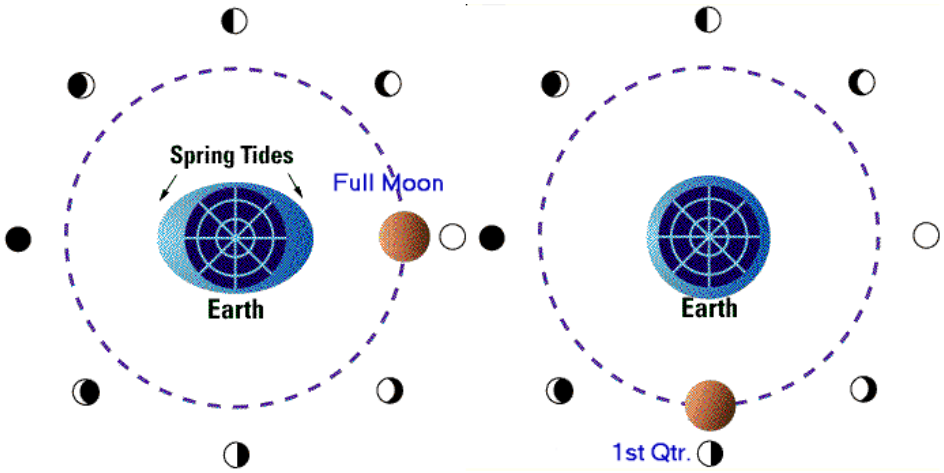

Figure 15 - Influence of Moon on tides. (a) Spring tides; (b) Neap tides [2]

The periods of tide oscillations can be semi-diurnal, daily or diurnal, bimonthly, monthly, and annual. Therefore, for each kind, the periods are different.

The first case occurs due to relation of Earth rotation on itself and the Moon position. Thus, two low and two high waters levels occur each day with small different between both levels, respective lows and highs. The period of semi-diurnal tides is 12 hours and 25 minutes (half of a lunar day). Figure 16 illustrates a semi-diurnal type tide in Boston, USA (Nathaniel-Bowditch, 2002).

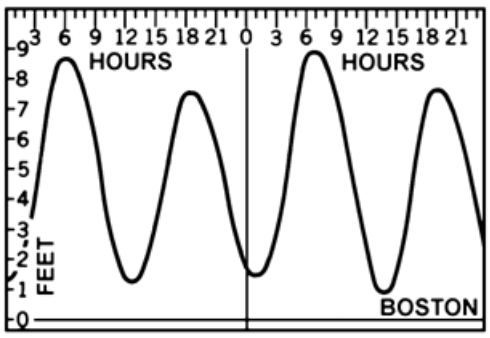

Figure 16 - Semidiurnal tide in Boston, USA (Nathaniel-Bowditch, 2002)

When the same happens with the Sun position (when lunar forces do not have so much influence), a daily or diurnal tide occurs. It is similar to the previous one, but there is only a single low and single high water level per day. A daily tide lasts 24 hours and 50 minutes (lunar day). Figure 17 shows an example of a diurnal tide in Pei-Hai, China (Nathaniel-Bowditch, 2002).

For monthly tides, the period varies due to rotation of Moon around Earth. Consequently, the period has the same value of a lunar month, 29.5 days. When the interference is due to the distance of Earth to Sun (solstices and equinoxes), tides suffer monthly cycles. Figure 18 demonstrates the variation of tides along a month (Nathaniel-Bowditch, 2002).

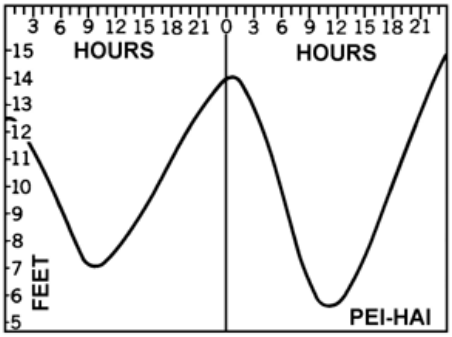

Figure 17 - Diurnal tide in Pei-Hai, China (Nathaniel-Bowditch, 2002)

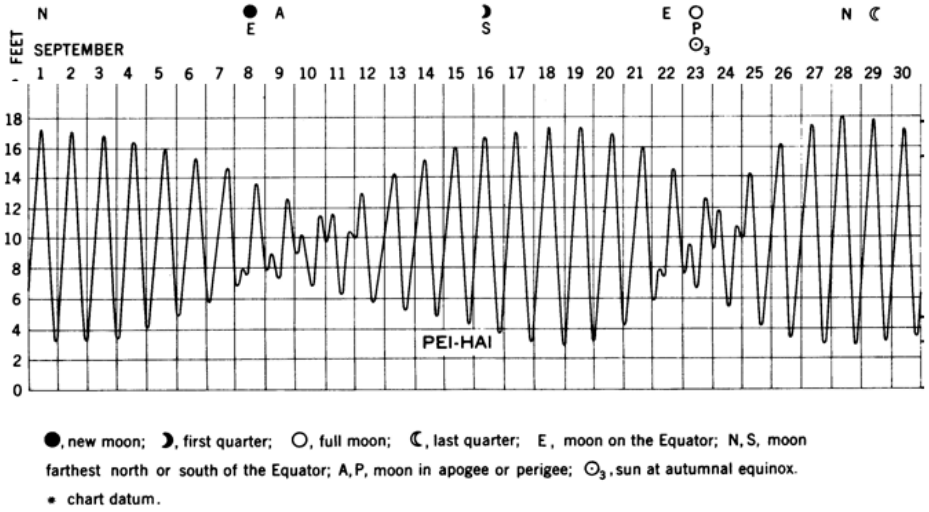

Figure 18 – Monthly tide cycle in Pei-Hai, China (Nathaniel-Bowditch, 2002)

There are also meteorological tides caused by the wind and atmospheric pressure oscillations. In general, onshore winds raise the coastal water level and offshore winds lower it. In general, these actions have a very small effect in comparison to equilibrium tides (Kamphuis, 2010), in open coastlines, but may have more significant effects in partially enclosed water bodies.

2.5.3. WAVES

2.5.3.1. Generation of Waves

Waves are a result of the interaction between the wind and the sea surface. In the generation zone, when the wind blows over the water, the generated turbulent eddies will periodically touch down, overcoming the water surface tension and causing local disturbances on the surface (small ripples). These local disturbances lead to small waves called capillary waves. The properties of this kind of waves are influenced by surface stresses and, with the continuous blowing wind, waves became higher and higher in a cyclic process, due to the shear stresses and pressure differentials created over the sea surface. Normally, these processes occur in deep waters. The length of water over which a given wind blows to generate waves is called fetch. Within the fetch, propagating waves absorb wind energy and

the wave energy increase. Wind energy is transferred to waves most efficiently when they both travel at the same speed (Kamphuis, 2010).

Waves follow the direction of their formation and once they reach constant properties, they enter on the decay region. Such as the name implies, wave energy start to decrease slowly, mostly due to the friction with the atmosphere and internal friction. Because waves are still in deep water, the influence of the sea bottom is negligible. Figure 19 represents a sketch of the several regions of wave propagation.

There are several theories that may be used to describe ocean waves. The most known are Airy's, Stoke's, Cnoidal's and Solitary's wave theory. The first one is a linear wave theory whereas the others are nonlinear theories.

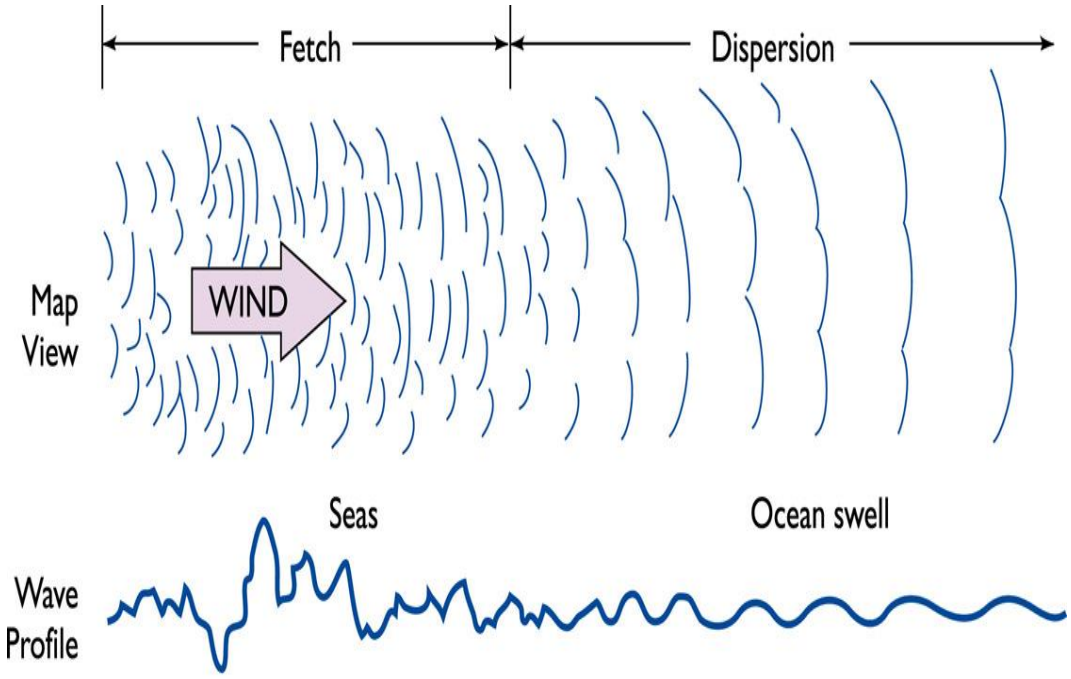

Figure 19 – Sketch of the generation zone [3]

2.5.3.2. Regular Waves

Airy's wave theory[4], despite being the most elementary wave theory, allows a reasonable estimation of the wave characteristics for a wide range of wave parameters. Nevertheless, the assumptions made in the development of this linear wave theory must be satisfied, namely:

- The fluid is homogeneous and incompressible; therefore, the density ρ is constant;
- Surface tension can be neglected;
- Coriolis effect due to the earth's rotation can be neglected;
- Pressure at the free surface is uniform and constant;
- The fluid is ideal or inviscid (lacks viscosity);

[4] Also named of first-order, small amplitude or linear theory was developed in 1845 providing a good approximation of wave characteristics and parameters (USACE, 2002).

- The particular wave being considered does not interact with any other motions; the flow is irrotational so that water particles do not rotate (only normal forces are important and shearing forces are negligible);
- The bed is a horizontal, fixed, impermeable boundary, which implies that the vertical velocity at the bed is zero;
- The wave amplitude is small and the waveform is invariant in time and space;
- Waves are plane or long-crested (two-dimensional).

Because it is the most basic wave theory, the correspondent wave profile will be simple too, being possible to assume that waves have a sinusoidal profile, Figure 20. A regular or monochromatic wave may be described by the following parameters (Thorpe, 1999):

- Wavelength – *L*;
- Wave period – *T*;
- Acceleration of gravity – *g*;
- Velocity of propagation or wave celerity – *C*;
- Wave amplitude – *a*;
- Wave height – *H*;
- Water depth – *d*;
- Water free surface elevation – η.

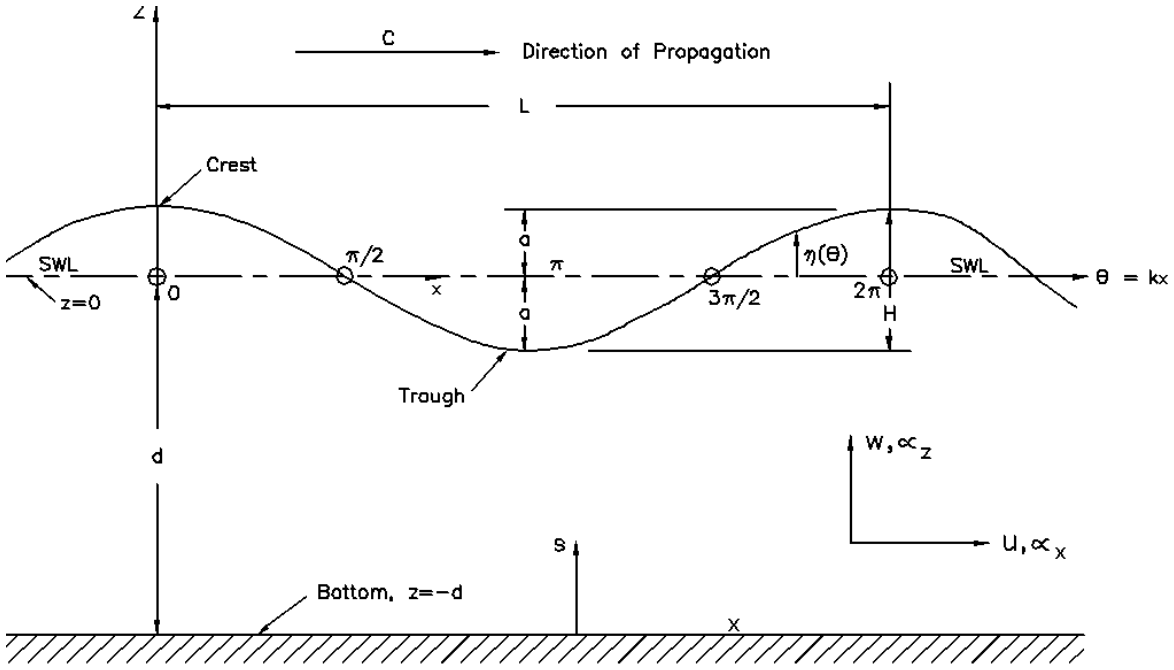

Figure 20 - Characteristics of a regular sea wave (SWL – Sea Water Level) (USACE, 2002)

The speed at which a wave propagates is designated the phase velocity or wave celerity (USACE, 2002). The wave celerity, the wave length and the wave period could be related to each other by Equation (1).

$$C = \frac{L}{T} \quad (1)$$

In deep waters conditions, Equations (2) and (3) can be used to determine the wave length and the wave celerity, respectively.

$$L_0 = \frac{gT^2}{2\pi} \tag{2}$$

$$C_0 = \frac{gT}{2\pi} \tag{3}$$

The index *0* refers to deep waters wave characteristic.

Linear wave theory predicts that water particles move in closed orbits, *i.e*. a fluid particle returns to its initial position after each wave cycle. The characteristics of water particles' movements depend on the water depth. In deep water conditions, water particles have circular orbits, whereas in transitional and in shallow water they have elliptical orbits, as shown in Figure 21. The more shallow the water, the flatter the ellipse.

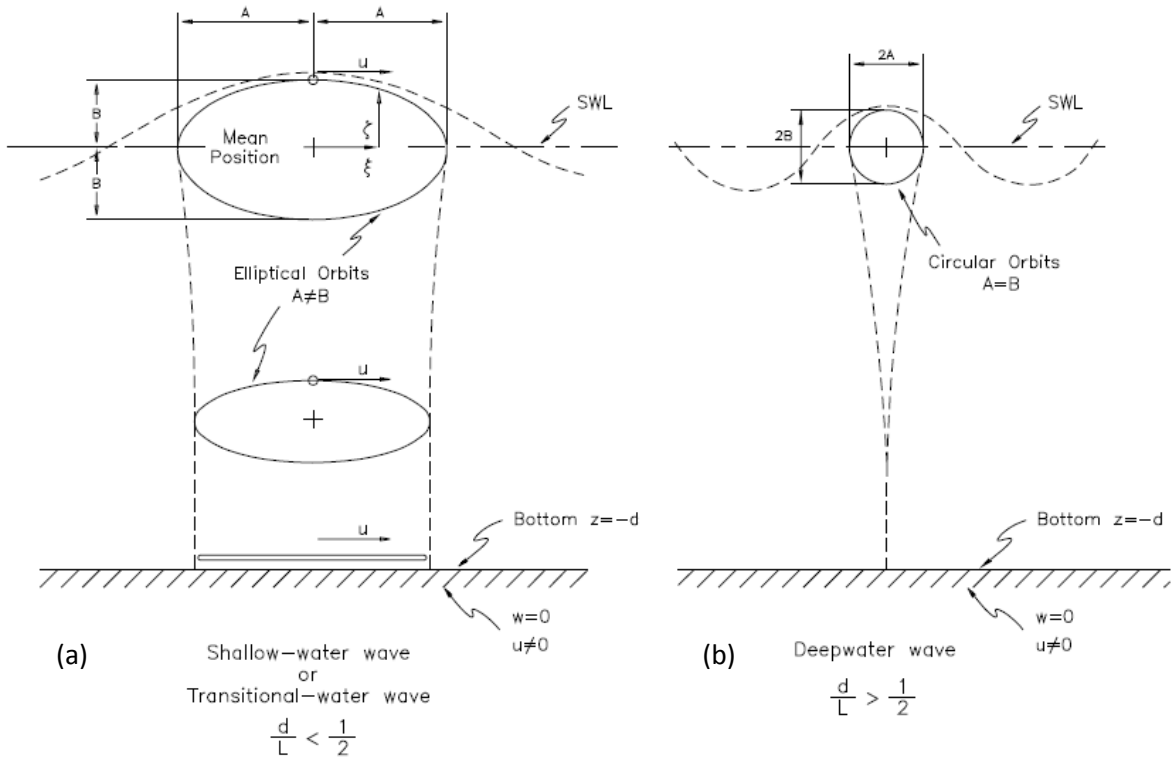

Figure 21 - Particles movement. (a) Shallow water; (b) Deep water (USACE, 2002)

The amplitude of the water particle movement is higher at the surface and reduces exponentially as the depth increases. The energy flux will have correspondence with those movement amplitudes (Figure 21). The higher the wave height, the more powerful it will be.

When ocean waves enter the continental platform, they start behaving as shallow water waves and being affected by the sea bottom. Mathematically, it means that wavelength is higher than the double value of water depth (Equation 4). Therefore, the characteristics of the wave in deep water will modify

with the variation of the water depth. Figure 22 represents the effect of the water depth reduction on the wave characteristics.

$$L > 2d \tag{4}$$

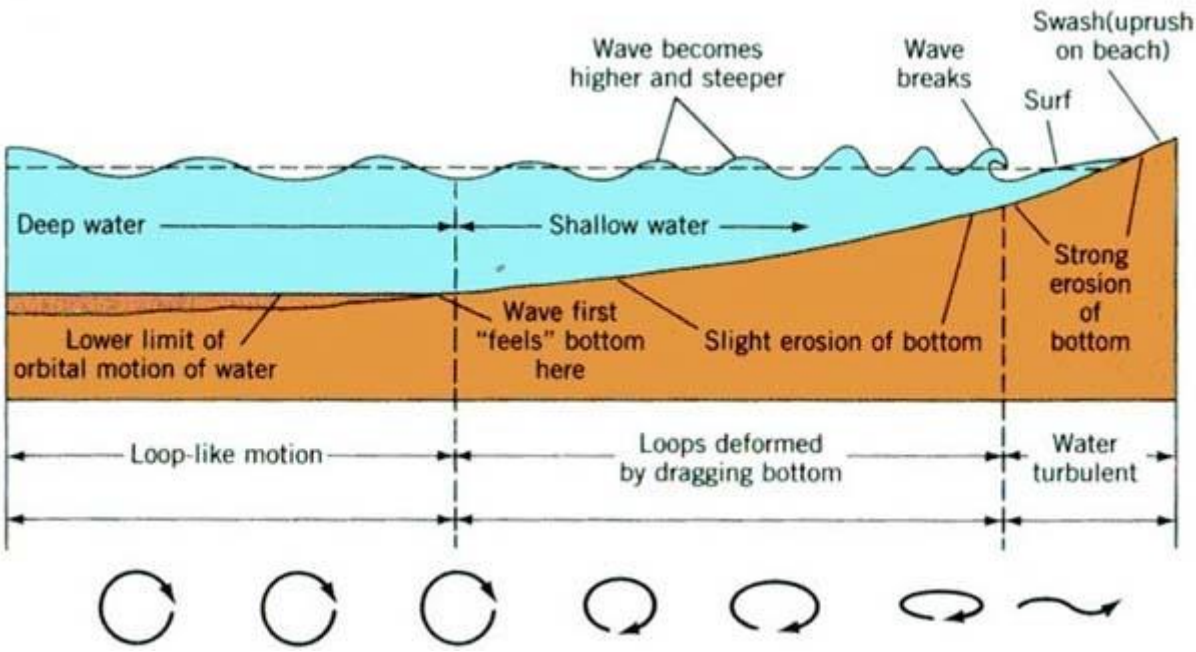

Figure 22 – Influence of continental platform on sea waves [4]

Equations (2) and (3) are only valid in deep water conditions. Equation 5 is more general and relates the wave celerity to wavelength and water depth, and is designated the dispersion relationship, being applicable to any water depth. It shows that waves with different periods travel at different speeds: the longer period waves will travel faster.

$$C = \sqrt{\frac{gL}{2\pi}\tanh\left(\frac{2\pi d}{L}\right)} \leftrightarrow C = \frac{gT}{2\pi}tanh\left(\frac{2\pi d}{L}\right) \tag{5}$$

The wave length may be determined by,

$$L = \frac{gT^2}{2\pi}\tanh\left(\frac{2\pi d}{L}\right) = \frac{gT}{2\pi}\tanh(kd) \tag{6}$$

The most used nonlinear wave theories are the Stokes' wave theories. The work of Stokes is based on the wave perturbations theory and the studies assumed that the wave steepness, *ka* (being *k* the wave number and *a* the wave amplitude), is small. Therefore, the perturbation solutions is expected to converge as more terms are considered in a power series in terms of $\epsilon = ka$; however, convergence does not occur for steep waves unless a different perturbation parameter is chosen. For a maximum

steepness, Stokes predicted mathematically that it is possible a wave to remain stable if one condition is fulfilled: the water particle velocity must be less than the wave celerity or phase velocity. For the cases that the $H_0/L_0 > 0.142$ (founded by Michell, 1893, and confirmed by Havelock, 1918), the wave becomes so large that the particle velocity at the crest exceeds the wave celerity, providing instability to the wave, leading to its breaking.

The fifth-order Stokes finite-amplitude wave theory is widely used in practical applications both in deep- and shallow-water wave studies (USACE, 2002).

The Cnoidal wave theory was developed by Korteweg and de Vries in 1895 and includes nonlinearity and dispersion effects. The use of this theory is pertinent for finite amplitude shallow water waves. The theory development is based on the Boussinesq, though it is only applicable to waves propagating in one single direction. In this case, the name of the theory came after the profile study. The profile has periodic sharp crests separated by large flat troughs.

In Cnoidal theory, waves behave as oscillatory or nearly oscillatory waves, *i.e.* water particles move forward and backward. On the contrary, the Solitary wave theory describes a wave without any trough, so the wave profile lies entirely over the still water level. It is difficult to form a solitary wave in nature. Normally, long waves such as tsunamis may approximately be considered a solitary wave. Likewise, if an oscillatory wave moves to shallow waters, the wave tends to become a solitary wave. The crest turns shorter and more pointed and trough goes longer and flatter. The wave period and the wave length are considered infinite, therefore only wave height and water depth characterize this kind of wave (USACE, 2002). Figure 23 presents the different wave theories explained previously.

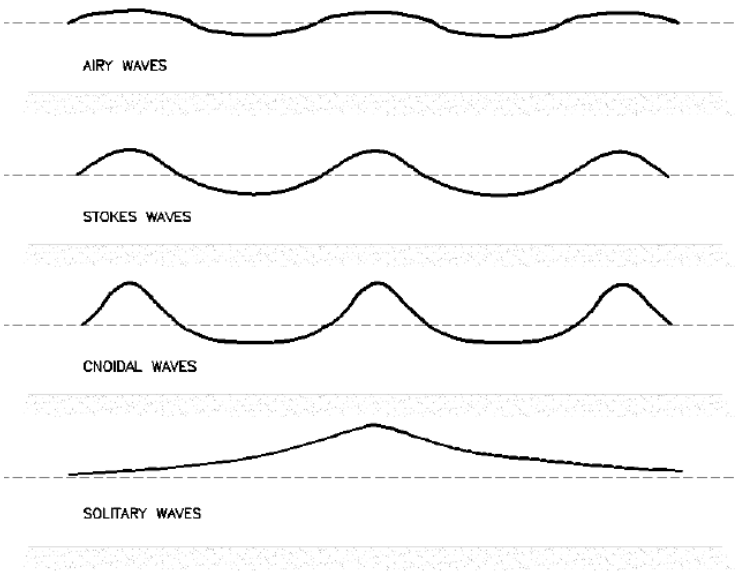

Figure 23 - Comparison of wave theories (USACE, 2002)

2.5.3.3. Irregular Waves

Elementary but rather unrealistic sea wave conditions were previously described. It was assumed that waves on the sea surface seemed to be nearly sinusoidal (constant height, period and direction, *i.e.* monochromatic waves). However, real sea states are composed of random waves with different heights, periods and directions. Therefore, it is fundamental to treat the characteristics of sea surface, not as constant, but in statistical terms. Despite complicating the analysis, it describes sea states more realistically.

Swell describes waves that may look like monochromatic waves in deep water, but it is fundamentally irregular in nature. In fact, during a storm, a sea state is always irregular and short-crested, but when travelling far from the generation region, swells may appear almost monochromatic and long-crest, as the range of characteristics variability reduces.

Figure 24 shows a standard water free surface elevation time series measured for an irregular sea state. As previously explained, wave characteristics are described in statistical terms; consequently several parameters with different designations may be used. When using these parameters, it is important to have into account that real sea states are composed of individual waves with values higher and lower than the ones used for design. There are two approaches to treat irregular waves: spectral methods and wave-by-wave (wave train) analysis. The first one is the most mathematically appropriate approach for analyzing a time-dependent, three-dimensional sea surface elevation record, but unfortunately it is more complex.

The other approach analyses the time-history of the sea surface elevation at a point, the undulations are then identified as waves, and later the statistics of the record are produced. In this method, each individual wave is defined by two successive zero-crossings. Therefore, first the mean level of the water surface is determined from the surface record and considered as the zero line. Then, a search is made for the point where the surface profile crosses the zero line downward. This point is taken as the start of one individual wave. Next, following the ups and downs of the irregular surface profile, the next zero-downward point is sought. This point will define the end of the first wave and the beginning of the next one. In the case of zero up crossings method, the points were the surface profile crosses the zero line upward are taken as the starting and ending points of individual waves.

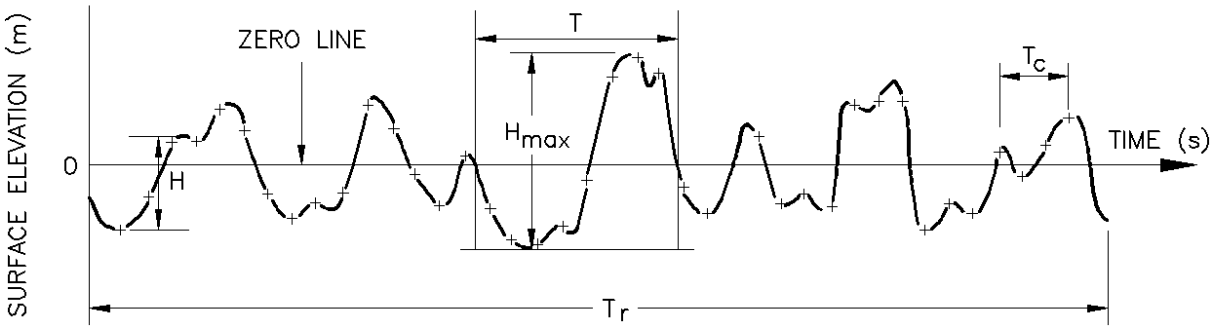

Figure 24 - Definition of wave parameters for a random sea state (USACE, 2002)

In Engineering, it is common to estimate or predict wave parameters using a time series of recorded water levels (Figure 24) and to develop a theoretical/statistical analysis to describe the sea state.

Taking Figure 24 as a reference, the characteristic parameters commonly used to describe a sea state are:

- Mean wave height – $\bar{H}$;
- Root-mean-square wave height – H_{rms};
- Significant wave height – H_s;
- Average wave height of the largest 1/n – $\bar{H}_{1/n}$;
- Maximum wave height – H_{max};
- Mean period – $\bar{T}$;
- Average zero-crossing period – T;
- Wave crest period – T_c;
- Peak wave period – T_p;
- Record length - T_r.

The vertical distance between the highest and lowest point between adjacent zero crossings points is defined as the wave height (H), disregarding small humps that do not cross the zero line, Figure 24, *i.e.*, it corresponds to the distance between a trough and a crest. The "distance" between the two successive zero crossings points defines the wave period (T) if the abscissa is the time.

However, other characteristic wave heights may be used to define an irregular sea state namely: the mean wave height, the root-mean-square wave height, the significant wave height, among others. The first one is the average wave height of all waves within the time series. The root-mean-square wave height is calculated by dividing the sum of the squared wave heights by the number of waves,

$$H_{rms} = \sqrt{\frac{\sum_1^N H_i^2}{N}} \tag{7}$$

where H_i is the ordered individual wave heights in the record and N the number of waves. H_{rms} is related with the statistical Rayleigh distribution. Considering Rayleigh distribution valid (individual waves defined by zero-crossing method in deep waters), the probability that a wave is higher than or equal to a design wave height H_d is calculated by Equations (8) and (9) may be used,

$$P(H > H_d) = e^{-\left(\frac{H}{H_{rms}}\right)^2} \tag{8}$$

$$P(H \leq H_d) = 1 - e^{-\left(\frac{H}{H_{rms}}\right)^2} \tag{9}$$

The definition of the other characteristic wave heights requires the organization of all wave heights in a descending order, as in the example of Figure 25. Then, according to the index *1/n*, wave heights of the first *n* part of the distribution are used to calculate the average height of the n part $\bar{H}_{1/n}$. The significant wave height is defined as the average of the wave heights of the one-third highest waves, *i.e.*, the one-third part, $\bar{H}_{1/3}$. The highest one-tenth wave refers to an imaginary wave having as height the average of the wave heights of the one-tenth highest waves. A similar analysis could be used for the wave periods. For instance, the significant wave period is the average of the wave periods of the one-third highest waves.

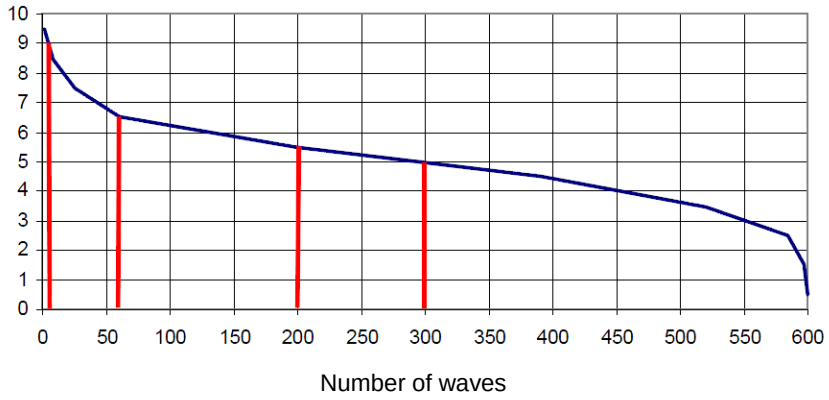

Figure 25 – Example of height waves descendant distribution

A wave energy spectrum is a graphical representation that presents the distribution of the energy over frequency or period. The spectral analysis is therefore a technique of decomposing a complex physical phenomenon into individual components, with respect to frequency (Figure 26). For instance, irregular sea states are composed of several sinusoidal components, with different frequencies and amplitudes, eventually propagating in different directions. Spectral analysis allows estimating the energy contained in each frequency/direction band, as well as the incident significant wave height, H_{m0}, also called the spectral wave height, the peak period, T_p, the average period, T_m, and the average wave period of the largest 1/n, $T_{1/n}$, among others.

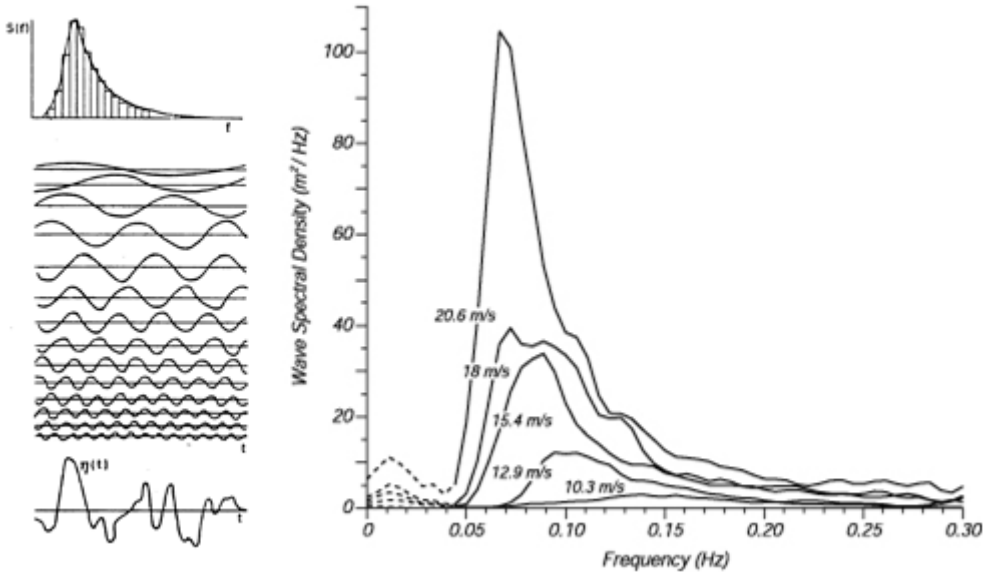

Figure 26 - Examples of wave spectrum. (a) Veloso-Gomes et al., 1986; (b) [5]

2.5.3.4. Wave Transformation

When sea waves approach the shoreline, they start to be affected by the seabed through processes such as refraction, shoaling, bottom friction, reflection and wave-breaking. In addition, if incoming waves meet any obstacle, structures or abrupt changes in the coastline, they will be transformed by

diffraction. Hence, this chapter describes what happens to waves when they travel from deep water (after generation) into shallow water (shore). Wave transformation is concerned with changes in wave height, wavelength, wave celerity and the wave angle with the sea bottom contours. Wave period remains approximately constant throughout the process.

When waves encounter an emerged reef, a beach or any sloping structure, they will run-up and then run-down or overtop the obstacle. These phenomena are intimately linked with the performance of the SSG wave energy converter and therefore will be analyzed in more detail in 2.2.4.5.

When ocean waves reach the surf zone or, in other words, the water depth decreases during the propagation, the wavelength reduces as well as the wave celerity.

An irregular wave train is composed of groups of waves. The group speed, which is the wave-energy transport velocity, C_g, is usually not equal to the speed with which individual waves within the group travel, and may be determined using,

$$C_g = nC = \frac{1}{2}\left[1 + \frac{4\pi d/L}{senh(\frac{4\pi d}{L})}\right]C \tag{10}$$

For waves propagating in deep or transitional water depths, the group velocity will be smaller than the phase velocity. In deep water, Equation 10 reduces to,

$$C_{g0} = \frac{1}{2}C_0 = \frac{1}{2}\frac{L_0}{T} = \frac{gT}{4\pi} \tag{11}$$

where C_{g0} represents the group velocity in deep water. Thus, in deep water, the group velocity is one-half of the phase velocity. In shallow water, Equation 10 reduces to,

$$C_{gs} = C = \frac{L}{T} \simeq \sqrt{gd} \tag{12}$$

where C_{gs} represents the group velocity in shallow water. Under these water depths, the wave group velocity is approximately equal to the phase-velocity of the component waves. As mentioned before, in shallow water, wave celerity depends essentially on the water deep, therefore all component waves travel at the same speed.

The total energy of a wave system is the sum of its kinetic energy and its potential energy. Applying the Airy theory, considering all waves propagating in the same direction, and determining the potential energy relative to the still water level, the potential and kinetic energy components are equal, and the total wave energy in one wavelength per unit crest width, E, is given by,

$$\mathrm{E} = \frac{\rho g H^2 L}{8} \tag{13}$$

where ρ represents the sea water density, g the acceleration of the gravity and H the wave height. The total average wave energy per unit surface area, $\bar{E}$, *i.e.*, the specific energy or energy density is given by,

$$\bar{E} = \frac{E}{L} = \frac{\rho g H^2}{8} \tag{14}$$

The wave power, *i.e.*, the average energy flux per unit wave crest width transmitted across a vertical plane perpendicular to the direction of wave advance is given by,

$$\bar{P} = \bar{E} C_g \tag{15}$$

Under stationary conditions, the total energy transport must be constant. Therefore, as the wave group velocity decreases with the reduction of the water depth, the energy density must increase, in order to maintain a constant energy flux. This phenomenon can be expressed as a shoaling coefficient. This interaction between the wave and the sea bottom is called the shoaling phenomenon, which depends on the wave steepness and the relative water depth. In shallow water, this phenomenon leads to an increase of the wave height that eventually results on wave breaking and consequently loss of wave energy in a turbulent water motion (Figure 27).

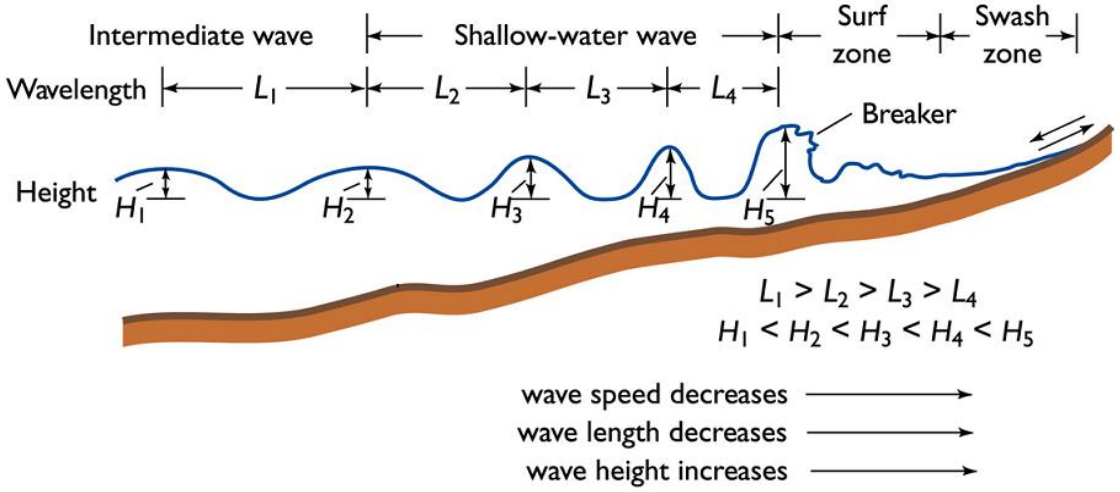

Figure 27 – Wave transformation with water depth reduction [3]

The bathymetry of the sea bottom and the coast line has also influence on several other phenomena, namely refraction, diffraction and reflection of waves. As a consequence of those effects, wave energy is focused in concentrated regions called “hot spots” (Thorpe, 1999).

It is well known from observations that waves tend to break parallel to the shoreline. Refraction (Figure 28) is the phenomenon that induces wave crests bending and changing their direction of propagation to align themselves with the sea bottom contours, resulting in wave directions more perpendicular to the shoreline. In fact, when waves reach the coast with a direction non perpendicular to it, the point on the extreme of the crest gets firstly to a smaller water depth. That results in wave celerity reduction. Therefore, the point next to the first one continues with the same velocity, so it can exceed the first point. After, the same event happens to the second point relative to the third one. And simultaneously it repeats with the first and second point with new values of depth. As the crest has infinite points, the visual result is a perception of the wave curving, and wave crests become parallel to the coast. That can result in different energy flux of each wave, depending on the wave direction. This occurrence will influence the quantity of water captured by an SSG device (Thorpe, 1999).

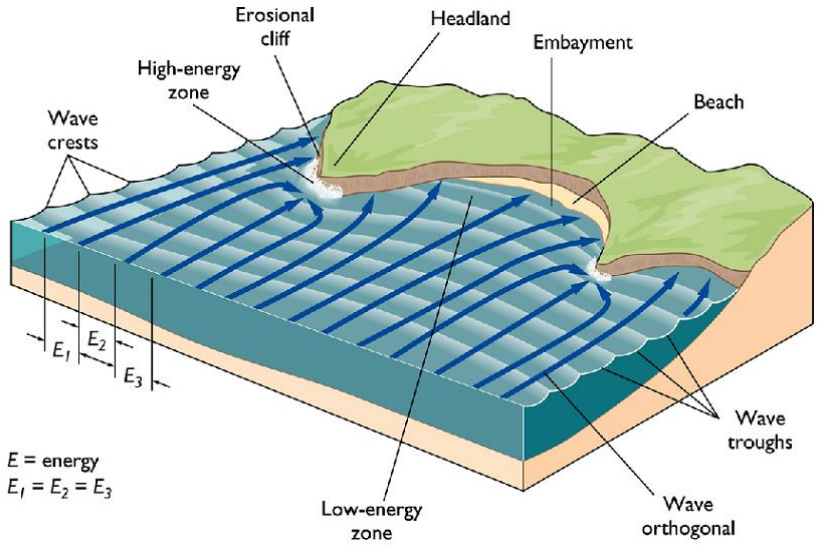

Figure 28 - Refraction of sea waves [6]

Diffraction (Figure 29) is the phenomenon that occurs when waves meet an obstacle, and it is related with the transfer of wave energy along the wave crests. Refraction and diffraction may occur together. However, there are situations that are mainly affected by refraction or by diffraction. Refraction is concerned with gently changing depth, causing the waves to shoal, and the wave crests and wave rays to bend. Wave diffraction is usually concerned with sudden changes in the wave conditions such as obstructions that cause wave energy to be forced across the wave rays (Thorpe, 1999).

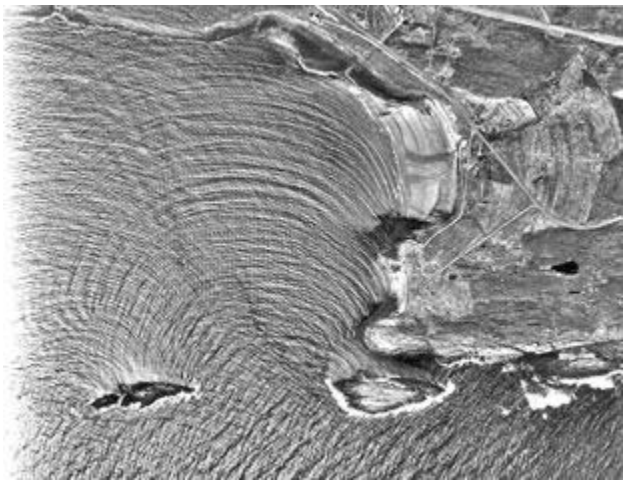

Figure 29 - Diffraction of sea waves [7]

When a wave encounters an obstacle, the wave continues with its direction (wave reflection may also occur), but on the extremity of the obstacle, the frontier point of the wave spreads, consequently, the wave energy is transferred along the crest and waves with smaller wave height appear contouring the obstacle.

Another consequence of the coast interference is the wave reflection (Figure 30). If a wave finds an obstacle but it does not have sufficient energy to break, the energy reflects on the surface of the obstacle and the wave comes back, propagating in the offshore direction (Thorpe, 1999).

Figure 30 - Reflection of sea waves [8]

2.5.3.5. Run-up and Overtopping

The study of run-up and overtopping is of paramount importance in the design and optimization of an overtopping based wave energy converter, such as the SSG wave energy converter. Run-up is defined as the maximum level reached by a wave when interacting with a beach or a coastal structure, and it is measured vertically from the mean water level. On the other hand, the rundown is defined as the minimum level reached by the wave as it goes down the slope.

Run-up and rundown depend on the characteristics of the incident waves, in particular of their height and period, and the characteristics of the beach or the coastal structure, namely the slope angle, surface roughness and porosity. The type of breaker and its location in relation to the slope is also of interest in the study of the run-up. There are several formulas and graphs for determining the maximum run-up on beaches and structures, defined as the one that is exceeded only by 2% of the waves, for irregular waves. Figure 31 presents the main parameters related with run-up phenomenon.

Overtopping occurs when sea waves go over the top of a structure. One kind of wave overtopping occurs when waves run-up the seaward sloping face of the structure and run-up levels are high enough to reach and pass over its crest. The water that passes over is called green water, according to Pullen *et al.* (2007). The other type is related to wave breaking on the face of the structure. Usually that causes a significant volume of splash. Along with wind, droplets result from the spray of water. This event can also occur either onshore or offshore. Although there are some research works about wind effect on overtopping, some models show that when discharges under 1 L/s/m happen, wind effect slightly increases the volume of green water. In these circumstances, the wind is strong enough to make water to overtop the structure, because water is essentiality spray.

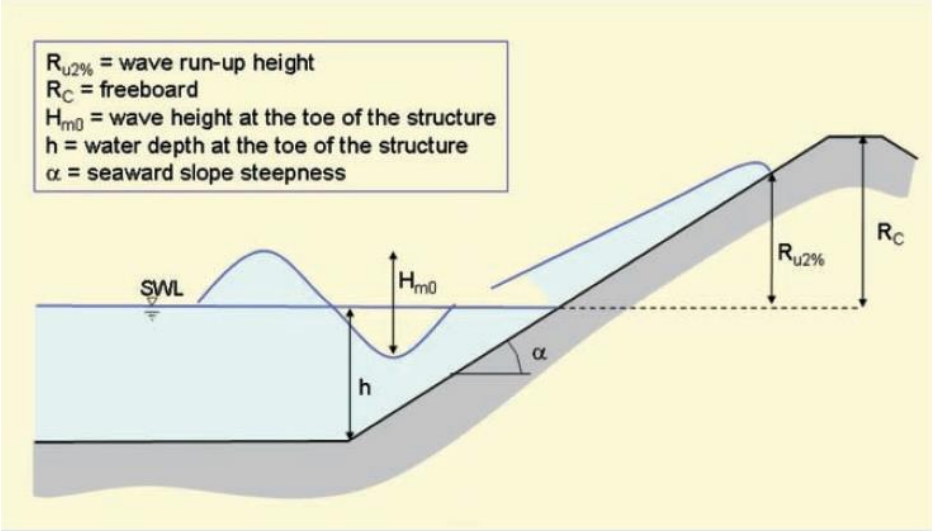

Figure 31 - Wave run-up parameters (Pullen *et al.*, 2007)

Besides wind, the slope of the breakwater (or the bottom of the sea) also has influence on overtopping. The slope of the seawall interferes directly in the values of the breaking parameter and the run-up. The more horizontal the slope is, the higher the probability of occurring overtopping is (assuming the same porosity). When the slope tends to be vertical, the overtopping probability is smaller, because more energy is needed to reach the crest of the structure without run-up.

The relative wave run-up height $R_{u,2\%}/H_{m0}$, *i.e.*, the wave run-up height exceeded by 2% of the incoming waves per incident significant wave height, is calculated by Equation (16). However, a maximum value for wave run-up is given by Equation (17). In order to approximate the calculations to real conditions, Equations (16) and (17) include the empirical coefficients c_1, c_2, and c_3, the factors γ_b, γ_f, and γ_β, to take into account berm, slope roughness and oblique wave attack effects, respectively, and the breaker parameter, $\xi_{m-1,0}$, which affects the run-up behavior and height (Pullen *et al.*, 2007).

$$\frac{R_{u2\%}}{H_{m0}} = c_1 \cdot \gamma_b \cdot \gamma_f \cdot \gamma_\beta \cdot \xi_{m-1,0} \tag{16}$$

$$\frac{R_{u2\%}}{H_{m0}} = \gamma_f \cdot \gamma_\beta \cdot \left(c_2 - \frac{c_3}{\sqrt{\xi_{m-1,0}}}\right) \tag{17}$$

The wave height value should be measured at the point of the toe of the structure. For sloped structures it begins where the foreshore meets the front slope. The wave steepness influences significantly overtopping. Wave steepness is calculated by Equation (18), where $L_{m-1,0}$ is the deep water wave length.

$$s_0 = \frac{H_{m0}}{L_0} \tag{18}$$

The wave steepness s_0 is included in a parameter that defines the type of wave breaking, called the breaking parameter (surf similarity or Iribarren number). The combination of the depth/structure slope

and wave steepness defines the type of breaking on a slope (spilling, plunging, collapsing and surging). This parameter is calculated by Equation (19), where L_0 is the deep water wave length. Wave breaking on vertical structures will not be discussed in this document because it is not directly related with this work. Figure 32 shows the different types of wave breaking (Pullen *et al.*, 2007).

$$\xi_{m-1,0} = \frac{\tan\alpha}{\sqrt{\frac{H_{m0}}{L_0}}} \tag{19}$$

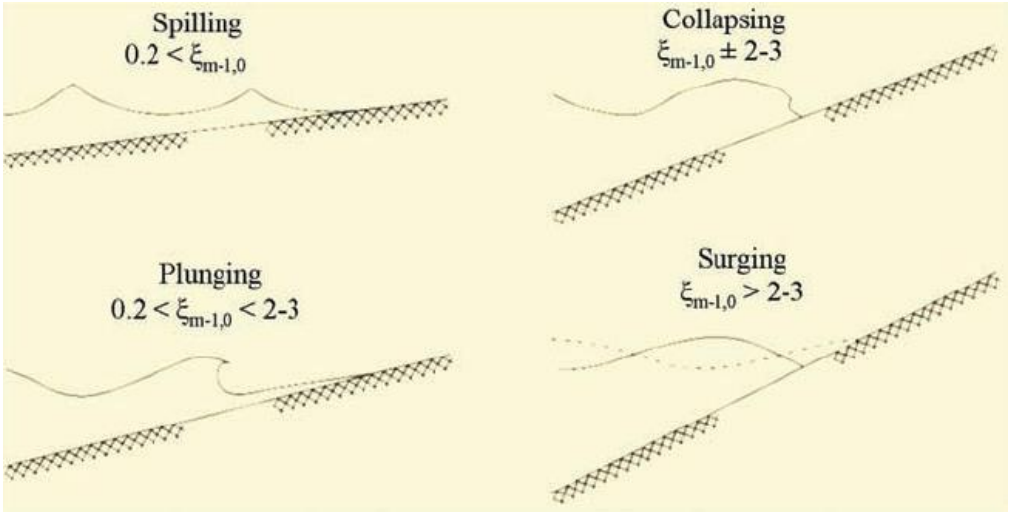

Figure 32 - Type of breaking on a slope (Pullen *et al.*, 2007)

Spilling waves occur on gentle foreshore and more than one breaker line can be found on such a foreshore. Plunging waves have steep and overhanging fronts. Also the wave tongue hits back washing water or a structure, in case of it. On collapsing waves, the wave front becomes almost vertical and a large water excursion is created (wave run up and run down). On surging conditions, there is no wave breaking. Wave runs-up and then it is reflected back to the sea (USACE, 2002).

The materials used on the slope affect other important parameters, such as permeability, porosity and roughness. These parameters affect the volume of water that can overtop a slope, therefore the wave power that can be absorbed by an overtopping based wave energy converter. If the slope is permeable, some water will be missed by the fact that water passes through the ramp. The permeability of the ramp is defined by the porosity of the material used for the slope. Also the slope roughness has effect on the energy losses in the overtopping process (Pullen *et al.*, 2007).

2.6. WAVE ENERGY CONVERTERS

2.6.1. INTRODUCTION

Since this work focuses on the study of a Wave Energy Converter (WEC), it is important to present a brief summary of the technologies already available to produce electricity from wave energy. Recent reviews have identified more than one hundred projects at different development stages (Falcão, 2010), and this figure is not expected to decrease as new concepts tend to substitute the ones that are being abandoned.

Due to the diversity of the technologies available, this section focusses in the WEC classification, according to: location, mode of operation, orientation relative to wave direction and dimensions in comparison with wave length. Overtopping based wave energy converters are then presented in more detail because the SSG belongs to this WEC category.

2.6.2. WEC CLASSIFICATION

Wave Energy Converters can be built in the shoreline, nearshore or offshore. Shoreline devices are built on shallow waters (water depths lower than 10 m), integrated on breakwaters or tidal dams, or fixed to cliffs. They have the advantage of allowing a good accessibility, easier installation and maintenance as well as simpler transportation of the produced electric energy. If the device is built in a bay, waves have a lower amount of energy available; therefore, it could be more advantageous to install these WEC in a cape, where the wave power is more concentrated. Other disadvantages are the existence of only a few locations for the installation, owing to environmental and social-economic impacts. When the equipment is installed in water depths in the range of 10 to 40 m, they are classified as nearshore devices, because normally these water depths are only found there. Usually these WEC are fixed to the sea bottom, avoiding the need of mooring systems, but they can also be moored, when local wave conditions and water depths do not permit that type of support. The disadvantage is that the device should resist to higher forcing loads from sea waves and the accessibility is more difficult. When WEC are installed in water depths higher than 40 m, they are called offshore devices. Frequently, these WEC are floating or submersible structures moored to the sea bottom. The advantages of onshore devices are the drawbacks of offshore devices and *vice-versa*. Offshore locations have more energy resource, but accessibility (human and energy transport) is more difficult and expensive (OTEO, 2012 and Ruiz, 2010).

Another kind of WEC classification is based on the orientation and relative dimensions in relation to waves. Point absorbers are characterized as objects of small diameter (compared to the wave length) and usually axisymmetric. Their shape allows capturing wave energy coming from all the directions. As a consequence of the incident waves oscillating movement, point absorbers action a linear generator. Attenuators are WEC with a long structure (compared to the wave length), applied in the same direction of wave propagation. They may have cylindrical modules connected with flexible articulations. The rotation between each piece permits the electric energy production. Terminators are as long as the attenuators, but are installed perpendicularly to wave propagation direction, causing the wave radiation effects. Figure 33 presents the WEC classification regarding orientation and relative dimensions (OTEO, 2012).

The last classification type concerns the WEC mode of operation. WEC could operate by submerged pressure differentials, by the Archimedes principle or the oscillating water column. The first type is based in a submerse point absorber and uses the variation of pressure that act on itself (maximum pressure for crest wave and minimum for trough). As the device works submerged, usually it is installed nearshore and fixed to the sea bottom. The second one is described as a semi-submerge chamber, usually installed on the shoreline, with an entrance on the bottom. The water enters into that chamber and causes the movement of the air (due to pressure oscillations) that passes through an air turbine to produce electric energy. Other WEC are based on the floating working mode. A floating WEC could work in group of devices or alone, using rotational and translational (either vertical or horizontal) movements or a combination of both. Another method is called “advance oscillatory

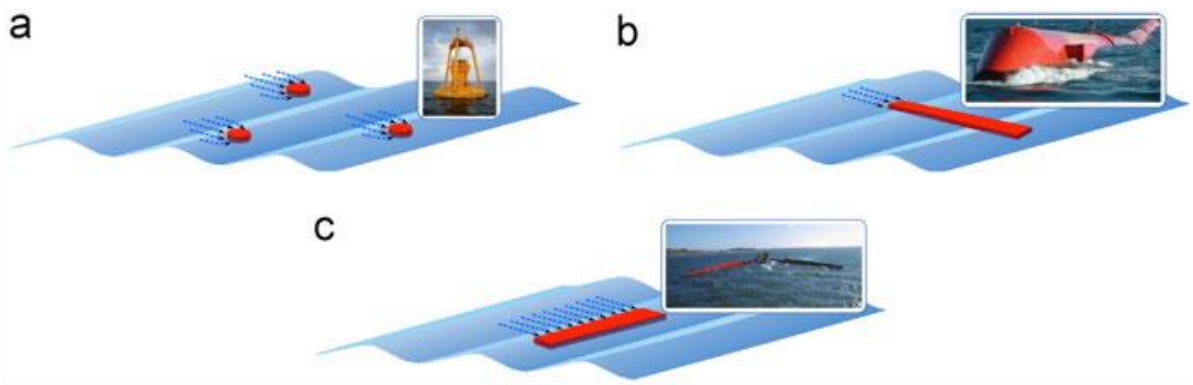

Figure 33 - Classification of WEC system regarding orientation and relative dimension with waves. (a) Point Absorber (OPT); (b) Attenuator (Pelamis); (c) Terminator (Wave Dragon) (OTEO, 2014)

system". It is composed of an articulated or flexible structure, which is installed perpendicularly to the direction of wave propagation, and moves forward and backward generating electric energy. Finally, the last mode of operation is named overtopping. These devices store the water that overtops sloping components in reservoirs installed at a higher level. The electricity is produced when the water returns to sea through low-head turbine. The Table 2 summarizes and presents examples of the WEC according to their classification.

2.6.3. Overtopping Devices

The Sea-wave Slot-cone Generator is not the only overtopping based WEC (Table 2). The Sea Power WEC, from Sweden, was one of the first devices using this mode of operation and reflectors to focus waves towards the slope, in order to increase overtopping (Kofoed, 2002).

This section intends to present some of the main overtopping based devices, such as TAPCHAN, Wave Dragon, Wave Plane and WaveCat. However, along the years, more WEC based on overtopping phenomena were developed, like the Sea Sucking Shaft, the Power Pyramid (Kofoed, 2002), the Floating Wave Power Vessel (Powertech, 2009), the WaveBlanket (Gatti, 2010), among others.

2.6.3.1. TAPCHAN

TAPCHAN (Tapered Channel Wave Energy) is an onshore WEC that takes advantage of a channel tapering effect and collects the water in an elevated reservoir (Figure 34). The concept was developed in 1985 and a prototype was built (rated power 350 kW) in Toftesfallen, Norway. It was operating until the beginning of the decade of 1990 (Thorpe, 1999). However, this WEC requires a large area in order to smooth out the fluctuations in the flow of the overtopping water. This was probably the reason for not being used anymore (Falcão, 2010).

The device is composed of a collector (sloping channel with a variable cross section) that increases wave height as a consequence of the energy concentration. The sea water undergoes a run-up process before entering an onshore reservoir, increasing its potential energy due to rising hydraulic head. The captured water is then available to be converted into electric energy by a standard hydroelectric power plant and returned to the sea. This conversion device has no moving parts and it is exclusively passive (Evans and Falcao, 1985).

Table 2 – WEC characterization (adapted from OTEO, 2014)

		Mode of operation					
		Submerged pressure differential		Floating mode		Overtopping	Oscillatory system
		Oscillating water column	Archimedes principle	Multiple structures	Singular structures		
			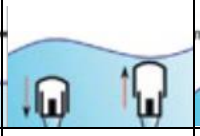	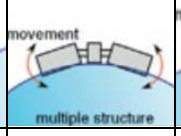	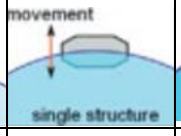		
Localization	Onshore	Pico Plant (PT) 				SSG WAVEnergy (NO) 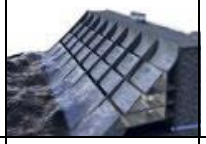	
	Nearshore	Oceanlix Energetech (AU) 	CETO III REH (UK) 	Wave Star (DK) 	Seareaser Ecotricity (UK) 	Wave Plane (DK) 	Oyester Aquamarine (UK) 
	Offshore	OE Buoy Ocean Energy (IRL) 	AWS Ocean (UK) 	Pelamis PWP (UK) 	PowerBuoy OPT (USA) 	Wave Dragon (DK) 	Langlee (LWP) (NO) 

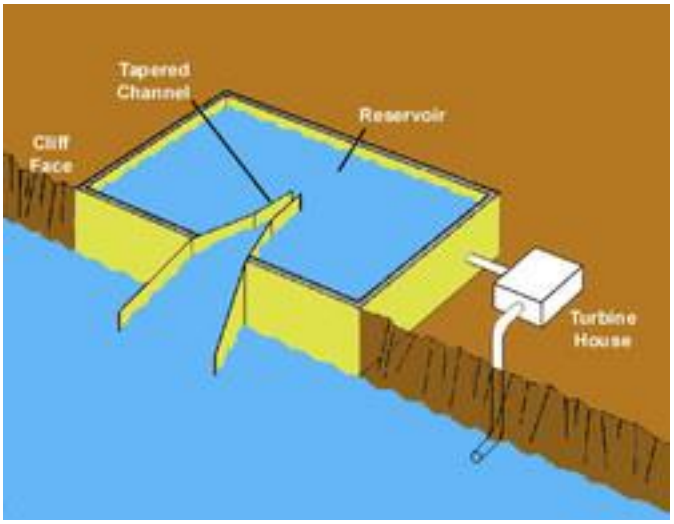

Figure 34 - Example of a TAPCHAN device [9]

2.6.3.2. WAVE DRAGON

Wave Dragon (WD) is a floating device that captures sea water due to wave run-up. Figure 35 shows a sketch of WD (Frigaard *et al.*, 2004). Depending on how energetic the wave local climate is this device may produce nearly 4-10 MW. WD has two wave reflectors connected to the main structure that concentrate incident waves toward the ramp, Figure 36 (Frigaard *et al.*, 2004).

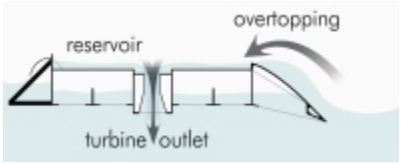

Figure 35 - Wave Dragon sketch (Frigaard *et al.*, 2004)

Figure 36 - Wave Dragon prototype (Frigaard *et al.*, 2004)

These patented reflectors increase energy capture (by raising the significant wave height) by 70% in typical wave conditions (Bevilacqua and Zanuttigh, 2011). However, according to Kofoed (2002), reflectors increase almost 100% the energy captured under the same conditions. The double curved ramp on the main structure (also patented) leads the water to a reservoir. The water returns to sea through a set of low head Kaplan-propeller turbines that convert the hydraulic head into electricity (Frigaard *et al.*, 2004, Kofoed *et al.*, 2006, and Bevilacqua and Zanuttigh, 2011).

2.6.3.3. WAVE PLANE

Wave Plane[5] (Figure 37) is the only WEC capable of converting pulsating waves directly into a fast and even rotation without any moving parts. Wave Plane is a floating device, wedge-shaped, moored with an anchor, which has a triangular top view (Frigaard *et al.*, 2008). The V-shaped ramp intends to reproduce a beach (Ruiz, 2010) and is responsible for inducing wave run-up and overtopping.

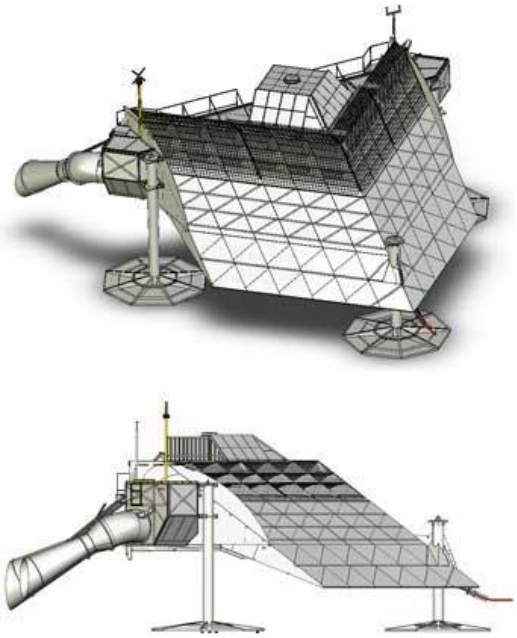

Figure 37 - Wave Plane design [10]

It uses the same principle of wave overtopping into several reservoirs, placed at different levels, and then, overtopping flow is returned back to the sea by passing a low head turbine (Kofoed, 2002). The ramp that captures incident waves is a V-shaped construction and anchored (Holmberg *et al.*, 2011). The device is composed of a series of funnel-like pockets that always face the waves. Therefore, water goes through the funnels into a horizontal pipe in a spiral-shaped flow, creating a torque moment that is converted into mechanical energy and, afterwards, into electric energy. This principle may also be used to oxygenate the bottom layers of polluted lakes and fjords (Energies, 1999). Wave Plane concept has been started at the Danish Maritime Institute and since May 1999, a 1:5 scale model has been under study in the Mariager Fjord, Jutland, Denmark (Energies, 1999). The overtopping flow may reach 500 m^3/h for waves with a high of 0.20 m high (Ruiz, 2010).

2.6.3.4. WAVECAT

WaveCat is another overtopping WEC and was developed by University of Santiago de Compostela. This floating WEC operates with oblique wave overtopping on offshore locations. WaveCat has two hulls, as a catamaran (hence its name), but forming a wedge in the plan view (converging hulls) and not parallel. The angle that both hulls form at the stern may be changed depending on the sea state,

[5] http://www.waveplane.com/

due to hinge joint placed at the stern. The draught and freeboard can also be varied in accordance with sea state (Figure 38).

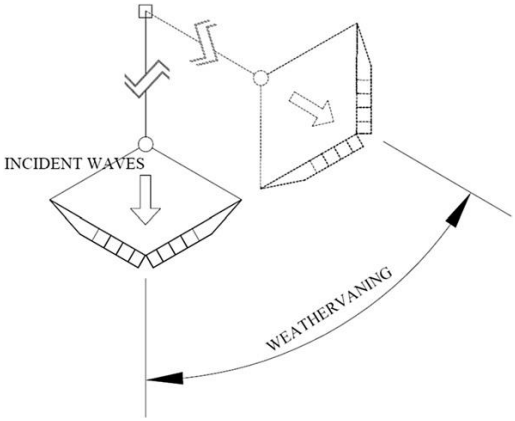

Figure 38 - WaveCat sketch of the direction variation (Fernandez *et al.*, 2012)

The freeboard of each hull decreases along with the length towards the stern, allowing a continuous overtopping, as incident waves propagate between both hulls. If freeboard were kept constant, wave height would decrease and the run-up height could not allow wave overtopping into the stern reservoirs. The main advantage of WaveCat are the low (if not null) environmental and visual impacts (due to the absence of superstructure), and the possible operation offshore, where usually the wave energy resource is higher than in nearshore shallow waters or onshore (Fernandez *et al.*, 2012).

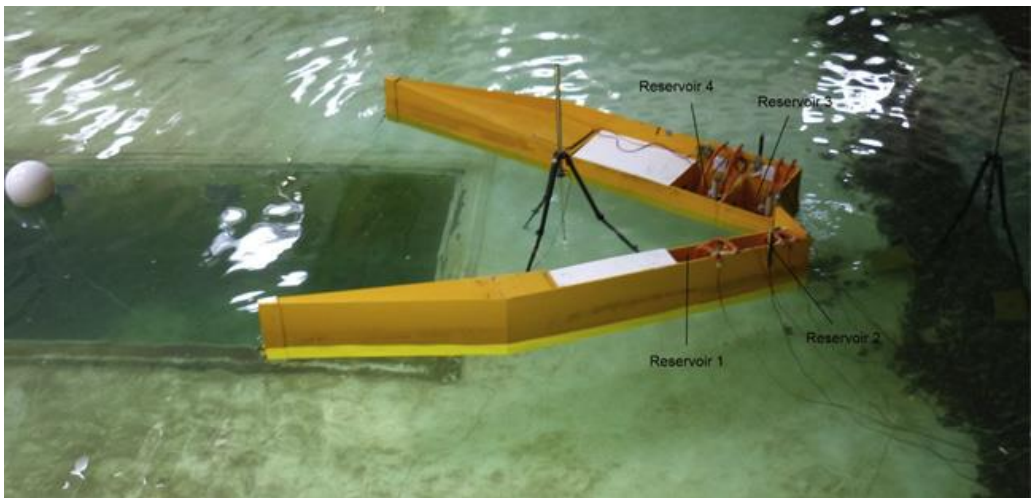

Figure 39 - WaveCat physical model in the wave tank of FEUP; location of the four reservoir for collecting overtopping water (Fernandez *et al.*, 2012)

2.6.3.5. SSG

In the year of 2003, a company named WAVE ENERGY AS from Stavanger, Norway, developed a WEC (Wave Energy Converter) identified as Sea-wave Slot-cone Generator, as known as SSG. This device (Figure 40) aims at converting the natural and renewable energy of ocean waves into electricity

taking advantage of wave overtopping (Margheritini *et al.*, 2009). The studies carried out ended with a pilot-project in 2008 for the Kvitsøy Island, Norway. However, this pilot installation was not built until the moment. In fact, when the theoretical studies and projects were concluded and the prototype was ready to be built, an individual did an official complaint at the Kvitsøy municipality against the construction approval and there has been no advance since then (Bakke, 2008).

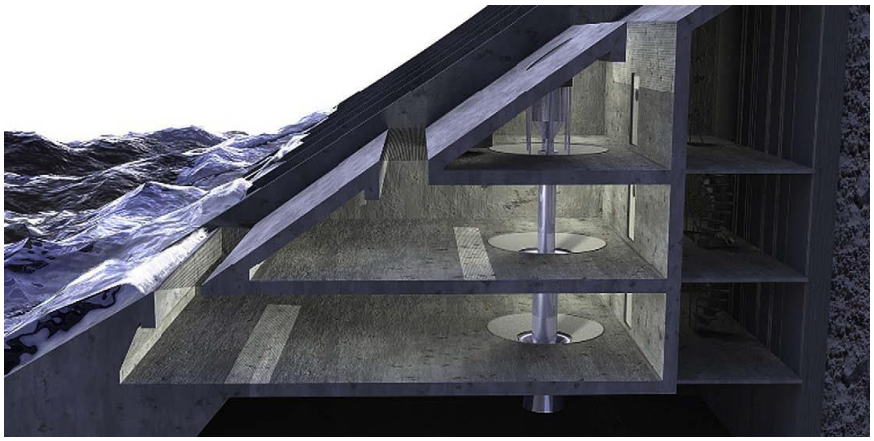

Figure 40 - Sea-water Slot-cone Generator (Vicinanza *et al.*, 2012)

2.7. SEA-WAVE SLOT-CONE GENERATOR

2.7.1. DESCRIPTION OF THE DEVICE

SSG is a wave energy converter with a profile designed to increase overtopping. Initial designs considered SSG an onshore device (Figure 41) due to the installation in breakwaters or in a cliff. However, an offshore solution (Figure 42) could be developed in order to reach more energetic sea climates (Margheritini *et al.*, 2009).

Figure 41 - Application of SSG on a breakwater (Margheritini *et al.*, 2009)

Figure 42 - Application of SSG offshore (Margheritini *et al.*, 2009)

So, when waves reach the sloping seawall they will run-up and then overtop the device, with the aim of making the sea water entering some openings at specified elevations that lead to the SSG reservoirs. These reservoirs store the water that has now a higher amount of potential energy: higher difference between the water level inside the reservoir and the MWL (Mean Water Level). Within the reservoirs, the water flows to a conduit where a multi-stage turbine is installed. In order to prevent air pressure from obstructing water storage, some ventilations openings must be created in the reservoir. The water flow makes this turbine spinning, generating mechanical energy that in turn will be transformed in electric energy. In order to improve the efficiency of the energy conversion process, it is under development a Multi-Stage Turbine (MST), which consists in a number of turbines (each section of the runner is connected to one of the reservoirs by concentric ducts) staggered concentrically inside each other, driving a common generator through a common shaft. Thus, it takes advantage of different heights of water head and, in addition the start/stop sequences are minimized because it only operates if one reservoir is supplying water (Vicinanza *et al.*, 2012).

The best place to install this unit is incorporating it in breakwaters. That means the breakwater, as a coastal or harbor protection structure, will have a better overall performance because its combined operation mode will efficiently dissipate wave energy. Consequently, economically is more rentable once it will be a single construction instead of two different ones. Kaplan turbines are recommended for this application because they have to work with low head and they have to be protected with floodgates in order to dry the turbine for eventual repairs or other exceptions. For that reason, the generators are allocated at a higher level in order to prevent the risk of floods. Those floodgates must operate with conditions 100 times worse than daily operation due to storms intensity.

As previously stated SSG has a “robust” appearance and low cost, because it may be incorporated in breakwaters or installed in a continuous front in a breakwater or cliff. In spite of these particularities, the key characteristic of this device is its geometry.

Research is still lacking to optimize the SSG geometry and operation strategies for environmental conditions typical of Portuguese coast. This will allow enhancing its currents performance harvesting wave power and consequent electric power generation. Each place where a SSG device will be used needs a deep study involving the characterization of the local conditions (waves, tides, currents and, local of installation) and the assessment of the SSG performance according to those local conditions (Vicinanza *et al.*, 2012).

2.7.2. ENERGY PERFORMANCE

The main goal of this equipment is to produce electric energy in an efficient way. Four steps are generally considered in overtopping based WEC to get the intended electricity. Unfortunately, energy transfer involves some dissipation. The steps are:

- Wave to crest of the structure;
- Crests to reservoirs;
- Low head water turbines;
- Electrical generator and electrical equipment.

The first topic means that the different waves need to have sufficient energy to run-up and pass over the crest levels of the reservoirs. Then the potential energy gained is slightly reduced due to the fall between the crest level and the level of the water inside the reservoir. After the water goes through the turbine transforming water motions in mechanical energy. Lastly, the mechanical movement will generate the electric energy (Vicinanza *et al.*, 2012).

2.7.3. STUDIES PERFORMED

As previously written, the idea of an on-shore overtopping based WEC started in 2003, but only one year later the physical and numerical modelling studies have begun. At Aalborg University, more precisely at the Laboratory of Hydraulic and Coastal Engineering, the behavior of the SSG was studied experimentally with regular and irregular waves, either 2D or 3D, using physical models built on geometrical scales between 1:60 and 1:15 (Bakke, 2008).

Since the end of 2005 to the middle of 2008, WAVE ENERGY AS coordinated a group of companies and European universities (partially funded by the European Union) to perform extensive research on a full-scale SSG device to be built in the island of Kvitsøy, Norway (Bakke, 2008). The SSG device designed for this pilot project was 10 m wide and it had an installed capacity nearly 200 kW. Unfortunately, this pilot project was never built due to a private individual complaint to the Kvitsøy municipal. However, the theoretical studies and the experimental works carried out during five years resulted in a complete design of the SSG mechanical and electrical equipment. In addition, during this project, the Aalborg University developed a helpful software that allows the simulation of sets of sea wave conditions and the estimation of corresponding energy production, taking into account the geometry of the SSG device, the characteristic of the electro-mechanic equipment and the chosen operation rules (Bogarino *et al.*, 2007).

The SSG efficiency depends, primarily, on the amount of overtopping water that enters the reservoir. Therefore, extensive experimental work has been performed at the Hydraulic and Coastal Engineering Laboratory of the Department of Civil Engineering of Aalborg University to analyze how wave, tide and structure parameters could affect the mean overtopping discharge, using regular and random waves, under either 2D or 3D conditions. The main parameters analyzed were the number of reservoirs, reservoir crest levels, ramp angle and ramp draught, front angles, horizontal distance between the reservoir crests, as well as the influence of the wave height and wave period.

The SSG optimization studies carried out for the pilot project of WAVEnergy AS were synthetized in Margheritini *et al.* (2009). It is worth mentioning that an innovated Multi-Stage Turbine (MST) was being developed for this project. This concept is a combined system of turbines depending on the number of reservoir (due to the low head available, it is advised to apply Kaplan turbines). All the turbines are connected by one vertical duct that makes it possible to use the head levels associated to different reservoir simultaneously in order to increase the overall efficiency of the power take-off

device. It may also be possible to install one more turbine at the lowest level (Margheritini *et al.*, 2009). Modelling results in 3D conditions were also presented (Margheritini *et al.*, 2008).

Later, in the year of 2012, a group of researchers worked on reviewing the studies and results that have been published on the devices installed all over the world. After many studies, the conclusions are always the same: improvement of the performance of SSG devices depends on a better combination of the parameters and variables of the environment conditions with the geometry of the structure as describe previously (2.3.2. Hydraulic Behavior), Margheritini (2009), Margheritini *et al.* (2012b), and Vicinanza *et al.* (2012).

Recently, Oliveira (2014) tested experimentally a SSG model in a wave tank in order to evaluate the geometry defined in previous works under wave conditions typical from the Portuguese west coast. In addition, Oliveira (2014) analyzed the influence of two reflectors installed on the SSG structure to concentrate wave power and increase the efficiency of the device (Figure 43). As expected from similar studies of others overtopping based WEC's, the use of reflectors increase the energy produced nearly to the double. This is justified because the wider entrance provides a higher wave capture width and the two reflectors form a slopping channel with variable width, causing a significant increase of the wave height. Therefore, the overtopping discharges increase and consequently the energy production grows too.

Figure 43 - Physical model developed (Oliveira, 2014)

Oliveira (2014) simulated SSG structures with reflectors with two configurations (Figure 44), despite the model without any reflector (case C1). Each reflector configuration was subject to three reflectors angles of 30º, 40º and 50º (Figure 45) that made with the normal of front ramp (on plan view). The second configuration (C2) has the reflectors converging in a point while in the third one (C3) the reflectors are parallel each other.

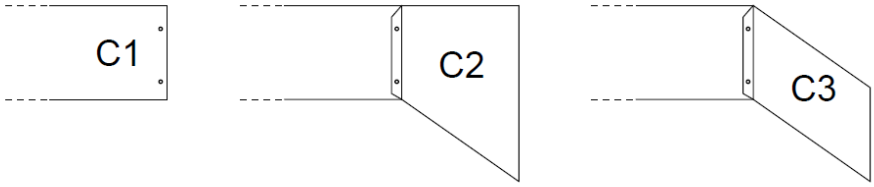

Figure 44 - SSG profile without reflectors (C1) and two different configurations with reflectors (C2 and C3) (Oliveira, 2014)

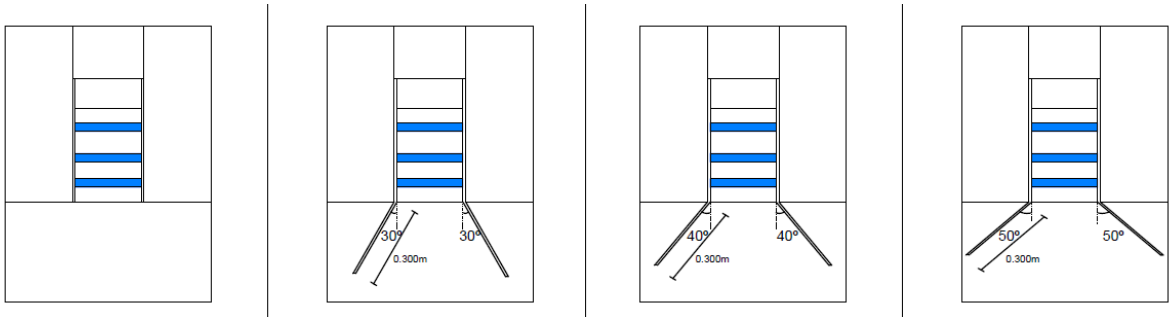

Figure 45 - Plan view of the different reflector angles with model measures (Oliveira, 2014)

The study was carried out with regular and irregular waves. The SSG configuration tested with the best overall performance was the C3 with reflector angle of 50º. The final power productions for each sea states carried out study are presented in Figure 46.

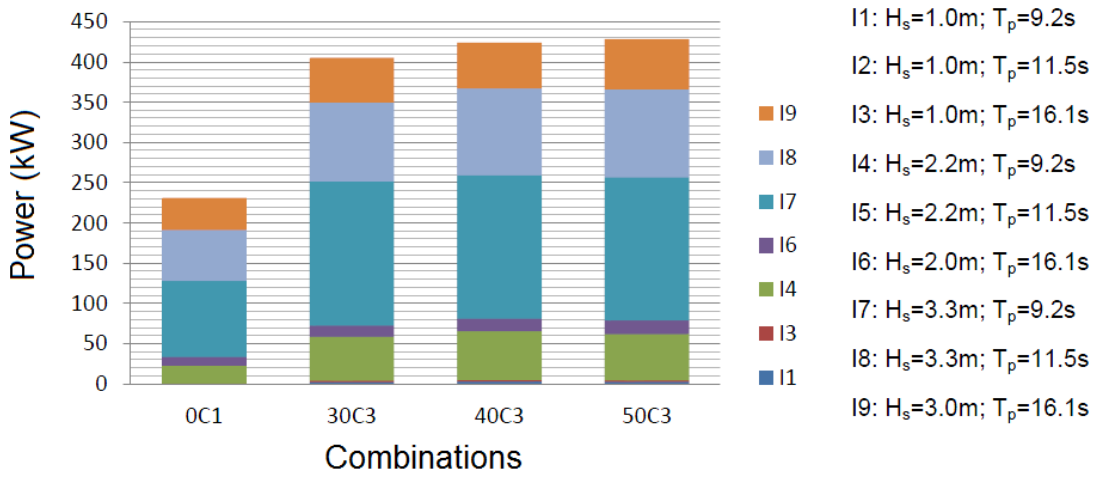

Figure 46 - Total power for different sea states tested (Oliveira, 2014)

2.7.4. HYDRAULIC BEHAVIOR

The Sea-wave Slot-cone Generator is a WEC that is still in a research and development phase; therefore it is not possible to state that it is a fully optimized device with the best possible performance. The amount of energy produced is directly related to the hydraulic behavior of the structure. The performance of the device may increase with the number of reservoirs, the reservoir crest levels, which define openings that allow the access of sea water to the reservoirs, the distance between those entrances, the angle of the ramps and the depth of the reservoirs. The optimization study should consider energy price.

The number of reservoirs affects the production of electric energy. More reservoirs may mean that there is more potential energy available. However, it is important to take in consideration the sea states on that location, *i.e.*, the wave heights, wave periods, wave directions, as well as the amplitude of tides. If typical sea wave conditions at site are characterized by a large range of wave heights or tide amplitudes, a SSG with several reservoirs may be required. However, if sea states do not have those characteristics, the used of several reservoirs may be unnecessary, otherwise, there will be reservoirs that do not collect water.

Another very significant variable is the level of the entrance to the lowest reservoir. Along with the wave heights, the entrance crest elevation can be higher or lower, enabling the entrance of more or less volume of water inside the reservoir, respectively. However, it is worth mentioning that a lower crest level means that the hydraulic head available to produce energy is smaller. For each case, the wave heights and the variation of tide levels must be considered.

For a SSG design with three reservoirs (Res.), with crest levels at 1.5, 3.0 and 5.0 m above SWL, 2D physical model tests were carried out (geometrical scales ranged between 1/60 and 1/15). Those tests allowed confirming that the mean overtopping flow increases with the wave height. Figure 47 shows that relationship, in which the wave height was measured at the structure toe (Vicinanza *et al.*, 2012). The explanation of the different shapes of the trend lines is rather uncertain, however, it is thought that the horizontal distance between the reservoirs front ramps forms a gap which seems to set an upper limit to the entering volume of water, *i.e.*, the amount of water the lower reservoirs can capture. More detailed information is presented in Kofoed (2005a).

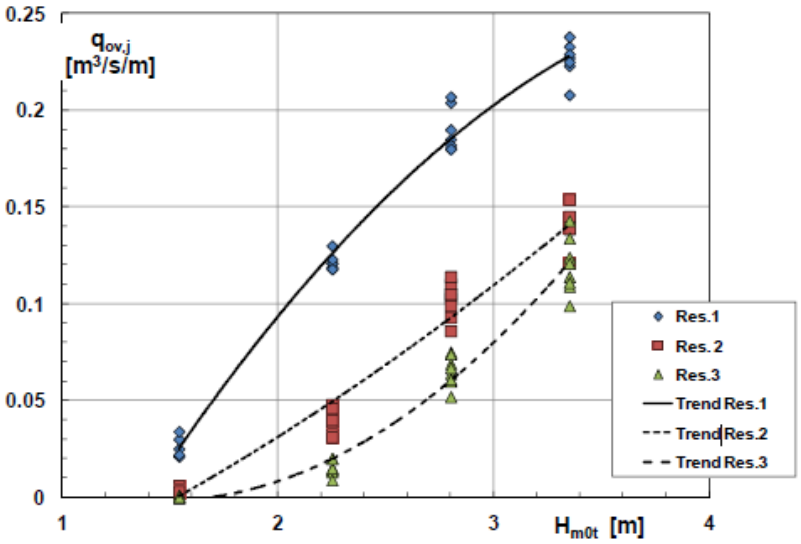

Figure 47 - Overtopping discharge vs. wave height (Vicinanza *et al.*, 2012)

However, if entrances are very high, the water does not go into the reservoirs. On the other hand, if the entrances are very low, the reservoirs may become submerged, particularly when the tide level is high. In both situations, the amount of the energy produced is null and the power from sea waves is unexploited.

Another SSG characteristic that influences the device performance is the horizontal distance HD between the front ramps. Enlarging the horizontal distance between the crests of the entrance of the reservoirs will increase the volume of water that enters into the reservoirs. When that distance is small compared to the wave height (according to Vicinanza *et al.*, 2012, $HD1/H_{m0,t} < 2$), the higher levels have an important influence on the water stored in the lower reservoirs. For large entrances, the device seems to respond like a single reservoir structure. On the other hand, when the distance is too large, the lower reservoirs collect more volume of water but the upper reservoirs do not, and the device starts to respond as a single reservoir structure (Vicinanza *et al.*, 2012). Figure 48 presents test results in the form of dimensionless overtopping discharges in the two reservoirs of the SSG structure as a function of the variation of horizontal distance between the front ramps, as explained previously. The SSG tested had no vertical front in the ramp ($d_r/h=1$) and a slope angle of 35º was selected for all the front ramps. A JONSWAP spectrum was used to reproduce irregular waves, and the peak wave steepness (Equation 19) had been varied between 0.005 and 0.05.

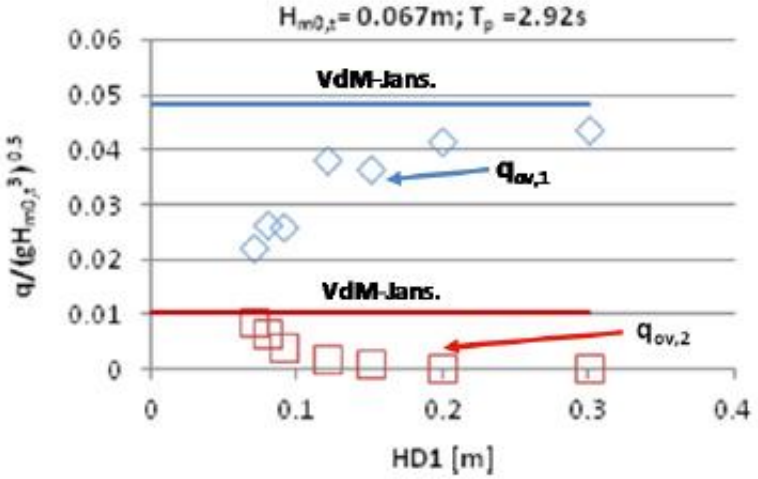

Figure 48 - Non dimensional overtopping rates in the reservoirs as function of HD1 (Vicinanza *et al.*, 2012)

The depth of each reservoir has an effect on power production, although it does not have influence from sea states. A reservoir with high depth allows accumulating more potential energy and the times of start/stop cycles of the turbines are larger, because when the reservoir is full, it takes more time to get empty.

The ramp angle also affects the performance being amplified by lower values. Three front ramp angles were tested with different sea states (Vicinanza *et al.*, 2012) and the results are presented on Figure 49. All the curves reducing for $H_s/h = 0.56$ due to breaking occurrence on the foreshore. Despite the 19º results in a better performance than the other angles (4% gain), it may potentiate the occurrence of plunging breaking and the production of air punches and consequently reduces run-up height, meaning major energy losses. Thus, the better solution is to increase the angle of the ramp so that non-breaking

waves happen. A study of sea state and ramp angle relation is advisable for each case of construction of SSG and also for each ramp angle.

As previously referred, the ramp height (value from the beginning of the slope of SSG and the crest of the entrance of the reservoir) of each entrance of the reservoirs is very important. Therefore, it is possible to calculate the mean overtopping flux using Equation (20). Bigger height increases the overtopping discharge and the hydraulic efficiency (Equation 21). The hydraulic efficiency can increase from 29 % to 34 % due to higher ramp draught as it is displayed in Figure 50 (Vicinanza *et al.*, 2012).

$$\frac{q}{\sqrt{gH_{m0}^3}} = a\, e^{\left(\frac{-bR_c}{H_{m0}}\right)} \tag{20}$$

where q is the average overtopping discharge per width, R_c the crest level of the reservoir, and a and b empirical coefficients.

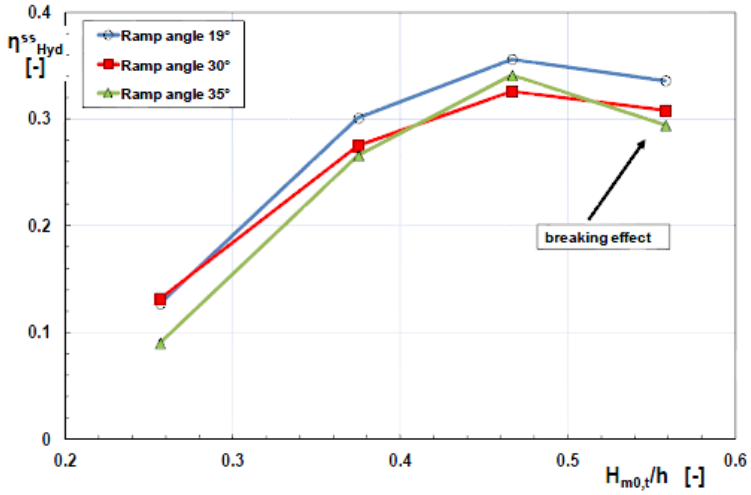

Figure 49 - Ramp angle effect on the hydraulic efficiency (Vicinanza *et al.*, 2012)

The hydraulic efficiency η_{in} is calculated by the ration between potential energy that overtops the crest reservoir P_{in} and the wave power by unit of length P_{wave}.

$$\eta_{in} = \frac{P_{in}}{P_{wave}} \tag{21}$$

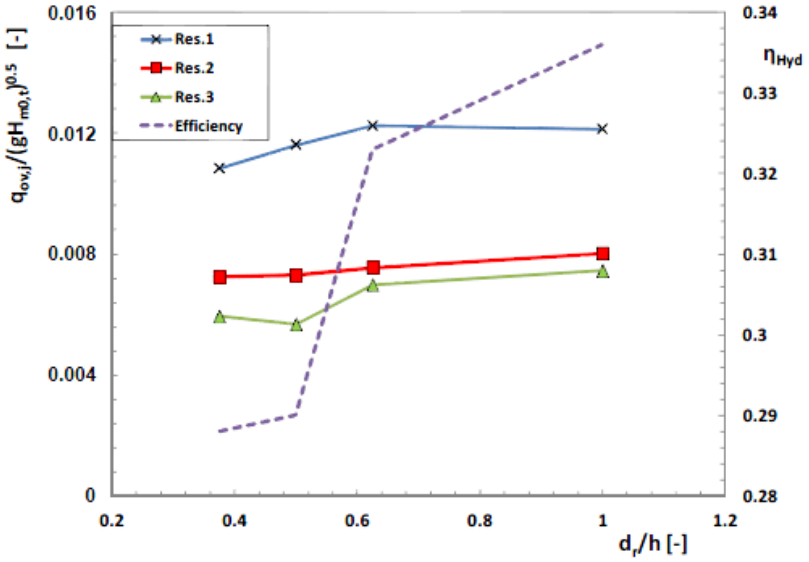

Figure 50 - Effect of the ramp draught on the overtopping rate and on the hydraulic efficiency (Vicinanza *et al.*, 2012)

So for higher values of wave height there are higher values of hydraulic efficiency according to Equation (22) estimated by Kofoed (2005a) by,

$$q_n(z_1, z_2) = \sqrt{gH_s^3}.\frac{A}{B}.e^{C\frac{R_{c,1}}{H_s}}.\left(e^{C\frac{z_2}{H_s}} - e^{C\frac{z_2}{H_s}}\right) \quad (22)$$

where g is the gravity acceleration, H_s the significant wave height, $R_{c,n}$ the crest level of reservoir n and z_1 and z_2 the lower and upper vertical levels of the reservoir, respectively, *i.e.* $z_1 = R_{c,n}$ and $z_2 = R_{c,n+1}$.

In 2D tests, the effect of wave directionality cannot be analyzed. Oblique waves reduce the volume of overtopping water; however, short-crestedness waves behavior is discussable. Van der Meer and Janssen defend that head-on short-crested sea-states reach the same run-up height as the long-crested on sloping structures. On the other hand, Franco and Franco (1999) achieve the opposite conclusion for vertical-face breakwaters (Vicinanza *et al.*, 2012). Therefore, irregular sea states as head-on long-crested wave attacks (2D, no obliquity, no directional spreading), head-on short-crested storms (no obliquity but different spreading levels), and oblique long-crested sea-states (wave directions between -15º and +15º and no directional spreading) have been run in order to understand the effect of wave directionality. Equation (23) was developed and Figure 51 shows the conclusions for the first and third reservoir of the initial SSG design.

$$S\,(D; D_0, n) = \cos^{2n}\left|\frac{D - D_0}{2}\right| \quad (23)$$

where D represents the direction of the generic Fourier component, D_0 the mean wave direction (taken from the normal to the SSG) and n the spreading index.

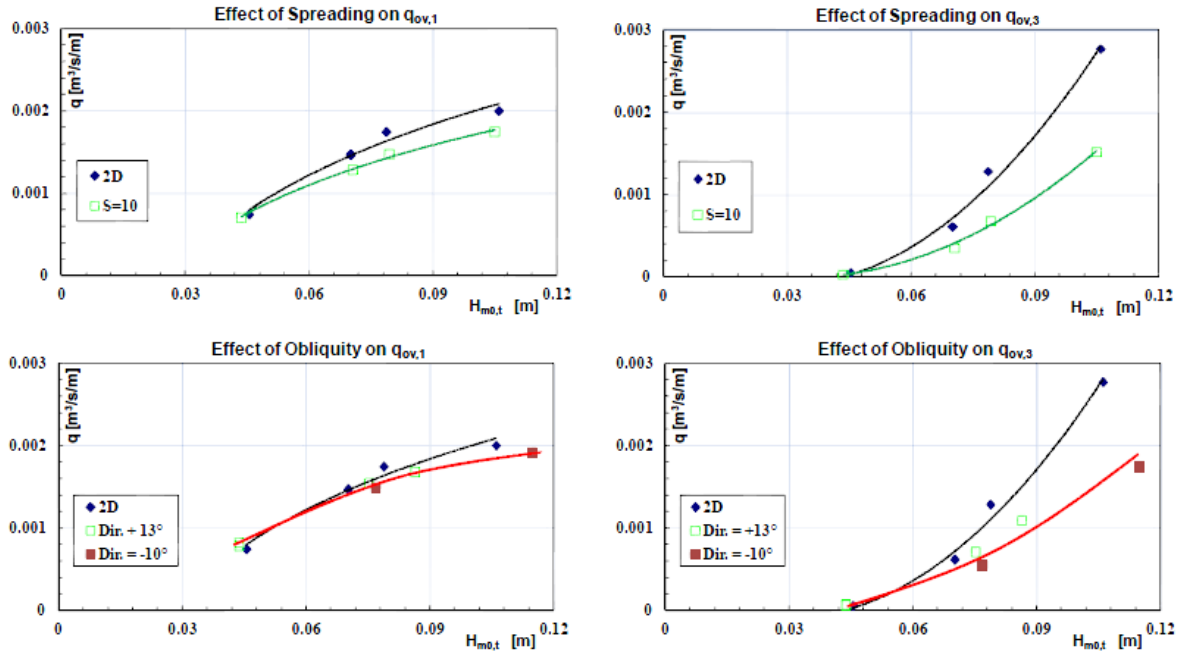

Figure 51 - Effect of directional spreading (up) and obliquity (low) on wave overtopping (Vicinanza *et al.*, 2012)

Analyzing Figure 51, the effect of short-crestedness and obliquity limits the volume of overtopping discharge. The reduction is well noticed for the highest reservoir while on the others not so much. Due to these effects, it is estimated that refraction and short-crestedness may decrease the hydraulic efficiency as much as 50% (Vicinanza *et al.*, 2012).

Finally, it is essential to study about the reflection of the waves on the seawall. From one point of view, SSG needs a steep ramp inclination in order to require large run-up heights but it will lead to large reflection rates. Contrary, steep slopes favor surging breaking occurrence in which little energy is dissipated. Another negative point is that high reflection rates could affect the structure stability if installed on sandy bottom (Vicinanza *et al.*, 2012).

2.7.5. Structural Behavior

The SSG wave energy converter is integrated in a breakwater or in a seawall (although offshore applications may also be possible). If located onshore, it will be subject occasionally to strong storms.

SSG technology is well accepted due to the low cost structure and its robustness. The material used to build the structure is concrete and despite the environmental impact (section 2.7.7.), maintenance and installation of the device are, respectively, low and medium-low classified due to be onshore and easily accessible, although it requires a large area in sites with steep slopes that overlook the deep sea (Bevilacqua and Zanuttigh, 2011).

It is possible to design the SSG structure using the method proposed by Goda (1974) for breakwaters, being required to increase wave loading between 20% and 50%. In fact, some experimental works were carried out with the aim of characterizing the nature and magnitude of wave loading in the structure and maximize the wave power capturing (Vicinanza *et al.*, 2012). It is also important to have

in mind that the SSG components, such as the floodgates that protect the turbines in case of emergency, may be exposed to conditions 100 times worse than the normal ones.

For that reason, 3D model tests with pressure transducers were carried out under extreme conditions in order to work out the design values for the construction of the concrete structure. Margheritini *et al.* (2009) and Vicinanza *et al.* (2012) tested a SSG prototype with 14 pressure cells, in 25 different positions on the structure under 32 wave conditions including waves with 100 years return period. The results of pressure values for the three ramps and the vertical wall in the upper reservoir of the initial design of SSG are presented on Figure 52. Impact pressures of 580 kN/m^2 on the vertical wall and 250 kN/m^2 on each ramp (values scaled to prototype) were registered. Figure 52 presents the results on the physical model where it was reproduced the surrounding bathymetry of Kvitsøy local. The values obtained by using the prediction formula developed by Takahashi *et al.* (1994) could be underestimated between 20 and 50%. The error occurs due to problem of scaling impact forces on prototypes. A cumulative distribution function that better describes the analysis results behavior is the Weibull distribution (Margheritini, 2009). The tests from Bakke (2008) also included 19 pressure transducers for measuring forces on the ramps, calculated by

$$p = \rho\, wgH \tag{24}$$

where p is the pressure, w is the water head, g is the gravity acceleration and H the wave height.

Another structural problem that may occur is the erosion of sea bottom in front of the device as a breakwater (Zanuttigh *et al.*, 2009). As explained in section 2.5.3.2, in intermediate and shallow water wave conditions, wave energy is distributed over the water column (although the wave power flow intensity diminishes downwards in the water). Consequently, the energy in the lower levels will disturb the sediments near the bottom of the structure, leading to erosion (scour). Because of this phenomenon, it is very important to design correctly the foundations of the SSG structure to prevent a global failure (Vicinanza *et al.*, 2012).

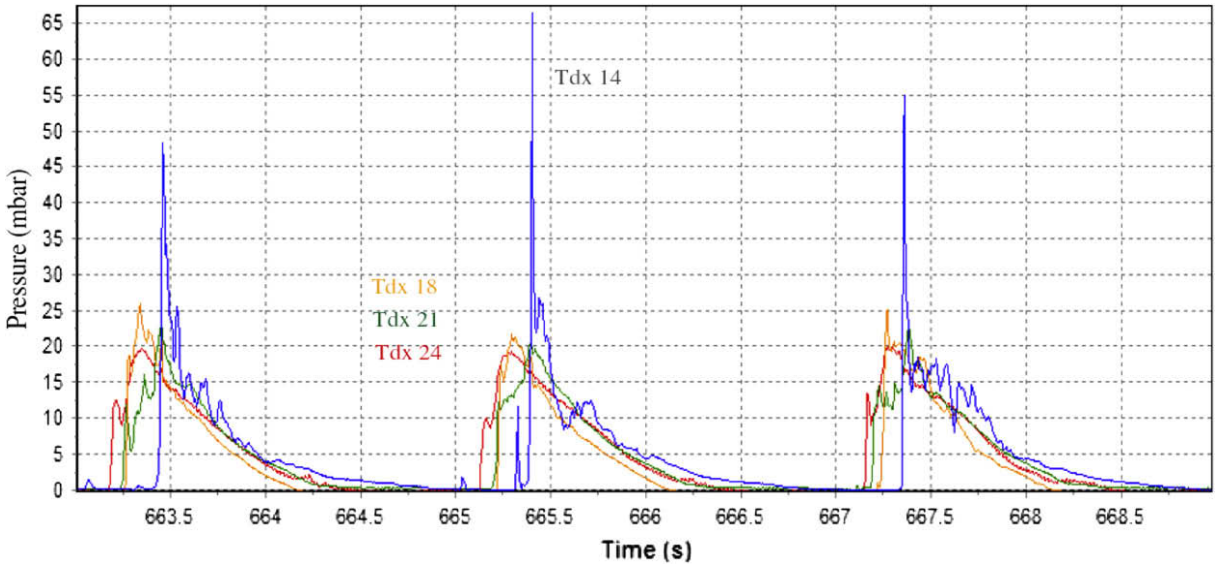

Figure 52 - Comparison of the pressures in the 3 front slopes (similar signals) and on the vertical real wall in the upper reservoir (Margheritini, 2009)

2.7.6. MULTI-STAGE TURBINE

Although the main studies of SSG were focused on the structural and hydraulic behaviour of the device, it was necessary to increase the performance of the conversion process of the potential energy to mechanic energy and therefore to electric energy. Thus, the study of Bakke (2008) focused on the turbine design, turbine control equipment, measuring and monitoring requirements, generator type, control system design, and grid connection in order to take better advantage from the turbines.

The Company WAVEnergy AS developed a new concept of the Multi-Stage Turbine to equip SSG structure in order to generate electric energy. It consists in a number of turbines (depending on the number of reservoirs) staged concentrically. The turbines are inside of each other linked to a single and common generator through a common shaft. Figure 53 illustrates a MST of three reservoirs (Margheritini *et al.*, 2009). Afterwards, the Technical University of Munich continued the study of MST in order to improve its performance.

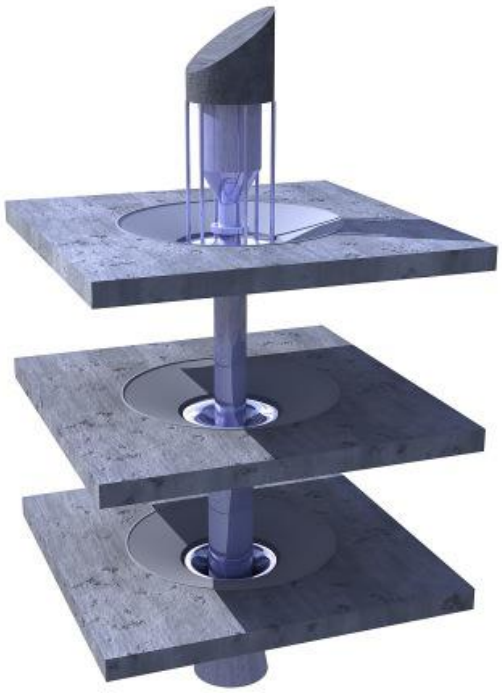

Figure 53 - Multi-Stage Turbine concept (Bakke, 2008)

The project started with the view to be applied on Kvitsøy pilot plant; however the progress took more time that it was anticipated due to some development and design challenges that were difficult to solve. Therefore, an alternative solution with Kaplan turbines was prepared in order to avoid a delay in the construction and installation of SSG. Despite the problem, the studies of MST continued (Bakke, 2008).

MST technology has the advantage of different heights of water head, so the number of start/stop sequences reduces. Also it operates when only one reservoir is capturing and supplying water to the turbine, resulting in a higher efficient rate (Bakke, 2008).

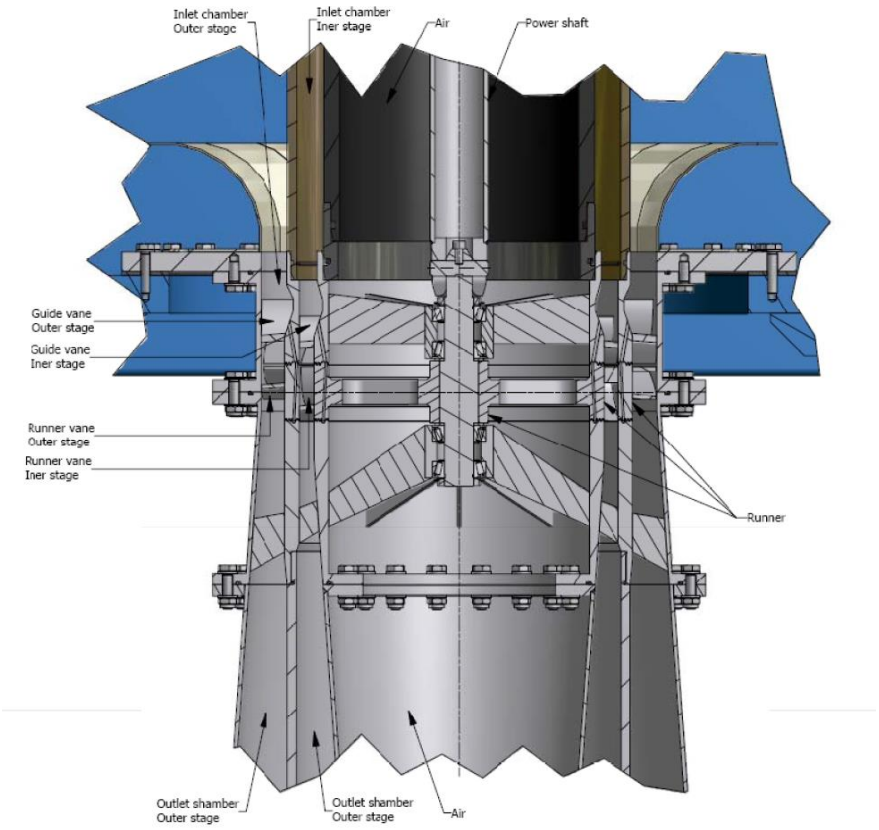

Figure 54 - Multi-Stage Turbine design (Bakke, 2008)

2.7.7. ENVIRONMENTAL IMPACTS

According to Margheritini (2009), a wave energy development is never fully ready due to the lack of understanding of interaction of the devices with the marine environment, as well as lack of coordination between competent Authorities regulation and conflicts of maritime areas utilization. Building a SSG will produce short and long term impacts on water and its aquatic communities. Because WECs are in a first phase, few studies about environment impact assessment (EIA) were carried out.

Most expected impacts for ocean wave energy devices are associated to the establishment and decommissioning phase, like sediment spill, incidents, accidents, oil spill, waste handling, pile driving, laying of mooring blocks, sediment depositing, marine archaeology, navigation hazards and increased shipping activity. However, during operational phase, WECs have influence on the marine mammals, fish, birds, and marine ecology that are necessary to be considered more deeply impacts before being given any judgment, such as behavior changes due to physical presence, noise and vibration, entanglement, entrapment and collision, loss or change of seabed habitat, change in distribution of prey items, change of wave climate or sediment transport leading to changes habitats, colonization of structure leading to increased biodiversity, navigation and coastal processes (CETN (1985)).

Therefore, a WEC must be followed by an appropriate monitoring program, both during construction and operation phase, so that data reflects the actual impacts and replace the previous ones (Kvitsøy, 2008). According to the author, five parameters for a preliminary EIA of WEC's can be recognized and classified:

- Distance of the installation to the shore – *D*;
- Kind of element used for stabilizing the device – *S*;
- Relative water column obstruction (vertical) caused by the presence of the device – *z/d*;
- Relative horizontal obstruction of a wave energy farm – *w/a*;
- The kind power take-off utilized in the installation – *P*.

For a SSG technology, environmental impacts have influence on local community, on coastal processing and coastal species, on geology, geomorphology and archaeology, on benthic habitats, on water column spices, and noise disturbance.

Margheritini *et al.* (2012a) classified devices built onshore as having major impacts on local community. However, the foreseen SSG pilot in Island of Kvitsøy, Norway, has benefited of the positive public acceptance, probably due to the projected demonstration center/museum that would bring tourist to the island. The visual impact could be contoured by applying natural rocks on the side of the concrete device to make it blend with the surroundings.

When a SSG is built in a breakwater of a harbor, the device will cause the same impact nearshore as a breakwater without a SSG installation would provoke, as the transport of sediments. For that question, it is an issue of coastal protection structures. However, the water quality in a harbor is improved as the outlet of water turbines on the leeside of the protection, is considered a positive effect.

The local seabed of the SSG installation has to be prepared to the construction. If the seabed is sandy, a gravel bed must be positioned previously, if it is rocky, the installation phase will consequently permanently partially degrade the morphology of interested area.

While the device is built, the natural conditions are disturbed and it is highly possible to cause the death of part of the benthic communities. Still, during operation phase, the structure offers new habitats and it becomes the "natural environment". In two years it is expected the repopulation from SSG device.

Fish and mammals are subject to lower distress than benthonic communities. Only during installation phase, they leave the area and come back within a short time. Therefore, the overall impact is considered negligible (Margheritini *et al.*, 2012a).

Another impact on marine life is the underwater noise. Piling and drilling during installation of a SSG technology can cause death or permanent damage to the fauna. In the meantime, Dr Jeremy Nedwell is researching and validating rates for this effect (Margheritini, 2009).

Summing up, only a limited number of issues concern the installation of the SSG device. The most impacted effects are the coastal processes in case of breakwater application, geology and coastal spices in relation to noise disturbance during installation.

3
NUMERICAL MODELLING

3.1. INTRODUCTION

Modelling is a useful tool used by researchers and engineers in the analysis of complex problems and in the design process. A model similar to the reality, but correctly simplifying some issues, is used in order to analyze, understand and solve real physical problems. The "solving process" is usually composed of physical/empirical modelling and theoretical/analytical modelling. The first part is carried out in laboratory and/or *in situ* where physical models are tested and results provide the required information to elaborate empirical and semi-empirical algorithms (CFLH, 2008).

The application/development of the theoretical models is composed of four main steps. The construction of a mathematical model for the corresponding physical problems with appropriate assumptions is the first step, which may take the form of differential or algebraic equations. Nevertheless, most of the engineering cases require a numerical solution because they cannot be solved analytically. Therefore, the second phase consists in the development of an appropriate numerical model or approximation to the mathematical model. It needs to be calibrated and validated against pre-existing data and analytical results, also considering an error analysis of the numerical model results. The implementation of the numerical model to obtain results for different test conditions only occurs in the third step. Finally, the fourth phase involves interpretation of graphics, charts, tables, or other ways capable to help and support engineering design and operation.

Nowadays, a wide diversity of numerical models is available and may be used by researches and engineers to allow obtaining results more easily and quickly, even when a large number of variables are considered. In this thesis, two different numerical models are applied: one to optimize the SSG geometry (WOPSim, v3.11) and the other one to simulate the complex interaction between incoming waves and a SSG structure (IHFOAM v2.1.1).

3.2. NAVIER-STOKES EQUATIONS METHODS

Numerical models based on Reynolds Average Navier-Stokes Equations Methods can nowadays be applied to solve many coastal engineering problems, namely to study the interaction between waves and breakwaters. The use of such models is especially important when viscous effects of boundary layer separation, turbulence, wave breaking and overtopping are important for the prediction of the hydrodynamic response of the structure, because other approaches, such as the potential flow methods cannot treat them directly (Li and Yu, 2012).

The Computational Fluid Dynamics (CFD) numerical models are commonly used in several fields (mechanical, aerospace, among others) and are becoming progressively more usual in the coastal engineering domain. Specific issues related with the wave induced flow are already successfully implemented in some numerical codes, namely in what concerns wave generation, wave absorption and porous media (*e.g.* IHFOAM, OpenFOAM, IH2VOF, IH3VOF).

Lara (2012) presents the following reasons to support the use of Reynolds Average Navier-Stokes models in Coastal Engineering:

- The number of underlying assumptions is quite low in comparison with other approaches;
- Non-linear flow characteristics are considered during wave transformation;
- Wave dispersion is intrinsically included in the equations;
- Breaking is not triggered artificially;
- Wave induced flows are solved in the vertical;
- Wave-induced turbulence can be considered.

There is also a huge potential to find new insights into physical process involved that due to their complexity, are commonly studied with simplified models. However, the computational cost of these models is still high, making the handling of large physical domains for long periods of time difficult or even impossible. The situation gets worse when dealing with problems with complex geometries.

The numerical model used to study the hydrodynamic behavior of the Sea-wave Slot-cone Generator is only presented in section 4.4.; however, this section briefly introduces the theoretical background of CFD code for solving three-dimensional (3D) fluid flow problems.

Briefly, the CFD principle consists of replacing the continuous problem domain by a discrete domain using a grid. Each flow variable is then only defined at the grid points, *i.e.* in the CFD, the relevant flow variables are only resolved at the grid points, being the values at other locations obtained by interpolation. The domain discretization may be done using finite-difference, finite-element or finite-volume methods. Most commercial CFD numerical codes use the last two methods because they are more appropriate for modelling flow past complex geometries (Juarez, 2014).

IHFOAM, developed by University of Cantabria, uses the finite volume discretization method. In this approach, the integral form of the conservation equations (mass, energy or momentum) is applied to the control volume defined by a cell to obtain the discrete equations for that cell. In 3D problems cells are usually hexahedra, tetrahedral or prims. When using a CFD code it is important to bear in mind that the code is finding a solution such that mass, momentum, energy or any other relevant quantities are being conserved in each cell. For instance, the conservation equation of incompressible flow reduces to,

$$\int_S \vec{V}.\hat{n}\ dS = 0 \tag{25}$$

where the integration is over the surface S of the control volume V with $\hat{n}$ for outward normal at the surface (Juarez, 2014).

The discrete equations mentioned above are applied to the cells inside the domain. For cells near or at the boundaries, a combination of discrete equations and boundary conditions must be used. CFD numerical codes present a variety of boundary conditions, such as velocity inlet, pressure inlet, among

others. At the end, a system of simultaneous algebraic equations is obtained, being the number of equations equal to the number of independent discrete variables. It is worth mentioning that a usual CFD application may have to deal with thousands to millions of unknowns in such discrete system, being necessary an iterative procedure: the longer one iterates, the closed one gets to the true solution.

The discretization of the equations introduces a truncation error that is directly proportional to the cell size, *i.e.* the numerical error decreases as the number of cells increases. When the numerical solutions, if correct, become independent of the grid as the cell size is reduced, within a level of tolerance specified by the user, they are referred to as "grid converged" solutions.

Iterative procedures are also used to deal with the non-linear terms of the conservation equations (*e.g.* the convection term in the momentum conservation equation) and to invert the matrix associated to the system of algebraic equations that represents the problem in analysis, due to its dimension, in order to reduce memory requirements. Therefore, for each iteration an approximate solution for the matrix inversion is obtained. The iterative process continues until some representative selected measure of the differences between iteratively obtained values, referred to as the residual, is small enough. It is important to stress that a converged solution may not agree well with the exact solution if truncation errors are relatively high. It is a waste of computational resources defining values too small for the residuals when a coarse discretization of the domain is used.

In those iterative procedures, convergence may be reached more or less slowly depending on the complexity of the problem and, in some situations, even divergence may occur. A numerical method is considered stable when the iterative process converges and unstable when it diverges. It is not possible to carry out an exact stability analysis for the Euler or Navier-Stokes equations. A common approach used in CFD codes for steady problems consists in solving the unsteady equations and to progress in time until the solution converges to steady state. In this time-marching to a steady state, and because the interest is only in obtaining accurately the asymptotic behavior at large times, the larger the time-step, the better (the steady state is reached in the least number of time-steps). However, there is usually a maximum allowable time-step beyond which the numerical scheme is unstable. In fact, if the time-step is too high numerical errors will grow exponentially in time causing the solution to diverge. The maximum allowable time-step depends on the numerical discretization scheme used. (Juarez, 2014)

The Courant-Friedrichs-Lewy (CFL) conditions is necessary for ensuring convergence while solving certain partial differential equations numerically, and appears in the numerical analyses of explicit time integration schemes, when these are used for the numerical solution. The CFL condition imposes a severe limitation on the maximum time-step and may be described by the Courant number, which may take the form,

$$c = \frac{v\,\Delta t}{\Delta x} \tag{26}$$

where v represents the flow velocity, Δt the time-step and Δx the cell size. The maximum allowable Courant number is problem dependent. CFD codes, as IHFOAM of OpenFOAM, allow the user to define the Courant number when using adjustable time-stepping. As mentioned before, using larger time-steps leads to a faster convergence to a steady state, within the limits of stability, consequently it is advantageous to set the Courant number as larger as possible (Juarez, 2014).

There are two very different flows states that are easily identified and distinguished: laminar and turbulent flow. Laminar flows are characterized by smoothly varying velocity fields in space and time in which individual "laminae" (sheets) move past one another without generating cross currents. Those

flows arise when the fluid viscosity is sufficiently large to damp out ant perturbations to the flow that may occur due to boundary imperfections or other irregularities. These flows only occur when Reynolds number adopts low-to-moderate values. On the other hand, turbulent floes are characterized by large, nearly random fluctuations in velocity and pressure in both space and time. These fluctuations arise from instabilities that grow until non-linear interactions cause them to break the action of viscosity. Turbulent flows occur in the opposite limit of high Reynolds numbers (Juarez, 2014).

The equations governing a turbulent flow are the same as for a laminar flow; however, the solution is much more complicated when this regime occurs. The approaches to solve the flow equations for a turbulent flow field are divided into two classes: Direct Numerical Simulation (DNS), which numerically integrate the Navier Stokes Equations, resolving all of the spatial and temporal fluctuations, without resorting to modelling. In essence, it is the same solution procedure as for laminar flow, except that the numeric must contend with resolving all of the fluctuations in the velocity and pressure fields. The disadvantage of DNS is that remains limited to simple geometries (*e.g.* channel flows, jets and boundary layers) and is extremely expensive to run. CFD codes usually solve the Reynolds Average Navier-Stokes (RANS) equations.

The averaging concept for the Navier-Stokes equations proposed by Osborne Reynolds significantly reduces the complexity of simulating turbulent flows, which is perhaps the most challenging area in fluid dynamics. The resulting Reynolds-Averaged Navier-Stokes (RANS) equations are formulated in terms of the (time-) averaged variables. Because those variables vary smoothly in space and in time, RANS equations become more amenable to computational fluid dynamics, but an additional Reynolds stress tensor appears as a result of the nonlinear terms of the original Navier-Stokes equations. These terms are unknown and therefore the equations are not closed: there are more unknown terms than equations. RANS turbulence modelling intends to close those equations and to provide a link between the mean velocity field and Reynolds stresses. IHFOAM and OpenFOAM support several turbulence models such as $k-\varepsilon$, $k-\omega$ SST and LES.

The Volume Of Fluid (VOF) method is a free-surface modelling technique for tracking the free surface (or fluid-fluid interface) often used in CFD. It is worth mentioning that the Navier-Stokes equations describing the flow motion have to be solved separately. This method is based in a so-called fraction function C, defined as the integral of fluid's characteristics function in the control volume (volume of a grid cell): when the cell is empty with no traced fluid inside, the value of C is zero; when the cell is full, C is equal to one; and when the interface cuts the cell, then C is between zero and one (Figure 55).

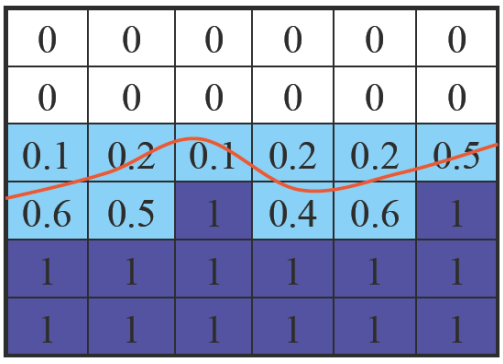

Figure 55 - Rate of water presence into a cell of the mesh (Lara, 2012)

3.3. DESCRIPTION OF THE NUMERICAL MODELS

3.3.1. SOFTWARE WOPSIM

WOPSim is an acronym for Wave Overtopping Power Simulation. This software was developed by the Aalborg University, Denmark, and aims at optimizing the geometry of overtopping based wave energy converters, such as the SSG or the Wave Dragon (Bogarino *et al.*, 2007), as well as the turbines operation strategy, by simulating the times series of overtopping flow into the WEC reservoirs and the energy produced by the turbines. This software can simulate a SSG device with N_{res} reservoirs, each one with its independent turbine setup, by inputting the various parameters that characterize the device geometry, the sea state conditions and the operation strategy.

The geometric parameters for each reservoir (SSG can have one or more reservoirs) are:

- Crest level – Rc;
- Freespace – f;
- Head – h;
- Draft – d_r;
- Length – L;
- Width – W.

Figure 56 helps to understand the meaning of the parameters that describe the SSG geometry. The crest level is the vertical distance between the Mean Water Level (MWL) and the highest point of the ramp, before the entrance to the correspondent reservoir. Freespace is the vertical distance between the entrance level and the water surface within the reservoir. The head represents the height between the water surface within the reservoir and the MWL. The draft corresponds to the distance between the MWL and the end of the overtopping slope.

The wave conditions are defined by:

- Peak wave period – T_p;
- Significant wave height – H_s;
- Probability of occurrence;
- Number of waves generated;
- Sea water level.

Figure 57 presents a print screen of the software WOPSim that shows the main parameters required to carry out a simulation, namely:

- computational settings;
- reservoir dimension;
- turbine characteristics;
- sea state characteristics.

WOPSim calculates the flow per meter of wave crest that overtop the crest freeboard using Equation (27), developed by Kofoed (2005b), for significant wave height H_s. This overtopping model is based on experimental data and is considered a reference for single level devices. Some authors, like Bogarino *et al.* (2007), called it as “reference single level” model.

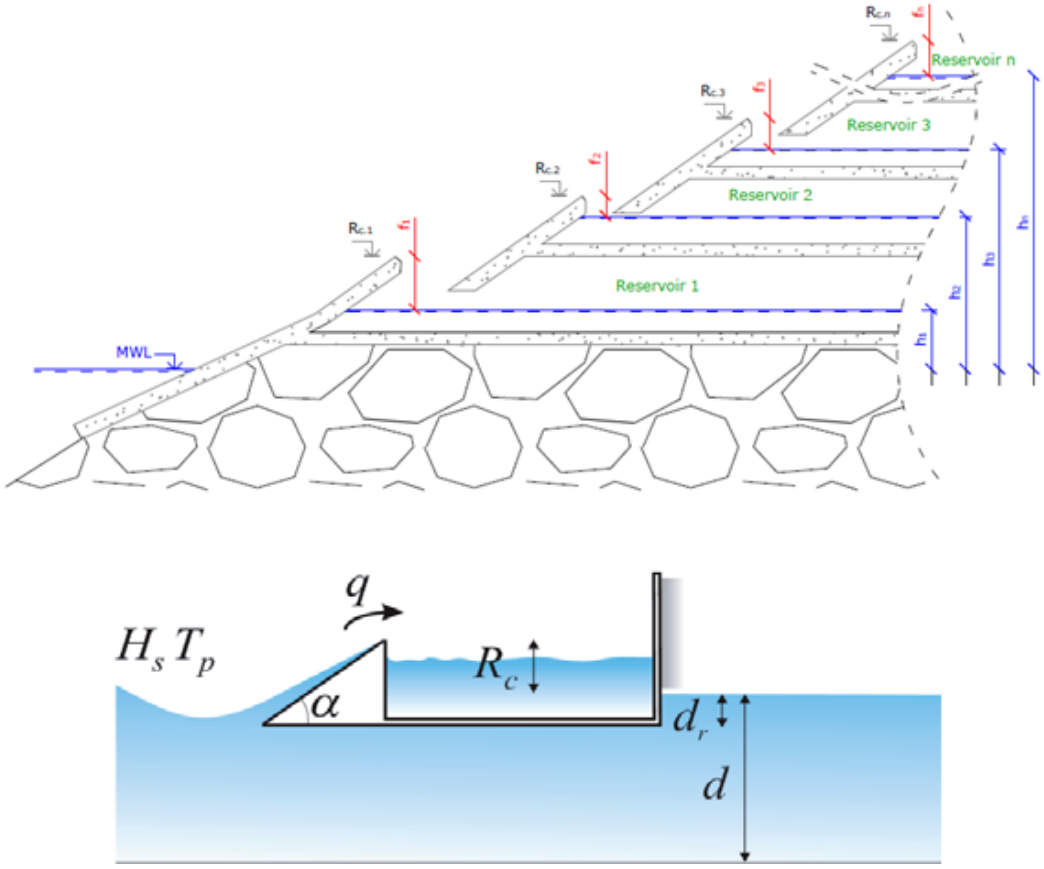

Figure 56 - SSG profile with geometric parameters (Bogarino *et al.*, 2007)

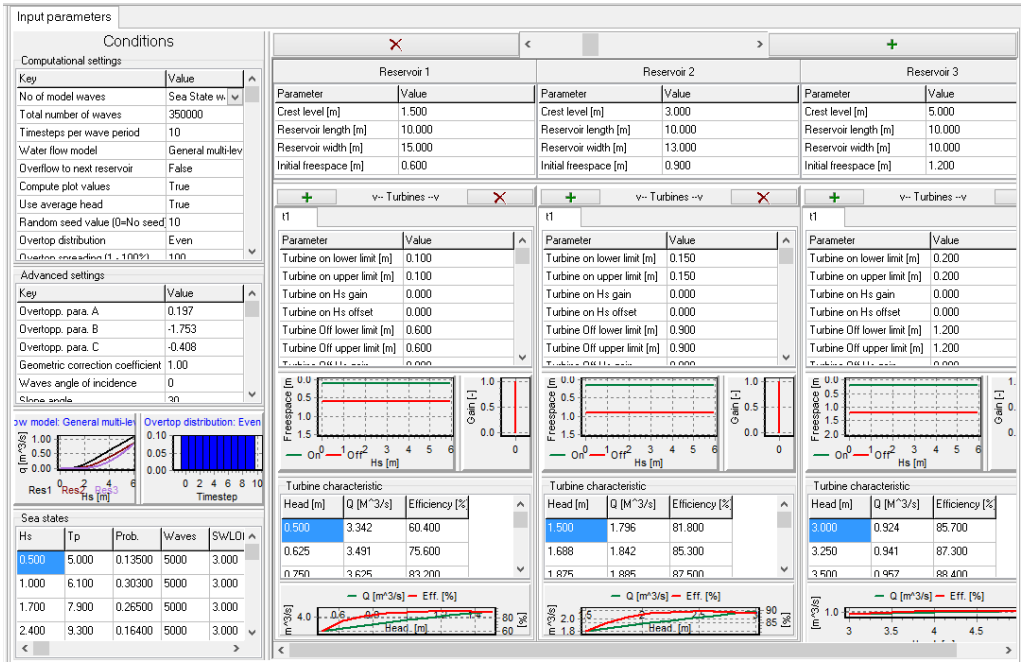

Figure 57 - Print screen of the software WOPSim

$$Q = \frac{q}{\lambda_\alpha \lambda_{dr} \lambda_s \sqrt{g H_s^3}} = A e^{C \frac{R_c}{H_s} \frac{1}{\gamma_r \gamma_b \gamma_h \gamma_\beta}} \quad (27)$$

A SSG device with three reservoirs was considered.

For non-breaking waves, Kofoed (2002) defines empirical constants A = 0.2 and C = -2.1. The coefficients γ express the influence of index parameters *r*, *b*, *h* and *β* that characterize the structure, respectively, the shallow foreshore, the berm, the roughness and the angle of wave attack. All these coefficients were considered equal to one, except the last one, that is calculated based on the angle of wave attack (in degrees), *β*, by,

$$\gamma_\beta = 1 - 0.0033\beta \quad (28)$$

The average overtopping discharge is slightly influenced by the slope angle α of the frontal ramp where the wave run-up occurs. The parameter λ_α allows taking that influence into account and is calculated by,

$$\lambda_\alpha = \cos(\alpha - \alpha_m)^3 \quad (29)$$

where α_m=30º is the optimal slope angle.

When the SSG ramp is not extending to the seabed, some energy passes under the device or may eventually be reflected back. In order to include that loss of energy, the parameter λ_{dr} is included in the overtopping formula. This parameter is calculated by,

$$\lambda_{dr} = 1 - k \frac{\sinh\left(2k_p d\left(1-\frac{d_r}{d}\right)\right) + 2k_p d\left(1-\frac{d_r}{d}\right)}{\sinh(2k_p d) + 2k_p d} \quad (30)$$

where k_p is the peak wave number and k is a constant equal to 0.41.

The coefficient λ_s appears after a comparison between the results of Kofoed (2002) and Van der Meer and Jansen (1995), and intends to extend their formulation to a larger range of experimental data, being determined by,

$$\lambda_s = \begin{cases} 0.4\sin\left(\frac{2\pi}{3}R\right) + 0.6 & if\ R < 0.75 \\ 1 & if\ R \geq 0.75 \end{cases} \quad (31)$$

where R represents the dimensionless crest level parameter (R_c/H_s).

The WOPSim program is based on the continuity equation (Equation 32), to ensure that the input and output water flows are the same,

$$Q_{in} + Q_{upper,over} = Q_{over} + Q_{turb} + Q_{res} \quad (32)$$

where Q_{in} (as $q_{ov,j}$), total overtopping flow rate to the j-reservoir, $Q_{upper,over}$ is the spillage from the above reservoir if it is full, Q_{over} is the overflow if the reservoir is full, Q_{tur} is the flow that passes through the turbines and Q_{res} is the flow in the reservoir.

The overtopping flow for each wave is calculated by a random process composed of two steps (Franco *et al.*, 1994, and Van der Meer and Jansen, 1995). The first one is the calculation of the probability that a wave does not overtops the crest of the reservoir P_{ov}, which is given by,

$$P_{ov} = e^{-\left(c\frac{H_s}{R_c}\right)^{-2}} \quad (33)$$

where c is a constant equal to 1.21.

The overtopping flow is bigger if that probability is low. The second step is the calculation of the overtopping flow according to the previous probability and the mean water flow into the reservoir. Hence, WOPSim calculates the overtopping flow into each reservoir by,

$$q_{in} = 0.84\frac{q}{P_{ov}}(-\ln(1-p_w))^{0.75} \quad (34)$$

where q is the average flow calculated by the previous formulas and p_w is a random number.

Based on additional experimental results, the overtopping formula presented in Equation (24) has been updated to allow the consideration of more reservoirs on the top of each other (Kofoed, 2002). The overtopping flow for each reservoir can be estimated by,

$$q_n(z_1, z_2) = \sqrt{gH_s^3}\frac{A}{B}e^{C\frac{R_{c,1}}{H_s}}\cdot\left(e^{B\frac{z_2}{H_s}} - e^{B\frac{z_1}{H_s}}\right) \quad (35)$$

where g is the gravity acceleration, H_s the significant wave height, and z_1 and z_2 the lower and upper vertical levels of the reservoir, respectively, *i.e.* $z_1 = R_{c,n}$ and $z_2 = R_{c,n+1}$. For the uppermost reservoir, theoretically the upper boundary is infinite, however, the software uses twice the lower boundary, *i.e.* $z_2 = 2.z_1$.

For a SSG device with three reservoirs, Kofoed (2005a), Allsop *et al.* (2005), Bogarino *et al.* (2007) and Vicinanza *et al.* (2012) recommend the use of Equation (35), with A = 0.197, B = -1.753, and C = -0.408. The values of these constants were determined by non-linear regression analysis.

Because the previous overtopping model is quite general it was named "general multi-level" flow model. Later, additional experimental work with a specific SSG geometry (reservoirs with crest levels at 1.5, 3.0 and 5.0 m, above the mean sea level) allowed defining a more accurate overtopping model, which cannot be synthetized as a formula, but that was directly included in the WOPSim software (Kofoed, 2005a). The Figure 58 compares the old and the new (case specific) flow model.

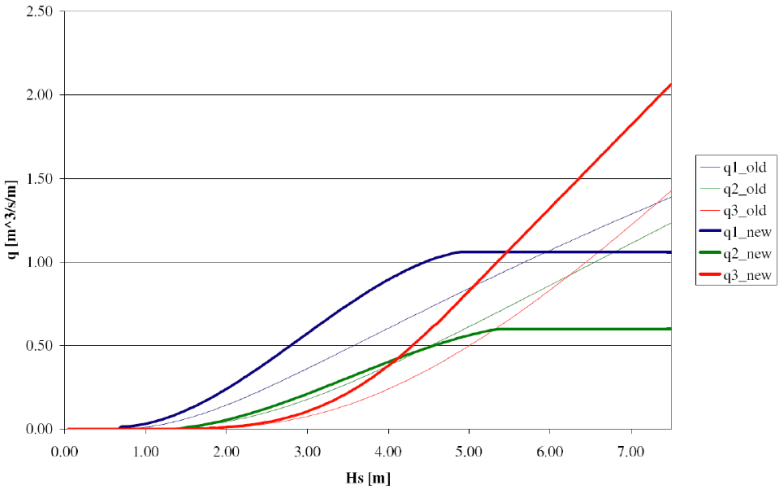

Figure 58 – Comparison of experimental data from Kofoed (April 2005) and Kofoed (June 2005) (Bogarino *et al.*, 2007)

WOPSim simulates the operation of turbines based on the defined operation strategies and the turbine characteristics. Turbines are characterized by the relationship between head, flow and efficiency. Then the software calculates the flow and the efficiency for each given head: the head varies in time because the water level goes down when water passes through the turbine and it goes up when water enters in the reservoirs due to wave overtopping. For simplification, the flow is calculated for an initial head or for an estimated average head. The higher the gradient of the turbine characteristic, the larger the error of the simplification is. So, to minimize this error, the user can specify a certain number of time steps to divide the wave period.

After, when the SSG geometry is defined (including reservoirs crest levels), the turbine characteristics for each reservoir need to be designated in order to convert the maximum wave energy possible. Another issue that must be considered is the spill out of large waves, that it is a loss of energy. This process will always happen, and oversizing turbines to minimize spill out might not be adequate due to higher costs and very low unjustified load factors.

In addition, the turbine operation strategy (*i.e.*, the turbine starting and stopping instant) is also a very important factor that affects the overall performance. This is a function of the distance between the reservoir crest and the water surface inside the reservoir, called freespace (Figure 56). Margheritini *et al.* (2008) suggest two different load factors for the study of turbine strategies.

After running the simulation with all the parameters set, the output results are:

- Water volume/flow into each reservoir;
- Water volume/flow through each turbine;
- Spillage volume/flow when the reservoirs are full;
- Produced wave energy;
- Average wave power;
- Hydraulic efficiency of wave overtopping into reservoirs;
- Efficiency of the reservoirs;
- Efficiency of the turbines;
- Total efficiency.

In order to compare different SSG geometries for several sea state conditions, efficient results are used. Every calculation of efficiency (whether hydraulic, from the reservoir of the turbines) uses the total available incoming wave energy per second, per meter of wave front, which may be determined by,

$$P_{wave} = \frac{\rho g^2}{64\pi} T_e H_s^2 \tag{36}$$

where the energy period may be estimated by,

$$T_e = \frac{T_p}{1.15} \tag{37}$$

The hydraulic efficiency in terms of overtopping (Eff_{Ov} or η_{in}) only has into account the geometry of the ramp, *i.e.* the potential energy overtopping the reservoir's crests. Therefore, if wave spill back occurs it is not considered.

$$\eta_{in} = \frac{P_{in}}{P_{wave}} \tag{38}$$

where the mean overtopping power in a sea-state is given by,

$$P_{in} = \sum_{j=1}^{N_{res}} Q_{in,j} R_j \rho g \tag{39}$$

The efficiency of reservoirs (storage efficiency) is determined based on the potential energy stored in the reservoirs. This efficiency will be smaller than the hydraulic efficiency, since the energy that overtops the reservoir's crests is higher than the energy that is effectively stored into the reservoirs. In this case, the wave spill back is taken into consideration because energy will be lost if the reservoir is full and the water returns to the sea. The stored efficiency is calculated by,

$$\eta_{res} = \frac{P_{res}}{P_{wave}} \tag{40}$$

where the mean power that may be theoretically converted into electricity by the reservoirs is given by,

$$P_{res} = \sum_{j=1}^{N_{res}} (Q_{in,j} - Q_{over,j}) \bar{h}_j \rho g \tag{41}$$

At least, the power production efficiency takes into account both turbine strategy and the turbine efficiency, and gives the relationship between the power that is effectively transformed into electric energy by the turbines and the incoming wave power. It is expected that this efficiency will be smaller than the others due to the start/stop cycles penalties and the turbine efficiency,

$$\eta_{turb} = \frac{P_{turb}}{P_{wave}} \tag{42}$$

where the mean power production of the whole SSG device is given by

$$P_{turb} = \sum_{j=1}^{N_{res}} P_{turb,j} \tag{43}$$

The index *j* represents the number of the reservoir and *P* the power of the corresponding index (respectively overtopping, reservoir, and power production).

Despite the use of WOPSim in a SSG device installed onshore, fixed to a structure, this software can also be used to study and optimize floating devices, such as Wave Dragon. To better describe the behavior of a fixed SSG or Wave Dragon, "advanced settings" should be modified in order to adapt the overtopping model to the desired conditions. In the case of a SSG device, those parameters are:

- Overtopping parameters – *A*, *B*, and *C*;
- Geometric correction coefficient – $\lambda_{m;}$
- Angle of wave incidence – β;
- Ramp slope angle – α.

When the values of the crest level of the ramp are given, it is used parameters *A* and *C* to compute the total overtopping flow. For multi-levels devices, parameter *B* is used to calculate the overtopping vertical distribution, depending on the reservoir crest level. Bathymetry, converging walls, and other components that affect the overtopping may be included by the geometric correction coefficient λ_m. When the direction of wave attack is not perpendicular to the SSG front, the parameter β includes this negative effect on the overtopping estimation. WOPSim considers an optimal angle of the ramp equal to 30º. When that ramp is not 30º, the software corrects the overtopping discharge ().

It was compared the relation between the physical model of Oliveira (2014) and the equation developed by Kofoed (2005a). Figure 59 shows graphically that there is a difference between the experimental results and the expected ones from the Equation (35). The physical model presents results with lower values than that were expected by using the equation developed. For lower values of wave height, that difference is not significant, however, as the wave heights increase, the relative error became higher too. The Figure 59 examples the relation of sea states tested by Oliveira (2014) that overtop the first reservoir.

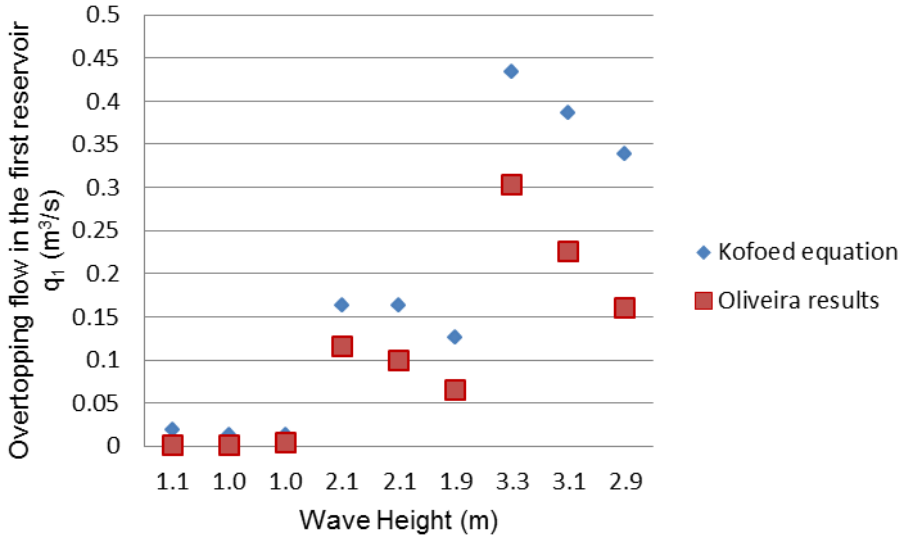

Figure 59 - Comparison of the Oliveira results with the Kofoed expression

3.3.2. SOFTWARE IHFOAM

The IHFOAM 2.1.1 is a two-phase solver numerical model developed at the University of Cantabria, Spain, based in "interFoam" (one of the solvers included in OpenFoam®), that includes additional built-in boundary conditions for wave generation and active wave absorption. The interFoam is used to solve the 3D Reynolds Average Navier-Stokes (RANS) equations for two incompressible phases using a finite volume discretization and the volume of fluid method (VOF).

This kind of discretization allows very complex free surface problems to be represented in a relatively easy way; however, some issues may arise when surface tension effects are important, what is not usually a difficult in the majority of the problems that occur in the coastal engineering domain.

The OpenFOAM® (Open Field Operation And Manipulation) is an open source CFD (Computational Fluid Dynamics) toolbox developed in C++ language. The program solves complex problems (such as turbulence, fluid flows and other problems outside of hydraulic domain), through mesh generation, setting field values, mesh decomposition and data sampling. One OpenFOAM® advantage is the possibility of using third party programs, such as Kitware ParaView, to post processing purposes. Another one is that the code structure is designed in a way to orient programming new solvers (such as IHFOAM), boundary conditions and new applications (Higuera *et al.*, 2013a).

The theoretical bases of IHFOAM are quite complex and consequently will not presented here. The implementation of wave generation and absorption in the model is described in Higuera *et al.* (2013a) and its validation in what concerns the simulation of coastal processes is presented in Higuera *et al.* (2013b). In addition, the simulation of the interaction between waves and porous coastal structures is detailed in Higuera *et al.* (2014a) and Higuera *et al.* (2014b).

The working methodology usually starts with the copy of a case similar to the pretended one. Thus, it is advised to eliminate and modify those files to reach the case under study. The information, for each case, is structured in three directories, which contain the files defining initial conditions, constant values and running procedures. The directory *0* contains files related with the boundaries conditions that will be used along the simulation, such as the VOF function *alpha1*, the dynamic pressure *p_rgh*,

the velocity *U*, the turbulence kinetic intensity *k*, the turbulent dissipation rate *ε*, and the turbulent viscosity *nut*. The directory *constant* has the files that define constants along the simulation, such as the acceleration of gravity *g*, the transport and turbulence properties, the mesh properties, the wave characteristics that are generated. Finally, the directory *system* includes all the files that control the simulation, such as the running time and the writing conditions of the variables calculations, and codes that refine the mesh and other numerical simulation settings and computational schemes. Figure 60 presents an example of case tree (the directories are in italic).

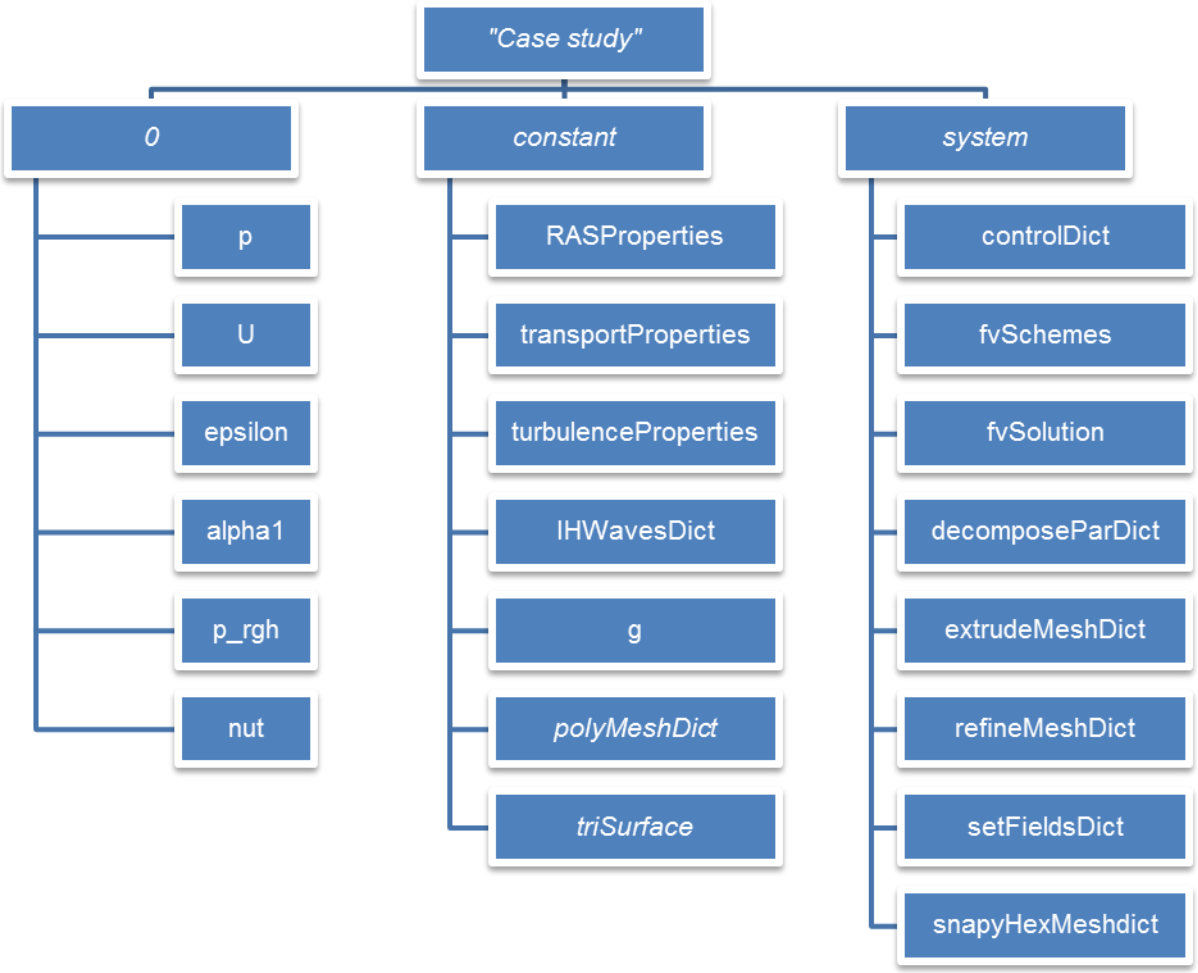

Figure 60 - Initial files of simulations tree in IHFOAM

The directory *polyMeshDict* contains the files that define the mesh characteristics and boundaries, whereas *triSurface* contains the files that define the SSG geometry.

Once done, it is necessary to create the mesh of the model to be simulated. The "interFoam" solver, as well the "ihFoam" solver, handles static meshes (*e.g.*, a Venturi pipe, a dam breaking event, run-up on a beach, etc.). However, there is also "interDyMFoam" and "ihDyMFoam" that handle dynamic meshes (*e.g.* movements of floating bodies or dynamic mesh refinement along the free surface). A check mesh command is available to assess the quality of the mesh and prevent errors that could appear afterwards.

The next step is defining the boundary conditions in terms of wave generation and wave absorption.

Proper wave generation defining is essential to ensure realistic results. The program allows the selection of the pretended wave theory, provided that it is available to read the code, such as the boundary conditions. When the software runs a simulation, the waves are generated following the profile of the wave theory selected. Those wave theories profiles are already predefined and the software calculates its equation, which defines that profile and theory, with the wave parameters inputted. The wave theories available in IHFOAM software are Stokes (first, second and fifth order), cnoidal, and stream function for regular waves, Boussinesq for solitary waves, wavemaker wave type and irregular waves (first and second order). Figure 61 shows the range of applicability of each theory.

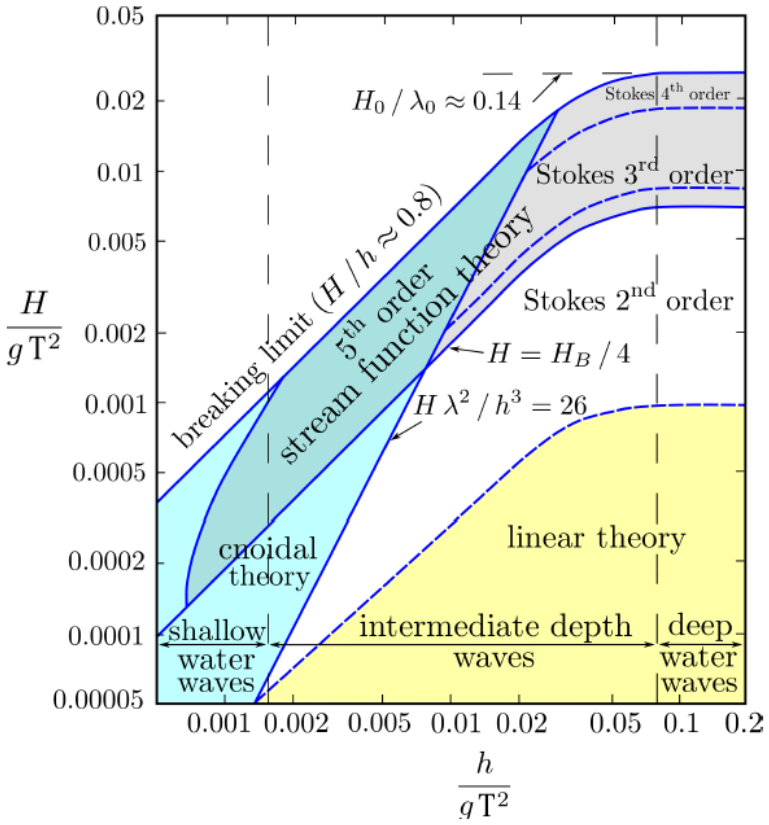

Figure 61 - Range of applicability of wave theories (IHCantabria, 2014)

The use of wave absorption is essential in physical and numerical modeling, of coastal engineering cases. If reflections are not taken into consideration, the results will be disturbed. One method used is based on modifying the wavemaker movement, based on a measured magnitude (feedback), so that it may continue to generate the target wave, while the re-reflection of other incoming waves are prevented. The supported active of wave absorption systems can be 2D, Quasi-3D or 3D (Juarez, 2014).

As mentioned before, the program resolves RANS equations, including continuity and mass conservation. RANS equations are the base mathematical equations which explain the pressure and velocity linking. Also, it is assumed that the fluid is incompressible, once that is the most common situation in coastal engineering practical problems.

The next step is setting the initial conditions. Each variable used in RANS equations must be defined, as the boundaries and the variable value (varying or not) within the range of boundary field. The turbulence properties can be defined as using Laminar, RAS (Reynolds Average Stress) or LES (Large Eddy Simulation) models. The first one is used for laminar flows (small Reynolds number). RAS, also known as Reynolds Averaged Navier-Stokes (RANS) are the governing equations that use ensemble-averaged form solving, including appropriate models for the turbulence effect. LES models are used for the cases of large turbulent structures in the flow, while modelling the effect of the sub-grid scales. By applying a filter on the governing equations, it is obtained the scale separation and it influences the form of SGS (Sub-Grid Scales) models. Therefore, the turbulence model used in IHFOAM simulations was RAS, which reproduces better the interaction between the waves and the structure.

At this point, only the initial conditions of the pretended simulation were defined, so none simulation was run. It is advised to check all the changes done to the initial similar case to avoid errors when running the simulation.

OpenFoam® and IHFOAM allow parallel computing, *i.e.*, to decompose the case study in parts and distribute them, so that all computer processors can run part of the simulation, to make it quicker. After, deciding whether or not using serial or parallel computing, the simulation can be run. If parallel computing is used, finally, the case must be reconstructed in order to compile the simulations results provided by the several processors. Then it is possible to post processing the data using the Kitware ParaView.

Within ParaView (Figure 62), the variation of the initial conditions and any other variable during the simulation time can be visualized, with color scales, such as the view of the block mesh (front and back, right and left sides, and up and down or any other view resulted from rotating). In addition, filters can be used for a better analysis of a specific variable. To understand what happens in the interaction between water and obstacles, it is possible to create a video animation with the successive frames (Appendix D).

The steps to interact with ParaView software are:

- Define “Decomposed Case” and check “List timesteps according to controlDict” in “Object Inspector” (1);
- Click “Apply” button in “Object Inspector” (1);
- Choose the parameter to analyze (2);
- Choose the representation (2);
- Change the colors presented and if necessary the scale (3);
- Play and time/steps controls (4);
- View controls (5);
- Quick access to filters (6).

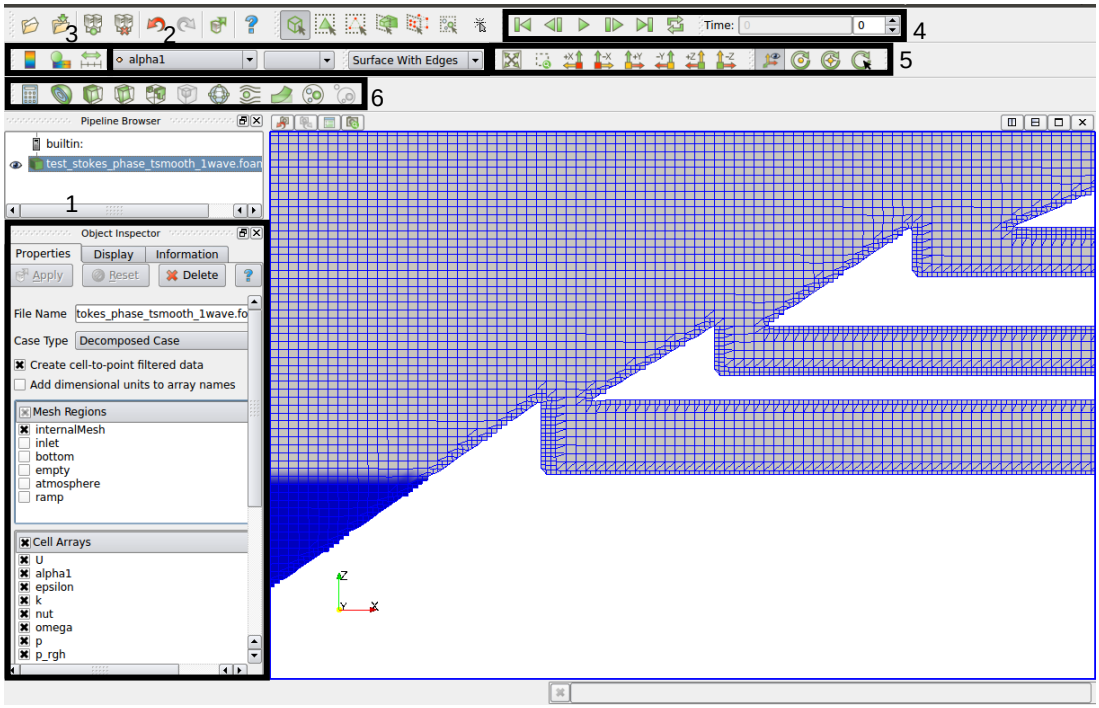

Figure 62 - Print screen of the ParaView window

4
CASE STUDY

4.1. CHARACTERIZATION OF THE CASE STUDY

The case study of this thesis consists in the development and optimization of a SSG device for a breakwater located in the river mouth, Porto, Portugal. Henriques *et al.* (2013) presents the wave characteristics at the site (11 m depth to MWL) that are used in this study. Those characteristics were obtained based on wave data measured offshore in deep water in Figueira da Foz, Portugal (from July 1990 to June 1994) that were then transferred to the hypothetical installation site, using an inverse-ray refraction model, taking into consideration the shoaling effect and the sheltering at the plant site (Henriques *et al.*, 2013). As expected, a decrease of the significant wave height and incident wave power was observed. Contrary, the energy period increased with the reduction of the water depth. This phenomenon was explained by the modifications experienced by the longer waves (longer period) are more strongly modified as waves approach the shoreline. The extreme values of sea state are not significant for the energy conversion (Henriques *et al.*, 2013). Table 3 summarizes the results obtained.

The bathymetry used in the study was an interpolated that from maps published previously by the Portuguese Hydrographic Institute[6] (Henriques *et al.*, 2013). As a consequence of the bathymetry, and as expected too, the mean wave direction rotates and wave crests become parallel to the coastline. The sea bottom characteristics and wind directions were considered in the work of Henriques *et al.* (2013). However, the ocean current effect was not taken into account.

For the tide variable, the predictions for 2014 provided by the Portuguese Hydrographic Institute were used (Table 4). Therefore, the number of occurrence for each 0.1 m tide level variation was counted and represented in ranges of 0.5 m.

Table 4 presents the probability of occurrence of the tide levels. The number of occurrences is defined as the sum of the times that a high or lower tide will be on that interval. The frequency of occurrence is calculated by dividing the number of occurrences by the total. The applicability of this method may be criticized, however it was considered to be appropriate for the purposes of the present study. For the calculations, the mean value for each range of tide levels was used.

The numerical simulations were carried out for a water depth in front of the SSG structure equal to 17 m, in accordance with experimental work carried out by Oliveira (2014).

[6] www.hidrografia.pt

Table 3 - Distribution of annual joint frequency for each class of wave height and wave period, for each 10º directional sector (Henriques *et al.*, 2013)

Direction (ºN)	**Peak Period (s)**	**Wave Height (m)**										**Sum**	**Sum**
		0.75	**1.25**	**1.75**	**2.25**	**2.75**	**3.25**	**3.75**	**4.25**	**4.75**	**5.25**	**(%)**	**(%)**
260	6	1.69	0.97	0.33								2.99	**8.32**
	8	0.91	1.09	0.87	0.83	0.29	0.01					4.00	
	10	0.18	0.19	0.16	0.29	0.24	0.17	0.01				1.24	
	12		0.05	0.01	0.01							0.07	
	14											0.00	
	16	0.01	0.01									0.02	
270	6	3.31	0.38	0.09								3.78	**46.81**
	8	4.84	3.03	1.04	0.54	0.17	0.02					9.64	
	10	3.10	3.83	3.18	1.77	1.00	0.42	0.11	0.01			13.42	
	12	2.09	2.89	3.57	2.28	1.09	0.77	0.33	0.15	0.08	0.03	13.28	
	14	0.28	0.45	1.03	1.04	0.92	0.45	0.39	0.27	0.10	0.04	4.97	
	16	0.04	0.08	0.19	0.30	0.27	0.17	0.11	0.27	0.18	0.11	1.72	
280	6	5.50	0.58									6.08	**44.11**
	8	10.01	5.84	1.78	0.12							17.75	
	10	3.60	4.21	2.75	1.50	0.39	0.07	0.01				12.53	
	12	0.60	1.35	1.31	1.02	0.53	0.22	0.11	0.11			5.25	
	14	0.07	0.20	0.45	0.43	0.34	0.20	0.18	0.15	0.06	0.03	2.11	
	16		0.01	0.05	0.07	0.03	0.03	0.11	0.03		0.06	0.39	
290	6	0.43	0.28									0.71	**0.76**
	8	0.02	0.03									0.05	
	10											0.00	
	12											0.00	
	14											0.00	
	16											0.00	
Sum (%)		**36.68**	**25.47**	**16.81**	**10.20**	**5.27**	**2.53**	**1.36**	**0.99**	**0.42**	**0.27**	**100.00**	**100**

Table 4 - Tides frequency

Tide range (m)	Tide mean value (m)	Number of occurrences (–)	Frequency (%)
] 0 ; 0.5]	0.25	124	8.79
] 0.5 ; 1.0]	0.75	356	25.25
] 1.0 ; 1.5]	1.25	224	15.89
] 1.5 ; 2.0]	1.75	1	0.07
] 2.0 ; 2.5]	2.25	16	1.13
] 2.5 ; 3.0]	2.75	285	20.21
] 3.0 ; 3.5]	3.25	327	23.19
] 3.5 ; 4.0]	3.75	77	5.46
Total		**1410**	**100**

4.2. OPTIMIZATION OF SSG

The first goal of this research work was to define an optimized geometry for a SSG device to be installed in the case study to the Portuguese west coast previously described, having into account the local conditions, namely the wave conditions and tide regime. Then, with the optimized geometry, a better estimation of the energy production could be obtained.

As a starting point, the same geometry described by Oliveira (2014) was used. Hence the initial SSG geometry had three reservoirs, with the following crest levels: R_{c1} = 1.5 m, R_{c2} = 3 m and R_{c3} = 5 m. The front openings were 10 m wide. The lowest reservoir had a length of 24.8 m, the middle one 21 m and the highest reservoir had 17.4 m length. The front angles were 35º and the horizontal distance between reservoirs was 1.2 m. The structure crest level was 15 m in relation to the SWL (Sea Water Level).

Then, the procedure was to input the representative sea states from the Portuguese case study and simulate then with the software WOPSim (section 3.3.1.). The parameters necessary to characterize the sea states are: significant wave heights, peak wave periods, probability of occurrence, number of waves, and associated sea level. There are two additional input parameters that are not directly related to the characterization of the sea states, but are required to define the geometry of the SSG device and have an important influence on wave run-up and overtopping. Those parameters are the slope angle of the SSG ramp and the angle of incoming waves in relation to the SSG. The Appendix A presents an example of one of the simulations carried out with WOPSim.

Afterwards, one by one, each parameter was changed while all the others were maintained constant, in order to establish the values that result in better hydraulic efficiencies, considering only the influence of that parameter. The combination of wave height and wave period used in this stage was that higher probability of occurrence (third quartile). Therefore, the most representative sea states were considered to simplify the analysis as well as to reduce the number and the duration of the simulations. The variation of tide level and the angle of wave incident on the SSG were also considered. Following this, the differences on the hydraulics efficiency, according to the parameters variation was analyzed.

The first SSG geometry parameter analyzed was the number of reservoirs. For that, the wave heights and tide amplitudes were taken into consideration. Since the probability of occurrence of small wave heights is greater than that of high wave heights (Table 3), it was necessary to considerer a reservoir at a low level, to take advantage of the power transported by those small waves. Figures 63 and 64 show the relationship between the hydraulic efficiency and the wave height, respectively, for long and short wave periods, *i.e.*, for the lower (1.5 to 10 s) and higher (6 to 14 s) values of wave period. It is possible to observe that the simulated SSG device has better performances for waves with 3 m of wave height.

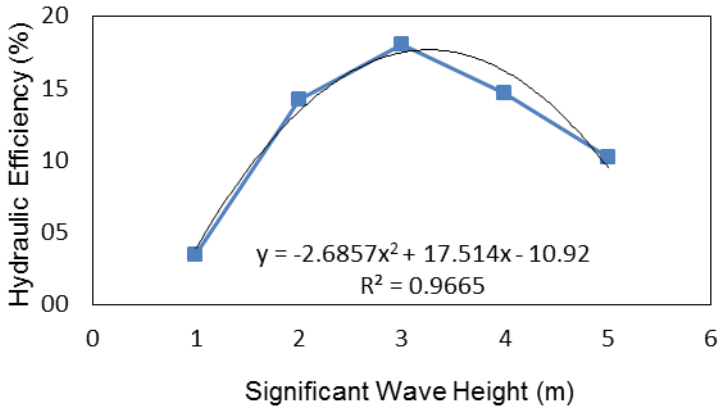

Figure 63 - Hydraulic efficiency vs wave height for long wave periods

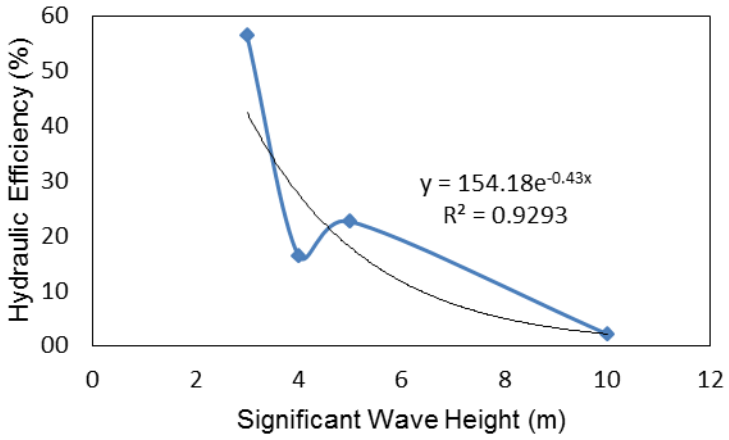

Figure 64 - Hydraulic efficiency vs wave height for short wave periods

In addition, the number of reservoirs was increased from the initial geometry (with three reservoirs) because the Portuguese west coast may have tides with a peak-to-peak amplitude range of nearly 4 m. Other works and studies carried out for the North Sea conditions, where tidal range is around 0.5 m, and the study of Oliveira (2014), did not considered the tide variation. The use of three reservoirs may not be appropriated under typical conditions of Portuguese west coast. Joining both the sea state and tide characteristics, it was concluded that it is necessary to install reservoirs at low and high levels, to capture waves (all the range of wave heights) during low tide and the lowest wave heights during high tides, respectively. Concluding, the new geometry of SSG has five crest levels, being R_{c1} = 1 m, R_{c2} = 1.5 m, R_{c3} = 2 m, R_{c4} = 3 m and R_{c5} = 4 m.

The second parameter analyzed was the wave crest angle, considered null for the direction of 270ºN. Since the difference between the most two probable directions (270ºN and 280ºN) is 0.65% (not significant in terms of hydraulics efficiency), it was necessary to considerer other directions. Due to the highest probability of occurrence of the 260ºN wave direction than 290ºN (last column of Table 3), there will be more waves with a lower angle of incident, providing more energy available, if the direction 270ºN is considered as reference.

The front ramp angle influences the wave breaking parameter and, consequently, the wave run-up and the energy captured in the reservoirs. Therefore, several angles were simulated in order to obtain the best values in terms of performance. Following Figure 65, for ramp angles between 25º and 35º, the hydraulic efficiency does not vary significantly. However, there is a hydraulic efficiency peak of 23.7% for an angle of 30º. This was not unexpected since, according to the formulations that are the basis of WOPSim simulations, the optimal ramp angle is 30%. Those formulations were obtained from experimental data.

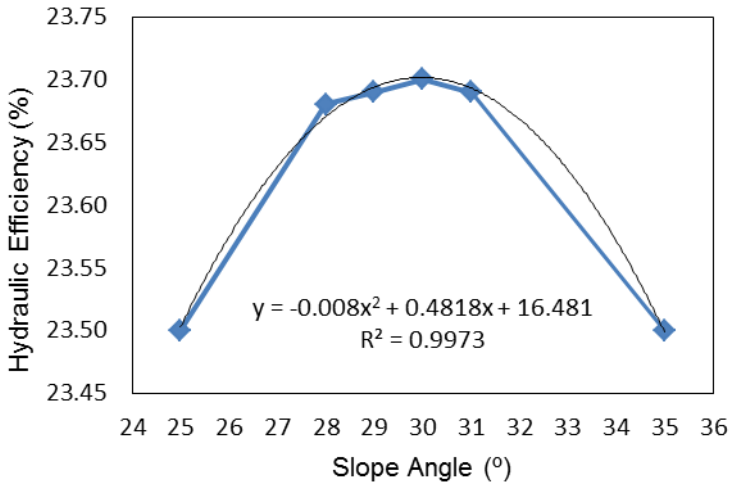

Figure 65 - Hydraulic efficiency according ramp angle of SSG

The dimensions of the reservoirs were also improved. For a fixed width, the reservoirs length was changed and the repercussions in term of efficiency analyzed, Table 5.

Table 5 - Hydraulic efficiency according to the length of the SSG (m)

Length (m)	η (%)	Efficiency difference
5.0	14.1	-
10.0	16.0	1.9
15.0	16.9	0.9
20.0	17.5	0.6
25.0	17.8	0.3
30.0	18.1	0.3

Table 5 shows that the hydraulic efficiency η increases with the reservoirs length, however, it tends to stabilize. Therefore, the reservoirs length was fixed in 20 m due to the small difference of efficiency from the latest range (half of hydraulic efficiency loss). It is worth mentioning that other constrains may limit the maximum length of the reservoirs. In addition, larger reservoirs correspond to bigger and more expensive SSG structures.

Regarding reservoirs width, the selection process focused on a solution with a reduction of hydraulic relatively small. When the width increases, the efficiency tends to decrease because the program performs the calculations per meter of width. Table 6 shows that the hydraulic efficiency tends to stabilize for reservoirs widths higher than 15 m. Therefore, 15 m was chosen as the capture width at the entrance of SSG reservoirs.

Table 6 - Hydraulic efficiency according to the width of the SSG (m)

Width (m)	η (%)	Efficiency difference (%)
5.0	26	-
10.0	20.8	-5.2
15.0	17.8	-3.0
20.0	15.2	-2.6
25.0	13.4	-1.8
30.0	12	-1.4

After the simulations, a SSG geometry, optimized for conditions typical of the Portuguese west coast, was developed, namely for the river Douro mouth. Two additional reservoirs were included, and the crest levels of the others were changed. The crest levels of the reservoirs in the developed geometry are: R_{c1} = 1 m, R_{c2} = 1.5 m, R_{c3} = 2 m, R_{c4} = 3 m, and R_{c5} = 4 m. Each reservoir is 20 m long and 15 m wide. The ramp front angle is 30º and the horizontal distance between reservoirs was maintained equal. Figure 66 shows the SSG geometry optimized for the conditions of the Portuguese coast.

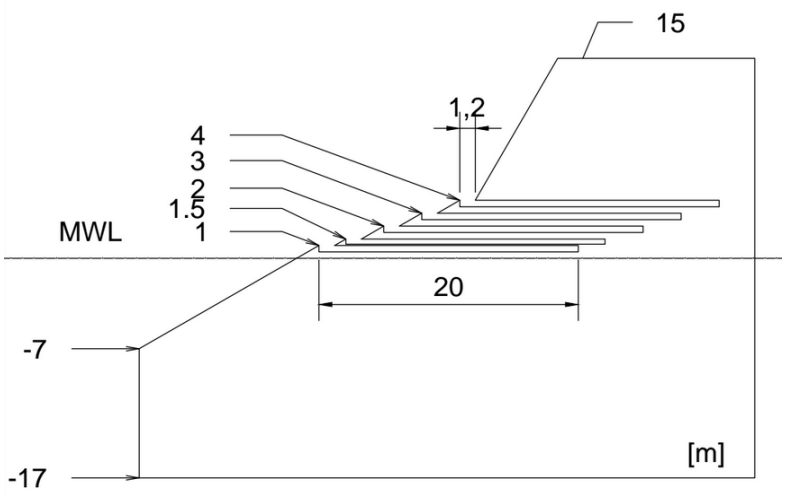

Figure 66 - Profile of the optimized SSG geometry

4.3. EXPECTED ENERGY PRODUCTION

As the WOPSim version used cannot simulate several sea states at the same time (maximum number of sea states is seven), it was necessary to develop a methodology to combine:

- wave heights;
- wave periods;
- tidal variation;
- angle of attack;
- probability of occurrence of each parameter.

For each case, the sum of the probabilities of the set of sea states simulated, was naturally, equal to 100%.

Each set of sea states corresponded to one line of Table 3, but with the normalized values of probability. Therefore, the values of probability corresponding to all the sea states simulated in one WOPSim run were adapted in order to totalize 100% probability (Table A 1). A weighted average was carried out at the end, as explained bellow. Also, each simulation was repeated for the mean value of the tidal ranges (tide value of Table 4).

After the simulation of all the sea states (line by line of Table A 1), the values were multiplied by the probability of occurrence of each sea state in the overall sea state probability (Table 3). After, the values of the hydraulic efficiency, flows and produced power of each simulation were multiplied by the probability of occurrence of the tide levels (Table 4). Ultimately, those values were multiplied by the probability of occurrence of each wave direction. Table 7 presents the global efficiency of each reservoir and the sum of all.

Table 7 - Reservoir Efficiencies

Res No.	Overtopping Efficiency (%)	Reservoirs Efficiency (%)
1	13.9	9.1
2	15.2	12.1
3	9.7	10.8
4	14.5	7.7
5	16.6	9.9
Sum	**69.9**	**49.6**

The final weighted average for each turbine production and its corresponding sum is presented in Table 8. It is worth mentioning that in this work the optimization was focused on the parameters that have influence, mostly, on the SSG hydraulic efficiency. Therefore, the power production is naturally underestimated. The optimization of the power production processes would require the definition of turbine operation strategies (and its fine-tuning), as well as the use of turbine characteristic curves (that relate head, flow rate and efficiency) suitable for the present study. This was considered to be outside the scope, of this work, which progressed to the simulation of the interaction between waves and the SSG structure, with the help of a Computational Fluid Dynamics model.

In comparison with the efficiency expected with a SSG structure with three reservoirs and a slope angle of 35º (geometry tested by Oliveira, 2014), the improvement was significant. The initial overtopping efficiency was 31.6 % for an associated 10.1 MWh/year produced power.

Table 8 - Produced Power

Res No.	Produced power (kWh/year)
1	1 075
2	3 283
3	3 982
4	5 368
5	8 525
Sum	**22 233**

Despite the produced power had increased around the double (from 10.1 to 22.2 MWh/year), the performance of the turbines was not improved, and consequently, the produced power could be higher than the present ones. For more realistic produced power expected, it is necessary to carry out a study focused in the turbine performance, such as the start/stop cycles, and the model turbines that take advantage of the turbine head available.

4.4. NUMERICAL SIMULATION

In parallel with the optimization of the SSG geometry for the conditions of the Portuguese case-study, this thesis also intended to study the interaction of incident waves with and its performance, using a computational fluid dynamics (CFD) numerical model (IHFOAM), and to validate simulations using the results of the experimental tests performed by Oliveira (2014). These tests were carried out at the wave tank of the Faculty of Engineering of the University of Porto (FEUP) and intended to assess the performance of an SSG device under wave conditions typical of the Portuguese west coast. The same regular wave conditions that considered the SSG geometry tested by Oliveira (2014) were simulated, in prototype dimensions, in the present work.

4.4.1. MESH CONDITIONS

The first step of the simulation consists in defining an appropriate mesh for the problem in analysis. In CFD, meshing corresponds to a discrete representation of the geometry of the problem. The mesh has the form of hexahedron (cells) inserted in a tri-axial coordinate system. Waves propagate along the *xx* axis; hence, this axis intersects one face of the domain that corresponds to the wave generation boundary and the opposite face represents the waves absorbing/reflecting boundary. In the present CFD application, the *yy* axis intersects two planes that are considered "empty", meaning that there is no boundary (2D problem). Finally, perpendicularly to the *zz* axis, the bottom face is defined as a wall (impervious boundary) and the top face is defined as atmosphere (open boundary: it lets water flow out as needed). In the *x* direction, the block has 100 m length: 50 m for the channel where the waves

propagate before reaching the structure and more 50 m to reproduce the SSG profile and more 50 meters for de development of SSG profile (Figure 67). In the *z* direction, the minimum elevation is -17.00 m, in agreement with the local water depth, and the maximum elevation is +15.00 m, matching the crest level of the breakwater where SSG device is installed. In accordance with the tests performed by Oliveira (2014), the simulation using IHFOAM were run for 2D conditions, therefore, in the *y* direction the SSG device was 0.02 m wide.

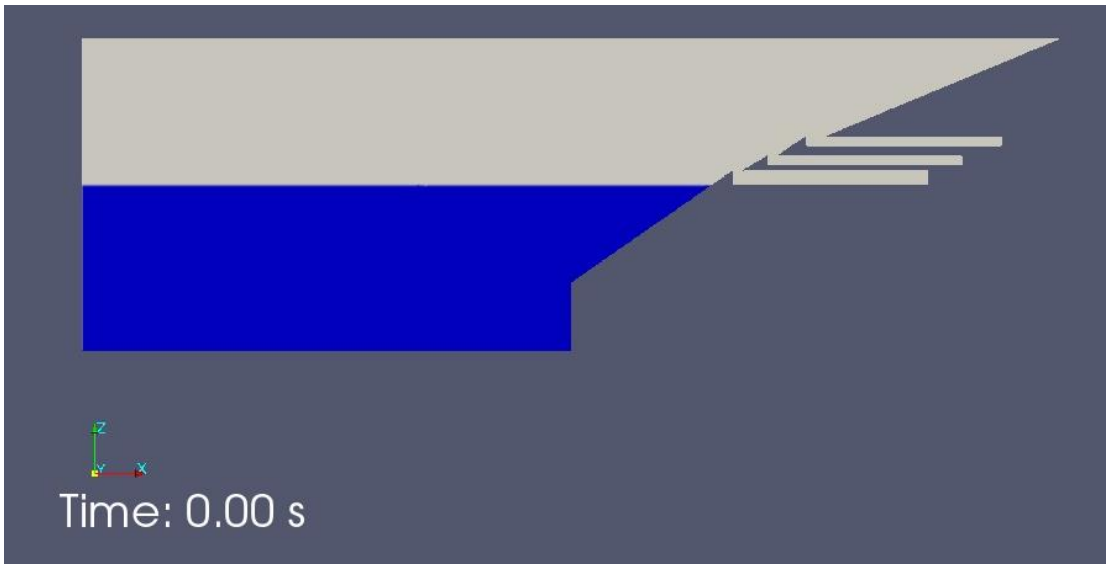

Figure 67 – Example of an IHFOAM simulation at 0.00 s (initial time of the simulation)

The number of mesh cells in each direction can be defined such as the cell expansion ratio, *i.e.* along each direction, the length of consecutive cells can increase or decrease, in order to get more detailed and refined information in a specified area (Figure 68). Since the objective of this study is the analysis of the interaction between waves and the SSG structure, the cell expansion ratio is smaller than one, in order to have more cells near the ramp than in the beginning of the channel (IHCantabria, 2014). This allows increasing the detail in the area of interest to better simulate the wave run-up and overtopping, while maintaining an affordable computational time.

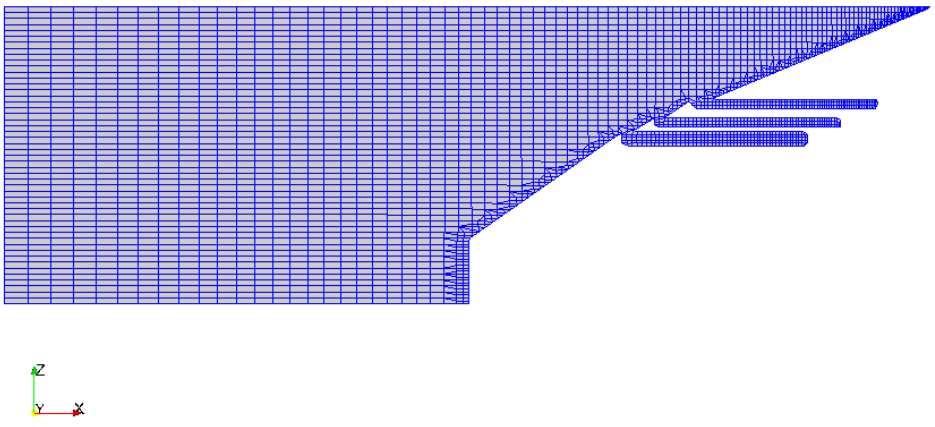

Figure 68 - Example of the expand ratio mesh along the xx axis

After having established the surrounding boundaries of the problem, the "absorber" face is modified in order to create a sloping face, with several entrances for the SSG reservoirs, *i.e.* to reproduce the profile of the SSG structure. This specific procedure is explained afterwards (section 4.4.3.).

4.4.2. Wave Conditions

The IHFOAM numerical model includes libraries that allow the consideration of several wave theories, to simulate regular or irregular waves. The values of wave characteristics used in the numerical simulations were the same that Oliveira (2014) used in the physical model study carried out in the wave tank of the Faculty of Engineering of the University of Porto (Table 9). Therefore, it would be possible to compare the numerical results with the experimental ones, qualitatively and quantitatively, and validating the numerical approach followed. Figure 61 was used to select the appropriate wave theory to be used in the simulation of each wave condition. The graphic representation uses dimensionless parameters for wave heights and water depths. Table 9 presents the initial wave heights considered in the simulations for a water depth of 17.0 m and the corresponding dimensionless parameters to be used in Figure 61 to select the appropriate wave theory.

Figure 69 presents the area where the results of Table 9 "fall" on the graphic of the range of applicability of wave theories by the blue dark ellipse. As it is possible to confirm visually, the corresponding wave theory is the 2nd order Stoke's theory.

Table 9 – Dimensionless parameters used in the simulations

H (m)	T (s)	h/gT^2	H/gT^2
2.5	11.5	0.151	0.0019
5	18.5	0.094	0.0015
1.8	11.5	0.151	0.0014
3.3	11.5	0.151	0.0025
3	16.1	0.108	0.0012
4.4	18.4	0.094	0.0013

The tests carried out by Oliveira (2014) with irregular waves were not used in this thesis as this would require the reproduction of several relatively long time series of waves, as generated and measured in the tests carried out at the wave tank of the Hydraulic Laboratory of FEUP.

4.4.3. Evolution of Simulated Conditions

In regard to this subject, several meshes and wave conditions were simulated in order to understand how the IHFOAM works and what could be modified with the purpose of taking a better advantage of this numerical code.

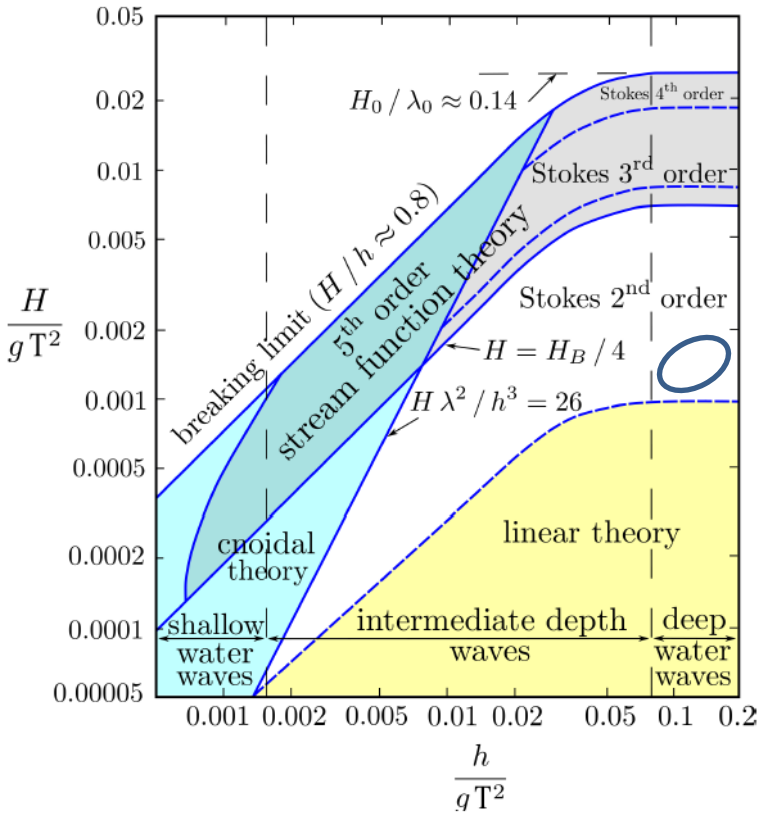

Figure 69 - Range of applicability of simulated wave theories (adapted from IHCantabria, 2014)

Initially, only a simple block with an inclined face was tested in order to understand the wave run-up phenomena on a sloping obstacle (Figure B 1 in Appendix B). It was necessary to test the numerical mode in order to avoid errors, increase the performance of the mesh, prevent running crashes and understand how it works. It is possible to mention that the main part of the errors can be solved by re-fining the mesh. In this work, one of the advantages of simulating in 2D problem was the reduction of the number of errors (Figure 70).

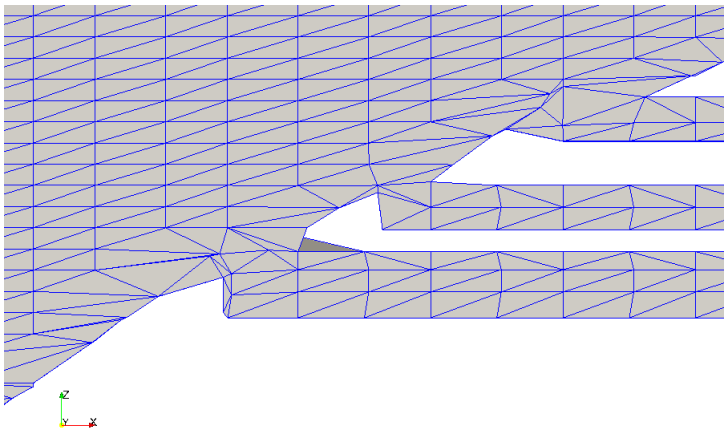

Figure 70 - Non re-fined mesh

After this initial work, a more complex case was reproduced: a ramp ending in a reservoir. The wave conditions were the same as before. In this simulation, it was possible to observe wave run-up, followed by a wave overtopping and, finally, the sea water entering the reservoir (Figure C 2 in Appendix C). The following step was adding another reservoir.

The first difficulty experienced was defining the mesh. As a compliment of the waves simulated and with the purpose of taking advantage of the software capacities, such as the mesh definition and detail, several meshes with diverse bases parameters of the ramp definition and mesh refinement were tested, in order to improve the quality of the simulation. The command runs in three steps. The first one and the most important, the program works by determining a border block mesh, from which the shape of the structure is removed. That shape is described by points that define a line (that connects those points). All the cells on the right side or below that cutting line (in a coordinate system with the smaller values on the left and the higher values on the right) are removed. For that, the software refines the intersected cells in the level that are defined previously. Those levels represent the refinement resolution, i.e. each time a level is increased the resolution is double. As the software works in 3D, the number of final cells per cell increases very rapidly (2^{3n} where n is the level). It is essential to take into account that as the new cells are smaller by level increasing; the time step of the running simulation tends to decrease, otherwise the Courant Number would increase. In the second step, the software snaps the mesh to the surface. The third one adds layers at the boundaries. However, during a preliminary study of different meshes and mesh creation techniques, it was concluded that more layers do not improve the mesh definition. It is also necessary to run a command to refine the mesh, allowing mesh lines to approximate each other better (Figures 71 and 72).

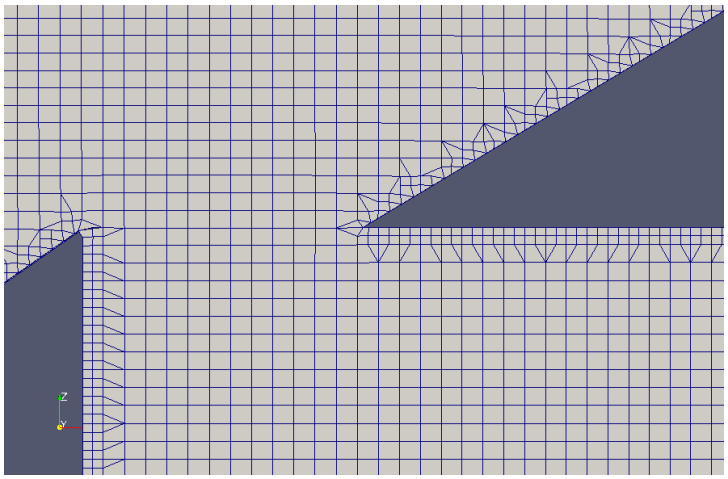

Figure 71 - Re-fined mesh on the entrance of a reservoir

As the goal of these simulations is the study of the interaction between the waves and the SSG ramps, the expansion ration along the *xx* axis was reduced in some cases, *i.e.* the mesh in the channel where waves propagate before reaching the structure was not so detailed as it was in the ramp and the SSG structure (Figure 66). Unfortunately, when meshes with an expansion ratio different than 1 were simulated an error occurred. Therefore, simulations were run with a constant base mesh: 6.25 cells per meter vertically and 5 cells per meter horizontally. This mesh resolution was considered also adequate for wave propagation.

Finally, a SSG with three reservoirs was reproduced (Figure B 3 in Appendix B). Consequently, this mesh was more elaborated and complex than before, and it was necessary to refine by introducing final adjustments to the initial mesh (Figure 72). Unfortunately, the mesh presented in Figure 72 was not used because several problems occurred due to the high memory the computer needed to calculate the variables during the simulation.

After defining the mesh and the boundary conditions, it is necessary to set the wave generation conditions. As explained before, the Stoke's 2nd order wave theory was selected to simulate the regular wave conditions, with a direction perpendicular to the SSG structure (no angle attack). The first simulation was run for a wave with a height of 2.5 m and a period of 11.5 s. In order to avoid initial disturbances caused by the sudden start of the wave generation process, a wave ramping time was used. Therefore, the "tSmooth" option was used and initial waves gradually increased to the desired wave height in the first seconds of the simulation (IHCantabria, 2014).

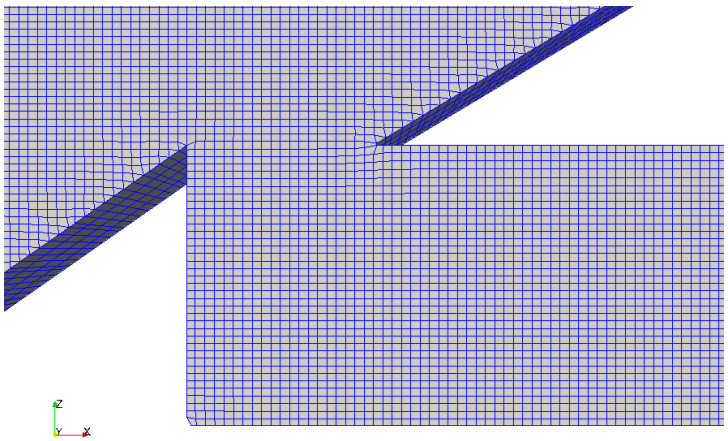

Figure 72 - Improved re-fined mesh on the entrance of a reservoir

4.4.4. FINAL CONDITIONS

The final model used in the simulations is presented in Figure 67. As described previously, the mesh has a channel where waves are generated and propagated until they find an obstacle. That obstacle is the face of SSG divided in two parts; a vertical front from the sea bottom to the elevation of -10.0 m, and a ramp with openings to the SSG reservoirs. The angle of the ramp with the horizontal plane is 35º. The crest levels of the three reservoirs (where overtopping water is stored) are 1.5, 3.0 and 5.0 m. Each opening is 1 m wide and each reservoir is 20 m long. Table 10 presents the coordinates of the vertices that define the SSG geometry.

Finally, all the parameters controlling the simulations can be changed. The simulation duration, the simulation time step and writing interval, among others, are defined. The duration of the tests ranged between 15 and 60 s, and for every 0.05 s the relevant variables computed were uploaded and written on independent files.

Table 10 - Coordinates of the SSG vertices

x (m)	z (m)
0	-17
0	-10
16.5	1.5
16.5	0
36.5	0
36.5	1.5
17.5	1.5
20	3
20	2
40	2
40	3
21	3
24	5
24	4
44	4
44	5
26	5
50	15

4.4.5. RESULTS

The second goal of this thesis was the validation of the numerical model with experimental results from the physical model tested by Oliveira (2014) in the wave tank of the Hydraulic Laboratory of FEUP. Therefore, IHFOAM (v2.1.1) was used to simulate the same conditions that were tested in the physical model and to study the interactions of waves with the SSG structure. After defining the mesh and the wave conditions, several conditions were tested.

The first simulation was run with regular waves, reproduced using cnoidal theory, which propagated in a channel until finding a slope/ramp. Figure C 1 (in Appendix C) shows a timeframe from ParaView as an example of that simulation.

After, in a second stage, a simple reservoir was added after the ramp. This geometry was initially tested under the action of waves simulated using cnoidal theory. Later 2nd order Stoke's wave theory was used. In both cases, some water overtops the ramp and enters the reservoir (Appendix B).

Then, the other two reservoirs were included in the mesh, increasing the complexity of the simulation. Similarly, the cnoidal and the 2nd order Stoke's wave theories were used. The goal was to understand how the sea interferes along the simulation, such as the running parameters (time interval, time of smooth, velocity of running, mesh detail, etc.). Figure 73 represents a timeframe from the simulation

of Stokes waves generation with 2.5 m height and 11.5 s for the period, with no phase neither angle attack and “tSmooth”.

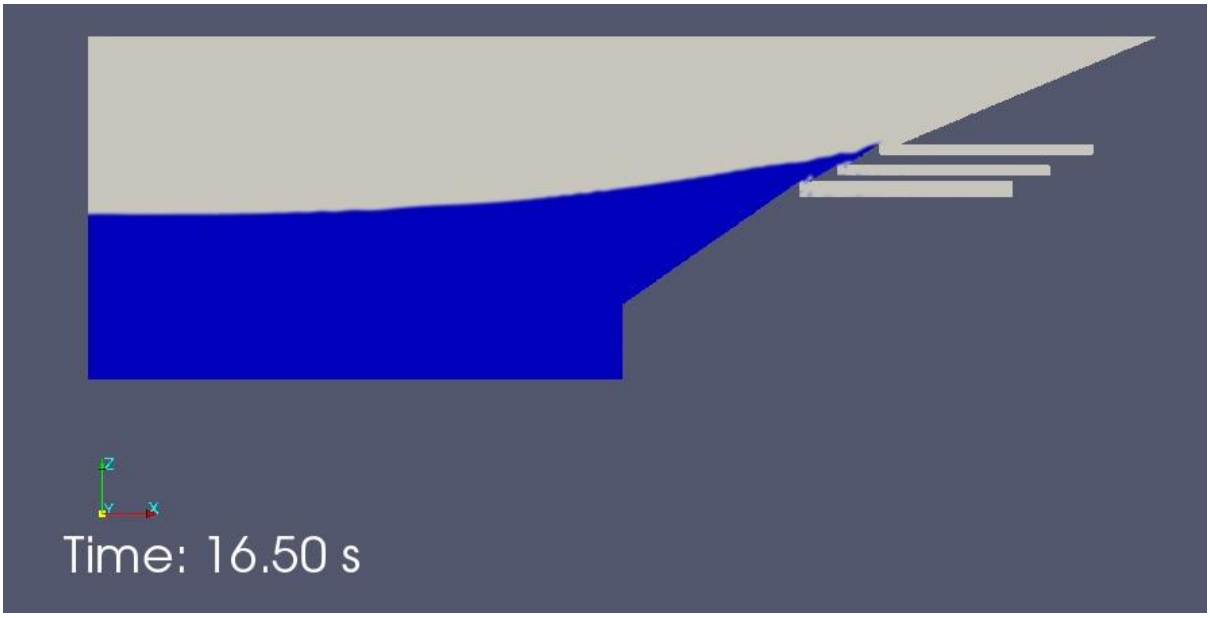

Figure 73 - Simulation at 16.50 s (water at the entrance of the reservoir 3)

For the sea state simulated (2.5 m wave height and 11.5 s wave period), a wave is generated and propagates in the channel until it finds the front ramp of the SSG structure. When that happens, the wave starts being affected by the ramp, once the depth water changes. Therefore, as a consequence, the wave runs-up the SSG slope until it finds the entrance of the first and lowest reservoir. From this instant, part of the wave continuous to overtop the structure, while another part enters into the first reservoir, where a certain amount of water is stored. The same occurs when the wave reaches the second reservoir. The wave may still reach the higher reservoir, however it has no sufficient energy to continue the overtopping. Therefore, the wave runs-down the ramp, originating turbulence near the reservoir entrances. Afterwards, the wave reaches its minimum run-down level in front of the structure and, then, another wave starts to run-up again the SSG structure and the process repeats again.

Figures 74 and 75 refer to the same timeframe of Figure 73 (16.50s), nevertheless present the variables turbulence kinematic intensity *k* and velocity *U*, respectively. As expected, the kinetic turbulence takes higher values (4.35 m^2/s^2) when the water enters into the reservoirs. In addition, velocity may increase up to 7 m/s.

During the simulation, and in accordance with the behavior of variable *alpha1*, the kinetic turbulence *k* and velocity *U* assume high values when turbulence occurs. Those disturbances take place when the waves propagate over the SSG ramp, during wave run-up and run-down, and at the entrance to the reservoirs, when the water goes inside.

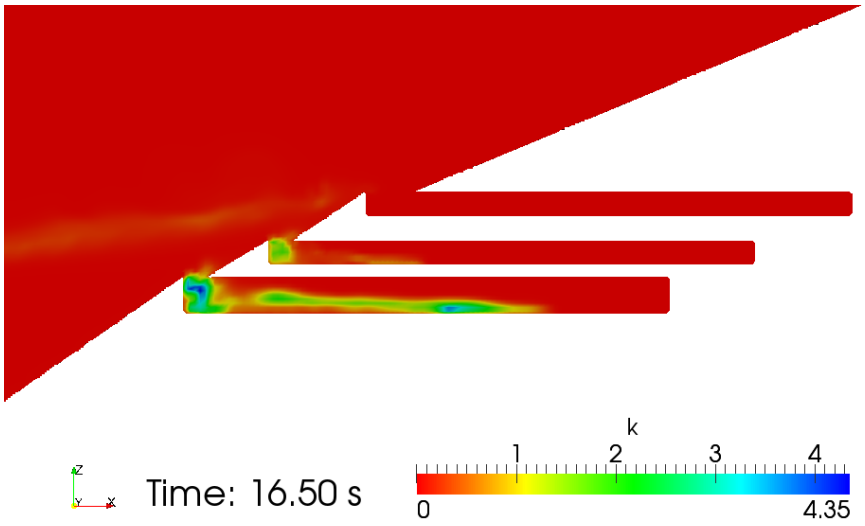

Figure 74 - Kinetic turbulence variation at 16.50 s at the entrance of the reservoirs (kinetic turbulence in m^2/s^2)

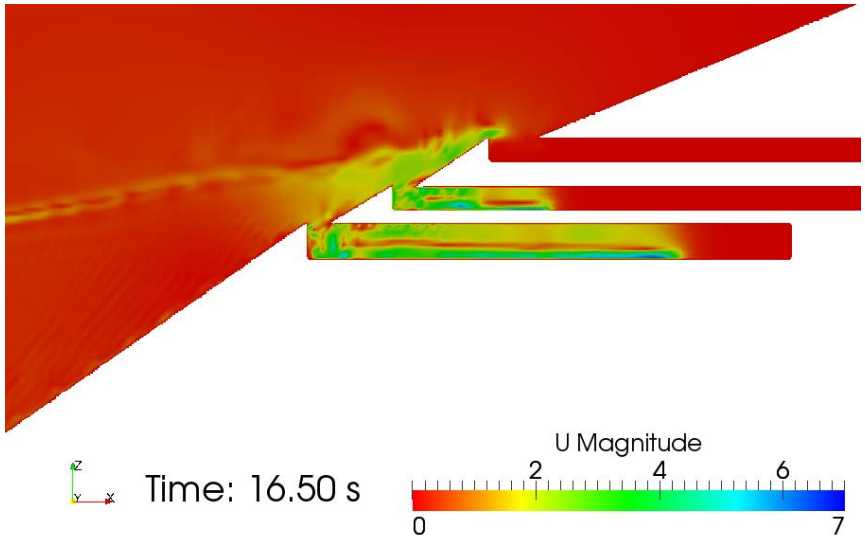

Figure 75 - Velocity variation at 16.50 s at the entrance of the reservoirs (velocity in m/s)

Later, a simulation for a wave height of 5.0 m and a wave period of 18.5 s was carried out. In general, the results are similar to the ones presented previously.

4.4.6. CALIBRATION AND VALIDATION

The validation of the numerical modelling results with experimental results from the physical model study carried out by Oliveira (2014) requires additional simulations. More time would be necessary to solve some issues related to the PC available memory and to perform all the simulations required. In this respect, future work should include the test conditions presented in Table 11.

Table 11 – Test conditions

Wave period (s)	Wave height (m)	Angle attack (º)	Phase (rad)
11.5	2.5	0	0
18.5	5.0	0	0
11.5	1.8	0	0
11.5	3.3	0	0
16.1	3.0	0	0
18.4	4.4	0	0

Thus, there were not enough time to run all the simulations planned neither to simulate numerically long test durations, like the ones considered by Oliveira (2014). The quantitative comparison of the results from this work with the results of the previous one was not possible. For that purpose, the use of numerical probes installed in the modelled domain will allow recording the free surface elevation of the water, namely inside the SSG reservoirs. Then, with these results it may be possible to estimate the volume of water in the reservoirs. Latter, the mean overtopping flow for each reservoir of the SSG device could be assessed and compared with the results obtained by Oliveira (2014).

5

CONCLUSIONS AND FUTURE DEVELOPMENTS

With the thesis, two analyses were carried out. The first one was the optimization of the SSG geometry when integrated in a breakwater located on the river Douro mouth, Porto, Portugal. The second part of the work aimed at the study of the interaction between incident waves and an SSG structure, after a intended validation of a Computational Fluid Dynamics (CFD) numerical model, with physical model results obtained in the experimental work carried out by Oliveira (2014) at the wave tank of the Hydraulics Laboratory of the Faculty of Engineering of the University of Porto, Portugal.

The optimization study of the SSG geometry reveled that an installation of this device in a breakwater located at the river Douro mouth requires a cross-section different from the ones developed for other locations. In fact, some of the previous works were carried out for installation sites in Denmark and Norway, which have similar wave conditions and tidal regimes (both countries are bathed by the North Sea). However, the Portuguese west coast has a different wave and tidal regime. The larger fetch area and depth of the Atlantic Ocean, in comparison with the North Sea, results in more energetic waves. On the other hand, the larger variability of the wave conditions along the year and the larger tidal range of the Portuguese west coast have influence on the SSG performance and should be considered in the design.

The SSG optimization study started with the same geometry used in the work of Oliveira (2014). The local wave conditions presented in Henriques *et al.* (2013) were considered in the simulations. The optimized SSG geometry is characterized by five reservoirs on the top of each other (instead of only three), 15 m wide and 20 m long. The length of the reservoirs in the upper levels may be reduced latter. The crest levels of the reservoirs, above the mean sea level, are: R_{c1} = 1.0 m, R_{c2} = 1.5 m, R_{c3} = 2.0 m, R_{c4} = 3.0 m and R_{c5} = 4.0 m. The slope angle of the structure has been considered equal to 30º.

During the simulations for the maxim tide levels, two issues occurred. One of them is the waste of the wave energy that is not entirely captured when the highest incident wave heights occur. However, the probability of occurrence of those wave heights, combined with the probability of occurrence of the high tide levels, is not significant, therefore the impact in the SSG overall efficiency is neglected. The other issue is that the lowest reservoirs became useless, because when the sea level rises, these reservoirs are submerged. However, it is important to mention that the lowest reservoirs are necessary due to the possible occurrence of low tides and low wave heights simultaneously.

After the definition of the optimized SSG geometry, the hydraulic efficiency of each reservoir and of the overall system, were estimated: 69.9% for overall overtopping efficiency and 49.6% for overall

hydraulic efficiency. The energy production was estimated in 22.23 MWh/year, which corresponds to 1.47 MWh/year per meter of SSG entrance against the 10.1 MWh/year of estimated energy production with the initial geometry (1.0 MWh/year per meter of SSG entrance). Despite the values of energy production being lower than the expected (values of around 5 to 10 MWh/year per meter were expected), the hydraulic efficiency is higher than the figures obtained in previous studies, *e.g.*, Margheritini and Kofoed, 2010. This discrepancy may be explained by the fact that turbine's restrictions and control strategies were not defined in the software WOPSim and the group of turbines was not optimized. This could improve the performance of energy conversion and the power production.

As further works, SSG geometries for other locations in the Portuguese coast could be studied and compared (*e.g.*, Sines). Other geometries could also be developed, even for the river Douro mouth, based on more detailed studies and eventually incorporating new data about wave conditions. In addition, new turbines, with performance characteristics defined based on the local conditions (head, flow, efficiency) and proper control strategies should be implemented as well. The group of turbines could also be optimized and to study the interaction with MST.

The second part of the thesis involved the study of the interaction between incident sea waves and the SSG structure, using a Computational Fluid Dynamics (CFD) numerical model (IHFOAM). The test conditions initially considered in the simulation were the same that Oliveira (2014) tested in a physical model. The goals were to calibrate the numerical model and to validate its results, qualitatively and quantitatively, with the results obtained in the physical model. Unfortunately, the validation was only performed qualitatively. The initial difficulties with the implementation of this recent numerical model, together with issues regarding the proper reproduction of the SSG geometry and the high computation efforts required by the CFD approach (several hours of CPU time to simulate a few seconds of a physical model test) explain the impossibility of carrying a comprehensive quantitative validation of the numerical results.

Nevertheless, some simulations were successfully completed that provides a starting point for further studies. One of those simulations reproduced a physical model test carried out for regular waves with a wave height of 2.5 m and a wave period of 11.5 s. The simulation time was 30 s, and hence included only the generation of two waves using the Stokes wave theory. It is important to mention that the simulation included a ramping time, *i.e.*, the IHFOAM started by generating a small wave (less than 2.5 m) due to the selection of the "tSmooth". During that ramping time, the wave height grows to the desired value. This approach avoided the numerical instabilities that occurred in previous simulations. At 11.40 s, the first wave reaches the front slope of SSG and starts to run-up. The wave overtops the reservoir crests, enters into them and starts to run-down the structure ramp. Some water is already stored in the SSG reservoirs when the second wave attempts to overtop its front slope (21.50 s of simulation time).

The post-processing of the simulations results with ParaView allows assessing other flow variables (*e.g.*, velocity, pressure, water level variation, kinematic turbulence, turbulence viscosity) in a range of colorful scales. This can be done for a specific time step or the whole simulation duration, any point in the numerical domain or the entire domain.

In future works, it is necessary to perform additional simulations for the other wave characteristics that were tested by Oliveira (2014), as well as to simulate the SSG geometry with wave focusing elements. To validate the numerical simulation, overtopping flows measured in the physical model will be used. Furthermore, the SSG geometry optimized with WOPSim for the conditions of the river Douro mouth (with 5 reservoirs) should be numerically simulated in order to better understand its performance and

to study its interaction with typical waves from the Portuguese west coast, not forgetting the study with reflectors.

REFERENCES

Allsop, William; Bruce, Tom; Pearson, Jonathan; Besley, Phillip - Wave overtopping at vertical and steep seawalls. *Proceedings of the ICE-Maritime Engineering*. Vol. 158. n.º 3 (2005). p. 103-114. 1751-7737

Bakke, Monika - WAVESSG, Full-scale demonstration of robust and high-efficiency wave energy converter. Wave Energy AS., 2008.

Bevilacqua, Giovanna; Zanuttigh, Barbara - Overtopping Wave Energy Converters: general aspects and stage of development. (2011).

Bogarino, Bruno; Kofoed, Jens Peter; Meinert, Palle - Development of a generic power simulation tool for overtopping based WEC. Department of Civil Engineering, Aalborg University, 2007.

CETN, V - 20 3/85. Biological effects of breakwater construction on aquatic communities in the Great Lakes. *Coastal Engineering Technical Note. CETN*. Vol. 20. (1985). p. 3.

CFLH - Velocity Variations in Cross-Hole Sonic Logging Surveys - Causes and Impacts in Drilled Shafts. Lakewood, United States of America: U.S. Department of Transportation - Federal Highway Administration, 2008.

Cruz, João - Ocean wave energy: current status and future prespectives. Springer Science & Business Media, 2008. 3540748954

Energies, CADDET Renewable - Denmark's clean energy future from waves. United Kingdom: CADDET Centre for Renewable Energy, 1999.

European-Council - Communication from the Commission to the European Parliament, the Council, the European Economic and Social Committee and the Comittee of the Regions - A policy framework for climate and energy in the period from 2020 to 2030. Brussels: 2014.

Evans, DV; Falcao, AF de O - Hydrodynamics of ocean wave-energy utilization. Springer-Verlag New York, Inc., New York, NY, 1985.

Falcão, António F. de O. - Wave energy utilization: A review of the technologies. *Renewable and sustainable energy reviews*. Vol. 14. n.º 3 (2010). p. 899-918. 1364-0321

Fernandez, H; Iglesias, G; Carballo, R; Castro, A; Fraguela, JA; Taveira-Pinto, F; Sanchez, M - The new wave energy converter wavecat: Concept and laboratory tests. *Marine structures*. Vol. 29. n.º 1 (2012). p. 58-70. 0951-8339

Frigaard, Peter; Kofoed, Jens Peter; Knapp, Wilfried - Wave Dragon: wave power plant using low-head turbines. 2004.

Frigaard, Peter; Trewers, Andrew; Kofoed, Jens Peter; Margheritini, Lucia - Conceptual Design of Wave Plane. Department of Civil Engineering, Aalborg University, 2008.

Gunn, Kester; Stock-Williams, Clym - Quantifying the global wave power resource. *Renewable Energy*. Vol. 44. (2012). p. 296-304. 0960-1481

Henriques, JCC; Cândido, JJ; Pontes, MT; Falcão, AFO - Wave energy resource assessment for a breakwater-integrated oscillating water column plant at Porto, Portugal. *Energy*. Vol. 63. (2013). p. 52-60. 0360-5442

Higuera, Pablo; Lara, Javier L; Losada, Inigo J - Realistic wave generation and active wave absorption for Navier–Stokes models: Application to OpenFOAM®. *Coastal Engineering*. Vol. 71. (2013a). p. 102-118. 0378-3839

Higuera, Pablo; Lara, Javier L; Losada, Inigo J - Simulating coastal engineering processes with OpenFOAM®. *Coastal Engineering*. Vol. 71. (2013b). p. 119-134. 0378-3839

Higuera, Pablo; Lara, Javier L; Losada, Inigo J - Three-dimensional interaction of waves and porous coastal structures using OpenFOAM®. Part I: Formulation and validation. *Coastal Engineering*. Vol. 83. (2014a). p. 243-258. 0378-3839

Higuera, Pablo; Lara, Javier L; Losada, Inigo J - Three-dimensional interaction of waves and porous coastal structures using OpenFOAM®. Part II: Application. *Coastal Engineering*. Vol. 83. (2014b). p. 259-270. 0378-3839

Holmberg, P; Andersson, M; Bolund, B; Strandanger, K - Wave Power. Surveillance study of the development. *Elforsk rapport*. Vol. 11. n.º 02 (2011).

IHCantabria - IHFOAM Manual. Cantabria, Spain: Institute of Environmental Hydraulic of University of Cantabria, 2014.

Juarez, Daniel Gonzalez - An intro to computational fluid dynamics. 2014.

Kamphuis, J. W. - Introduction to Coastal Engineering and Management. Canada: Queen's University, 2010. ISBN: 978-981-283-484-3

Kofoed, Jens Peter - Wave Overtopping of Marine Structures: utilization of wave energy. Videnbasen for Aalborg UniversitetVBN, Aalborg UniversitetAalborg University, Det Teknisk-Naturvidenskabelige FakultetThe Faculty of Engineering and Science, Institut for Vand, Jord og MiljøteknikDepartment of Civil Engineering, 2002.

Kofoed, Jens Peter - Experimental hydraulic optimization of the wave energy converter seawave Slot-Cone generator. (2005a).

Kofoed, Jens Peter - Model testing of the wave energy converter Seawave Slot-Cone Generator. Department of Civil Engineering, Aalborg University, 2005b.

Kofoed, Jens Peter; Frigaard, Peter; Kramer, Morten - Recent Developments of Wave Energy Utilization in Denmark. 2006.

Lara, J. - Numerical modeling of wave-structure interaction with RANS models. 2012.

Li, Ye; Yu, Yi-Hsiang - A synthesis of numerical methods for modeling wave energy converter-point absorbers. *Renewable and Sustainable Energy Reviews*. Vol. 16. n.º 6 (2012). p. 4352-4364. 1364-0321

Margheritini, Lucia - R&D towards commercialization of the Sea wave Slot cone Generator (SSG) overtopping wave energy converter. (2009).

Margheritini, Lucia; Hansen, Anne Merrild; Frigaard, Peter - A method for EIA scoping of wave energy converters—based on classification of the used technology. *Environmental Impact Assessment Review*. Vol. 32. n.º 1 (2012a). p. 33-44. 0195-9255

Margheritini, Lucia; Kofoed, Jens Peter - Definition of Geometry for SSG Breakwater at Hanstholm Location. Department of Civil Engineering, Aalborg University, 2010.

Margheritini, Lucia; Stratigaki, Vasiliki; Troch, Peter - Geometry Optimization of an Overtopping Wave Energy Device Implemented into the New Breakwater of the Hanstholm Port Expansion. International Society of Offshore and Polar Engineers, 2012b.

Margheritini, Lucia; Vicinanza, Diego; Frigaard, Peter - Sea Slot Cone Generator overtopping performance in 3D conditions. 2008.

Margheritini, Lucia; Vicinanza, Diego; Frigaard, Peter - SSG wave energy converter: Design, reliability and hydraulic performance of an innovative overtopping device. *Renewable Energy*. Vol. 34. n.º 5 (2009). p. 1371-1380. 0960-1481

Meinert, Palle; Gilling, Lasse; Kofoed, Jens Peter - Usual manual for WOPSim (Wave Overtopping Power Simulation). Aalborg, Denmark: Aalborg University, 2008. ISSN 1603-9874

Nathaniel-Bowditch, LL. D. - American practical navigator: an epitome of navigation and nautical astronomy. Bicentennial Edition. Bethesda, Maryland, United States of America: National Imagery and Mapping Agency, 2002.

Oliveira, Pedro - Aproveitamento da Energia do Mar através do Espraiamento de Estruturas Costeiras Portuárias. Porto, Portugal: Faculty ofEngineering of University of Porto, 2014.

OTEO - Estado da Arte - Relatório. Observatório Tecnológico para as Energias Offshore, 2012.

OTEO - Relatório das Tecnologias de Aproveitamento elaborado pelo Observatório Tecnológico para as energias Offshore. Porto, Portugal: Observatório Tecnológico das Energias Offshore, 2014.

Pullen, T; Allsop, NWH; Bruce, T; Kortenhaus, A; Sch, H; Van der Meer, JW - Wave overtopping of sea defences and related structures: assessment manual. (2007).

Ruiz, Manases Tello - Dynamics and Hydrodynamics for Floating Wave Energy Converters. Lisbon, Portugal: Technical University of Lisbon, 2010.

Thorpe, TW - A brief review of wave energy: A report produced for The UK Department of Trade and Industry. *ETSU-R120, May*. (1999).

USACE - Coastal Enginnering Manual, Part II. Washington, DC, USA: 2002.

Vicinanza, Diego; Margheritini, Lucia; Kofoed, Jens Peter; Buccino, Mariano - The SSG wave energy converter: Performance, status and recent developments. *Energies*. Vol. 5. n.º 2 (2012). p. 193-226.

Zanuttigh, Barbara; Margheritini, Lucia; Gambles, L; Martinelli, Luca - Analysis of Wave Reflection from Wave Energy Converters Installed as Breakwaters in Harbours. 2009.

[1] https://yearbook.enerdata.net/

[2] http://home.hiwaay.net/~krcool/Astro/moon/moontides/

[3] http://www.eeescience.utoledo.edu/Faculty/Krantz/Hazards/Hazards.Chap_03a.wave_basics.pdf

[4] http://i.stack.imgur.com/1cqfL.jpg

[5] http://www.wikiwaves.org/files/9/99/Fig16-7s.jpg

[6] http://homepages.cae.wisc.edu

[7] https://cyberchalky.files.wordpress.com/2008/03/seawave_diffraction.jpg

[8] https://imaginenewdesigns.wordpress.com/tag/volcanic-mushroom-clouds/

[9] http://taperedchannelwaveenergy.weebly.com/

[10] http://www.nordicgreen.net/startups/wavehydro/waveplane

APPENDIX

Appendix A – Probability of occurrence of each sea state equal to one

Table A 1 - Distribution of annual joint frequency for each class of wave height and period for each 10º directional sector when the probability of occurrence of each sea state is equal to one

Direction (ºN)	Peak Period (s)	Wave Height (m)										Sum
		0.75	1.25	1.75	2.25	2.75	3.25	3.75	4.25	4.75	5.25	
260	6	0.565	0.324	0.110								1
	8	0.228	0.273	0.218	0.208	0.073	0.003					1
	10	0.145	0.153	0.129	0.234	0.194	0.137	0.008				1
	12		0.714	0.143	0.143							1
	14											0
	16	0.500	0.500									1
270	6	0.876	0.101	0.024								1
	8	0.502	0.314	0.108	0.056	0.018	0.002					1
	10	0.231	0.285	0.237	0.132	0.075	0.031	0.008	0.001			1
	12	0.157	0.218	0.269	0.172	0.082	0.058	0.025	0.011	0.006	0.002	1
	14	0.056	0.091	0.207	0.209	0.185	0.091	0.078	0.054	0.020	0.008	1
	16	0.023	0.047	0.110	0.174	0.157	0.099	0.064	0.157	0.105	0.064	1
280	6	0.905	0.095									1
	8	0.564	0.329	0.100	0.007							1
	10	0.287	0.336	0.219	0.120	0.031	0.006	0.001				1
	12	0.114	0.257	0.250	0.194	0.101	0.042	0.021	0.021			1
	14	0.033	0.095	0.213	0.204	0.161	0.095	0.085	0.071	0.028	0.014	1
	16		0.026	0.128	0.179	0.077	0.077	0.282	0.077		0.154	1
290	6	0.606	0.394									1
	8	0.400	0.600									1
	10											0
	12											0
	14											0
	16											0
Sum		**6.193**	**5.152**	**2.466**	**2.032**	**1.153**	**0.640**	**0.573**	**0.392**	**0.159**	**0.242**	**19**

Appendix B – Simulation result from WOPSim

Simulation: Simulation 0, 09/12/2014 23:00:56

RESULTS (Flow):

==========

TOTALS:

FLOWS AND PRODUCED POWER:

Res No.	Water in [m^3/s]	Water overflow [m^3/s]	Water through [m^3/s]	Water.chg reservoir [m^3/s]	Produced power [kWh/yr]	Average power [kW]
1	1.355433	0.209606	1.329657	7.18E-06	40026.97	4.566261
2	0.770337	0.1838362	0.776372	4.68E-05	56251.53	6.417153
3	0.705726	0.1899186	0.55824	1.71E-05	65301.33	7.449551
4	0.246442	0.0424490	0.232744	-5.88E-07	43699.26	4.985195
5	0.136777	0.0287505	0.108022	5.30E-06	29356.57	3.348987
Sum	3.214716	0.209606	3.005034	7.58E-05	234635.7	26.76715

** Flow to next reservoir

RESERVOIR EFFICIENCIES:

Res No.	Eff overtop [%]	Eff. res. [%]
1	11.62615	5.559806
2	9.911313	6.615748
3	12.10668	7.358882
4	6.341542	4.925688
5	4.692809	3.204052
Sum	44.67849	27.66418

TURBINES EFFICIENCIES:

Res No.	Turb No. [%]	through turb [%]	Eff. work eff [hours/yr]	Turb Turb.on time [%]	Turb.on pct [%]	Turb charac eff [/hour]	No. of turn on/ turn off	Produced power [kWh/yr]
11	5.681865	3.891195	3392.562	38.70221	65.75397	19.50494	40026.97	
21	6.685175	5.468473	3774.054	43.05427	81.8	10.25674	56251.53	
31	7.407518	6.348243	5290.051	60.3487	85.7	4.304441	65301.33	
41	4.957058	4.248199	2201.147	25.11061	85.7	4.25167	43699.26	
51	3.232522	2.853884	986.2622	11.25124	56.3049	2.275369	29356.57	

Figure B 1 - Example of a simulation result from WOPSim

SIMULATED SEASTATES:										

					Model	Model	Prototype	Prototype	Wave	Average
No.	Hs	Tp	Offset	Prob	waves	time	waves	time	Energy	power
[-]	[m]	[s]	[m]	[%]	[-]	[s]	[1/yr]	[s/yr]	[kWh/yr]	[kW]
1	1.02	6	0.25	35.94	44125	220625	2268311	11341553	126104.9	40.02783
2	1.57	8	0.25	48.08	44273	295153.3	2275884	15172562	532912.8	126.4444
3	2.06	10	0.25	14.9	10976	91466.67	564237.5	4701979	355404.6	272.1102
4	1.46	12	0.25	0.84	516	5160	26507.8	265078	12077.27	164.0202
5	1	16	0.25	0.24	110	1466.667	5680.244	75736.58	2158.408	102.596
Sum				100	100000	613871.7	5140620	31556909	1028658	117.3489
RESERVOI	1									

FLOWS AND PRODUCED POWER:										
Sea	Water	Overflow	Water	Water	Water.chg	Produced	Average			
state	in	Water in	overflow	through	reservoir	energy	power			
[-]	[m^3/s]	[m^3/s]	[m^3/s]	[m^3/s]	[m^3/s]	[kWh/yr]	[kW]			
1	0.636217	0	0.000667	0.635355	0.000195	6110.937	1.939714			
2	1.553832	0.060947	0.088807	1.525794	0.000178	21426.57	5.083892			
3	2.45	1.028353	1.103295	2.37605	-0.00099	12085.23	9.252872			
4	1.552635	0.155768	0.270197	1.438858	-0.00065	360.2762	4.892878			
5	0.667688	0	0.002808	0.662782	0.002098	43.95629	2.089382			
Mean	1.355433	0.183836	0.209606	1.329657	7.18E-06	40026.97	4.566261			
RESERVOIR EFFICIENCIES:										
Sea	Eff	Eff.								
state	overtop	res.								
[-]	[%]	[%]								
1	15.99848	7.300629								
2	12.36914	5.812861								
3	9.06268	4.623903								
4	9.528121	4.226796								
5	6.550564	2.930233								
Mean	11.62615	5.559806								
TURBINES EFFICIENCIES:										
			Eff.	Turb		Turb	No. of	Produced		
Sea	Turb	through	work	Turb.on	Turb.on	charac	turn on/	power		
No.	No.	turb	eff	time	pct	eff	turn off			
	[%]	[%]	[hours/yr]	[%]	[%]	[/hour]	[kWh/yr]			
11	7.364896	4.845915	1629.781	18.59248	64.32379	14.79977	6110.937			
21	5.933175	4.020653	3899.075	44.4805	65.82175	23.07682	21426.57			
31	4.768602	3.400413	6023.025	68.71044	68.97133	19.32507	12085.23			
41	4.364471	2.983094	3657.415	41.72364	66.21111	21.62791	360.2762			
51	3.044212	2.036514	1662.53	18.96607	65.00209	12.27273	43.95629			
Mean. 1	5.681865	3.891195	3392.562	38.70221	65.75397	19.50494	40026.97			
Mean on t	5.681865	3.891195	3392.562	38.70221	65.75397	19.50494	40026.97			

Figure B 2 - Example of a simulation result from WOPSim (continuation)

APPENDIX C – PROGRESSION OF THE GEOMETRY

Figure C 1 - Cnoidal waves on a slope

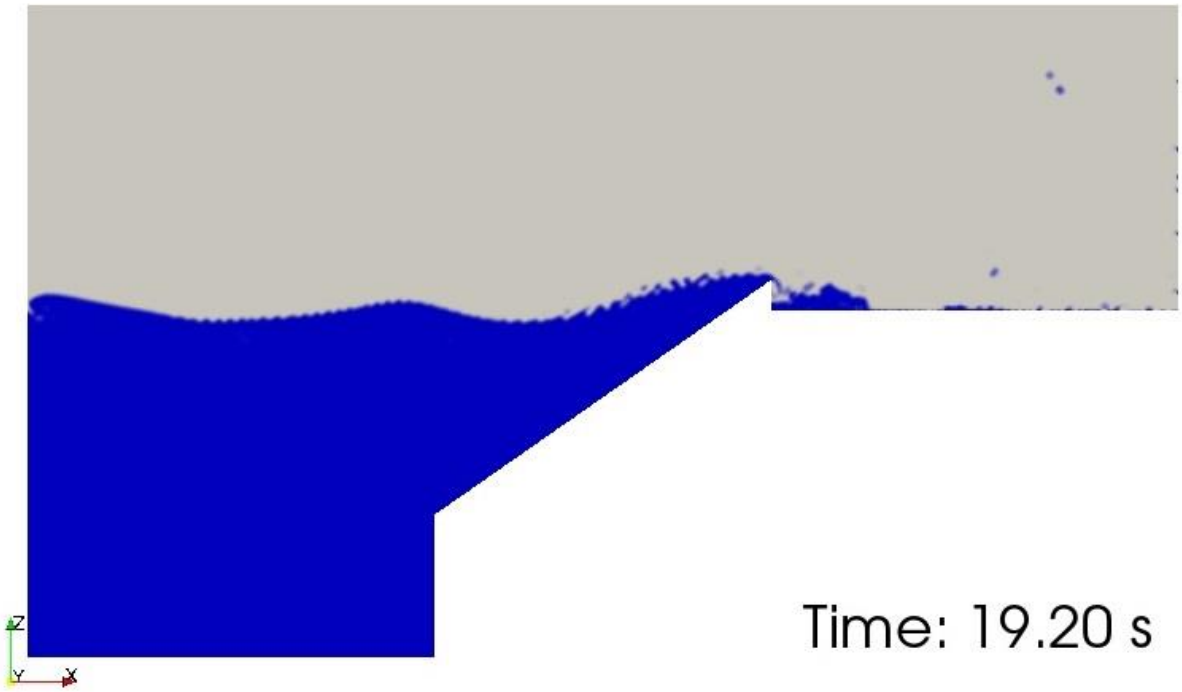

Figure C 2 - Stokes waves with a single reservoir

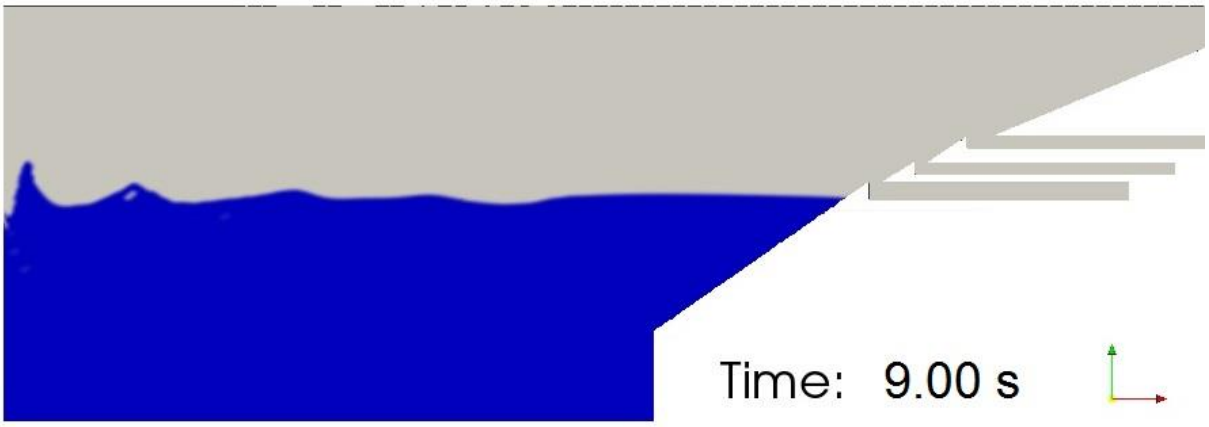

Figure C 3 - Cnoidal waves with three reservoirs

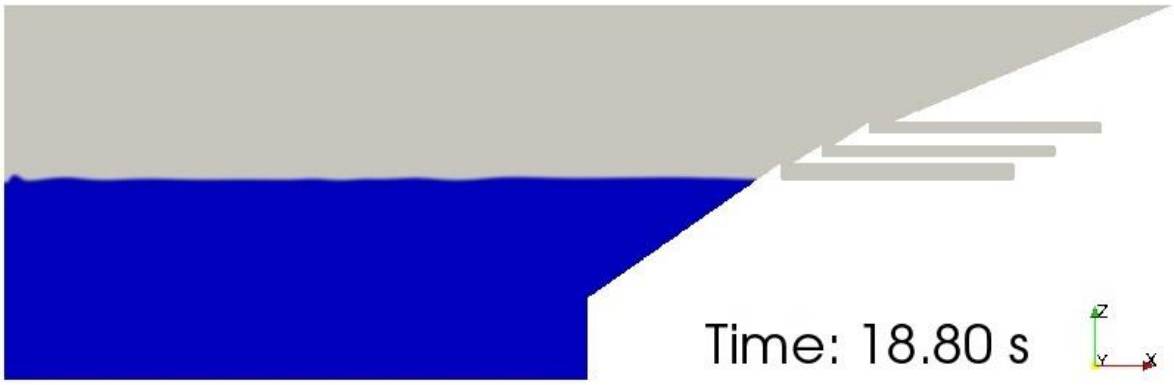

Figure C 4 - Stokes waves with three reservoirs

Appendix D – Progression of the Mesh

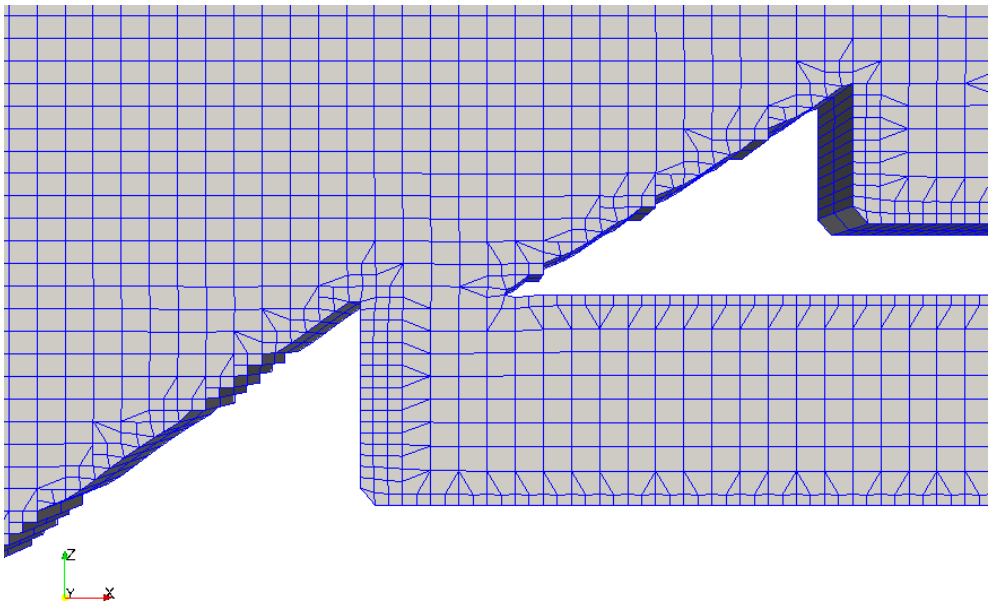

Figure D 1 - Non-refined mesh

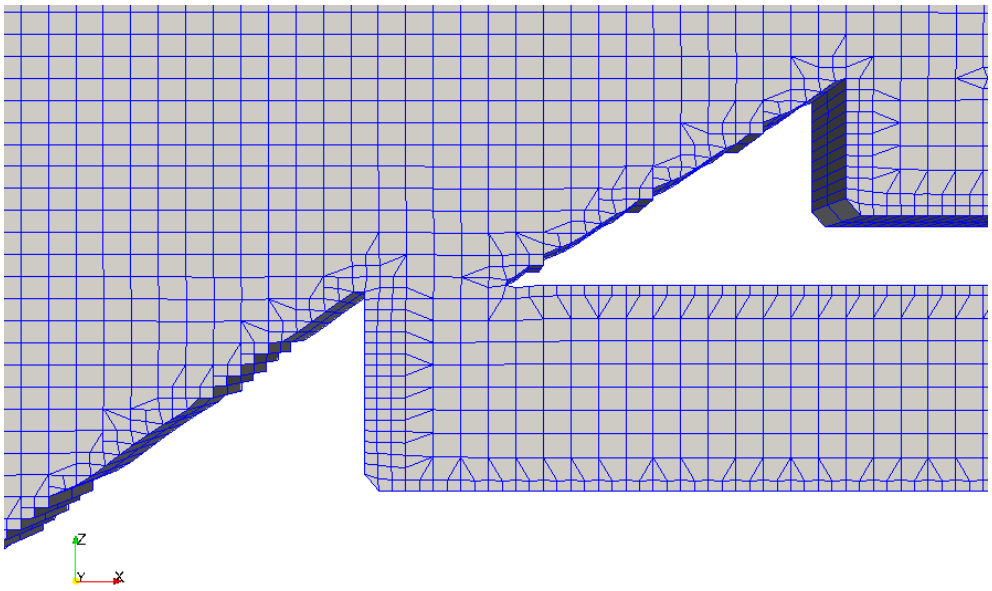

Figure D 2 - Refined mesh with command "seachableBlox" on

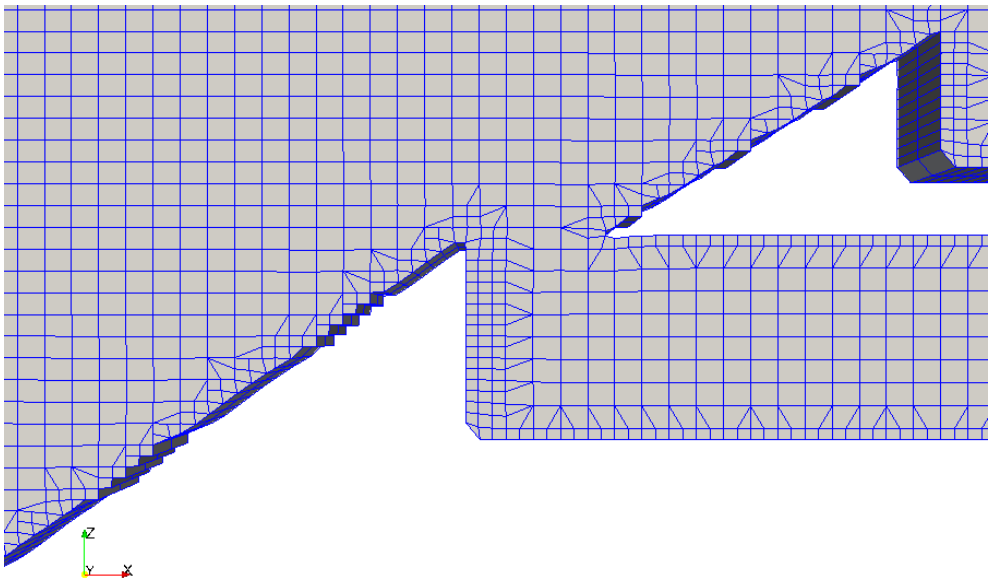

Figure D 3 - Refined mesh with addition layers

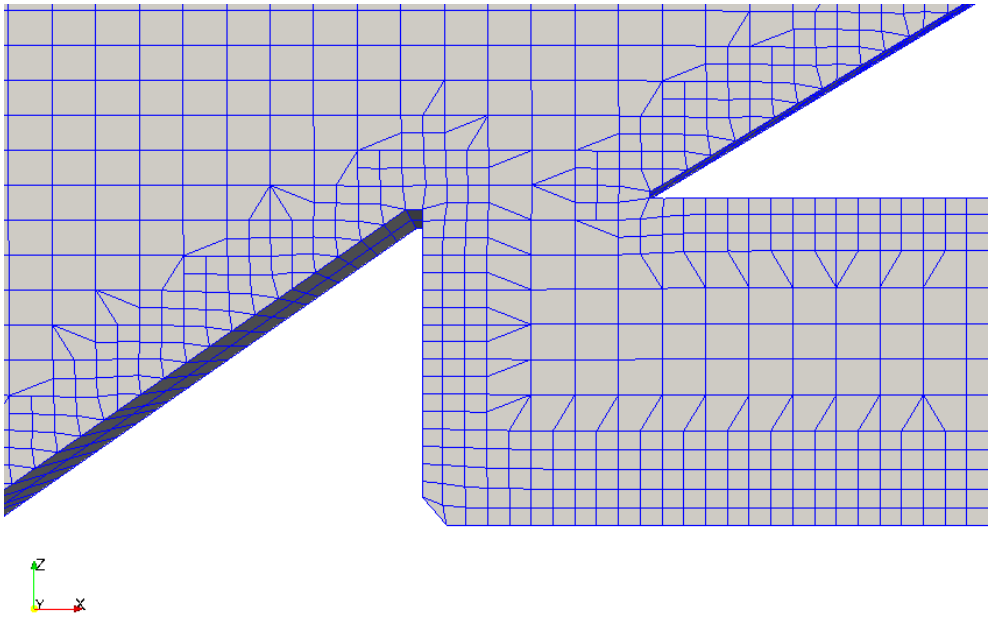

Figure D 4 - Re-fined mesh with number of cells between levels equal to 5

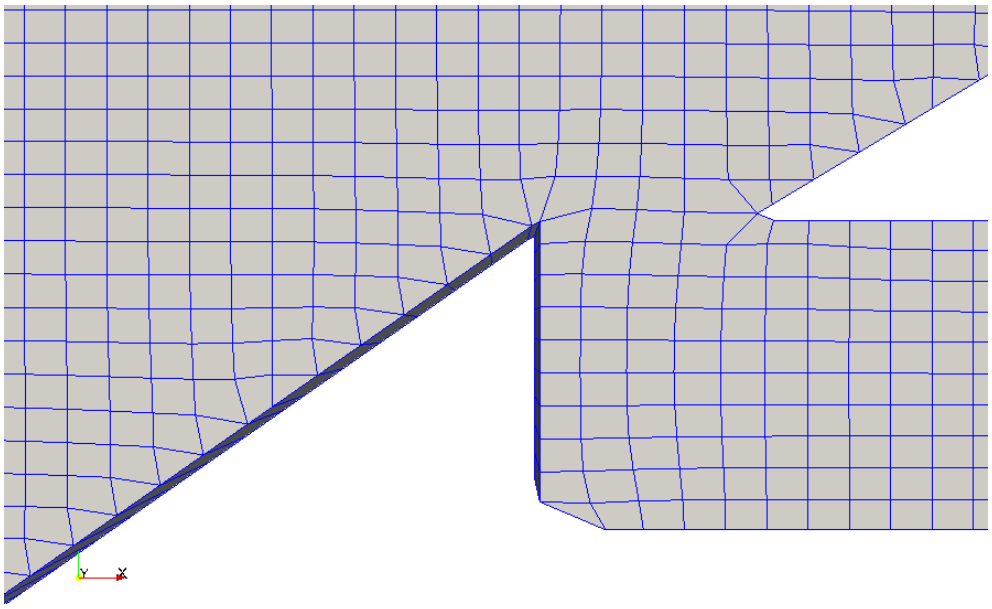

Figure D 5 - Re-fined mesh only with level 0 of refinement

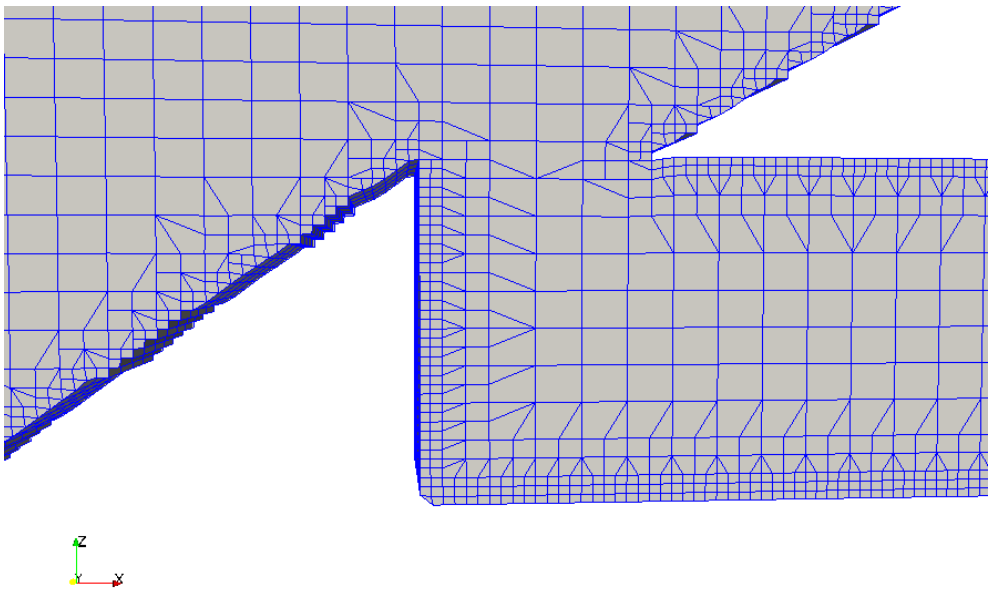

Figure D 6 - Re-fined mesh only with level 2 of refinement

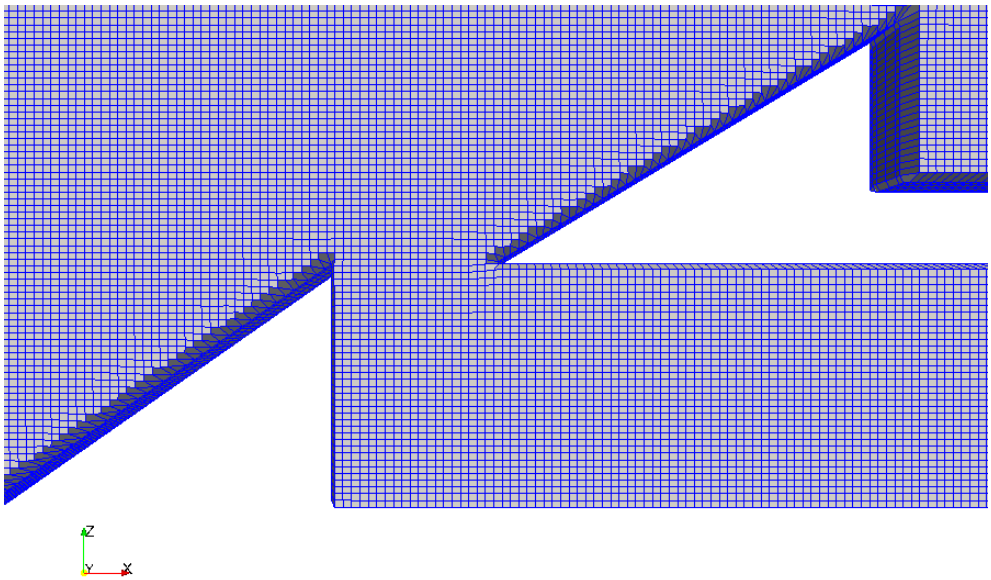

Figure D 7 - Re-fined mesh with level between 0 and 2 of refinement

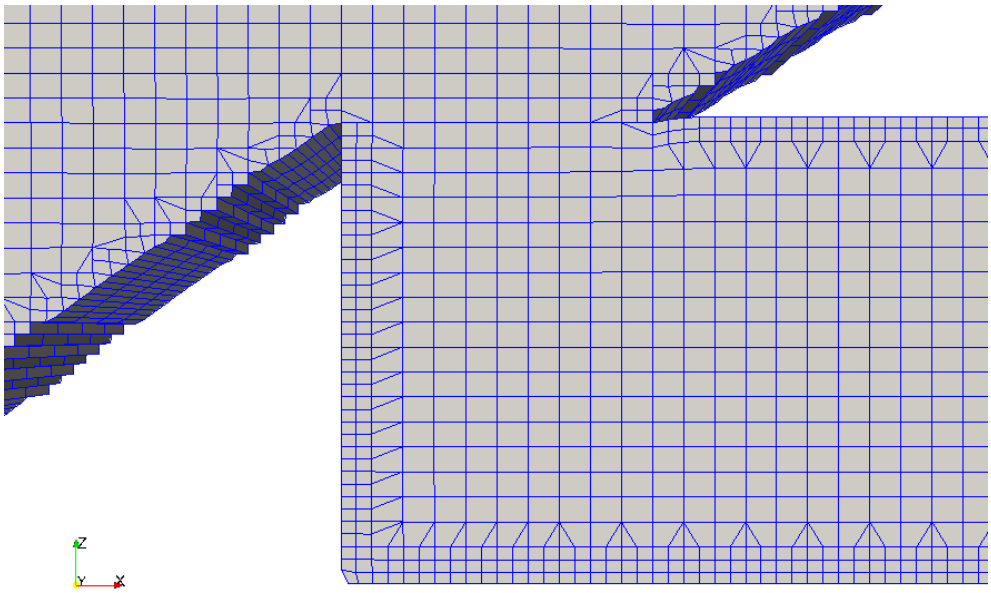

Figure D 8 - Re-fined mesh with feature angle equal to 35º

Appendix E – Simulation for 11.5 m of wave height and 2.5 s for wave period

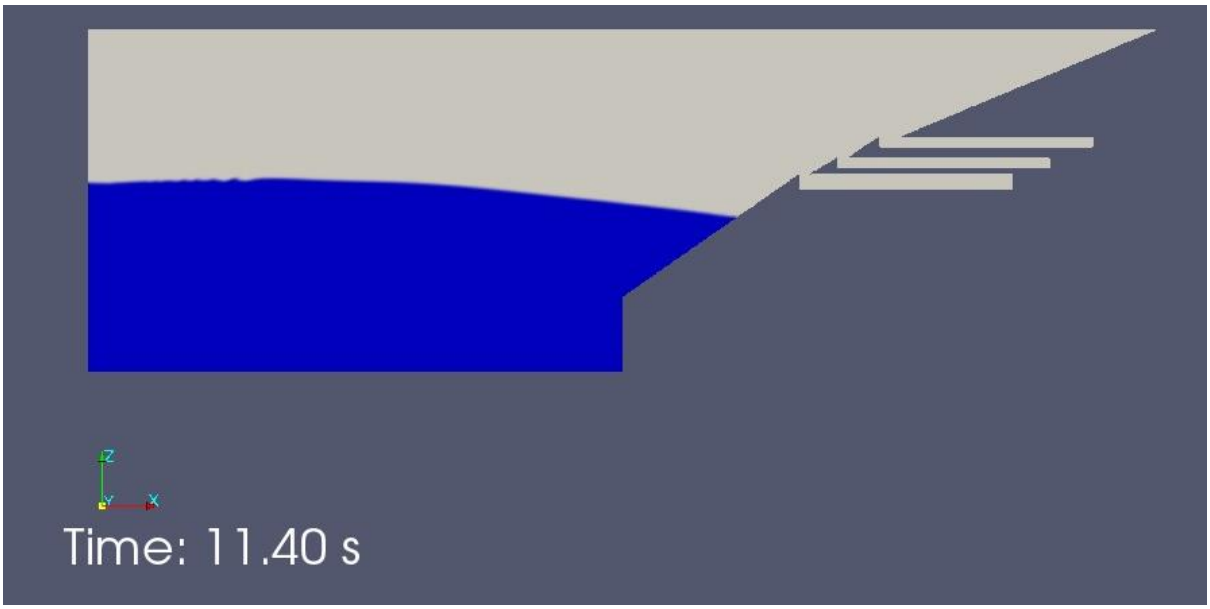

Figure E 1 - Simulation at 11.40 s (minimum water height in the first wave)

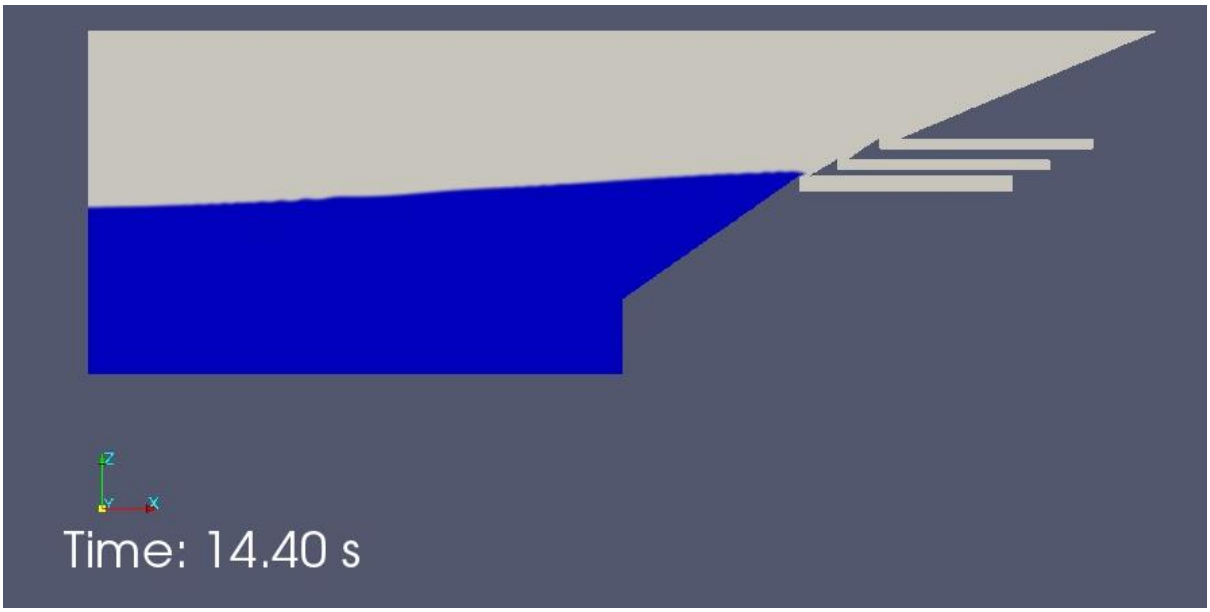

Figure E 2 - Simulation at 14.40 s (water at the entrance of the reservoir 1)

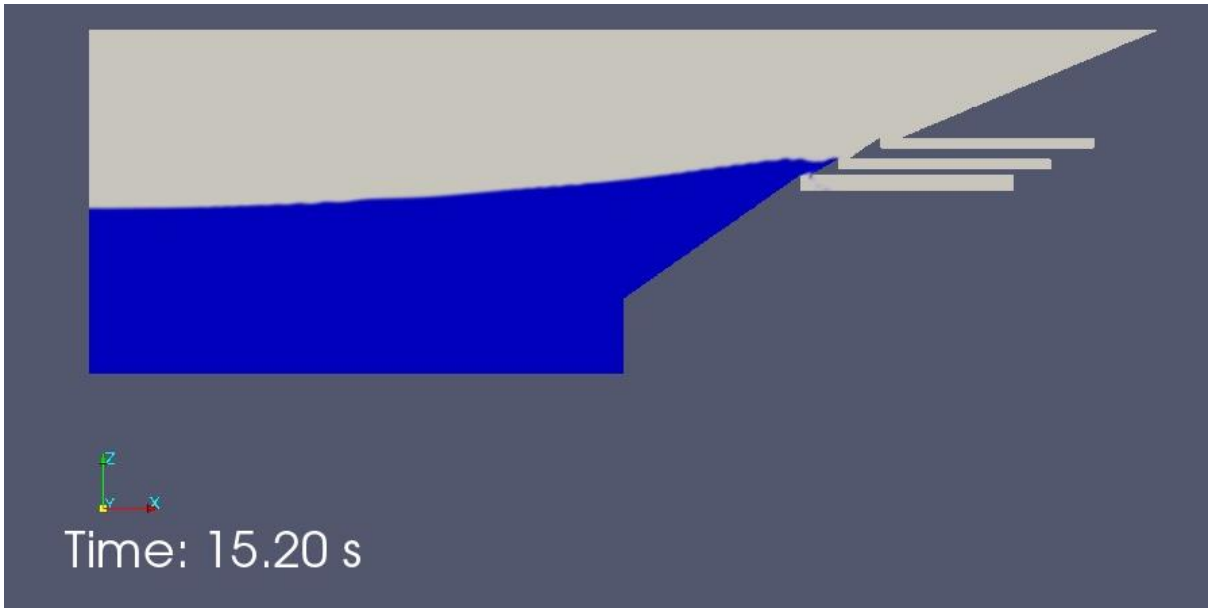

Figure E 3 7 - Simulation at 15.20 s (water at the entrance of the reservoir 2)

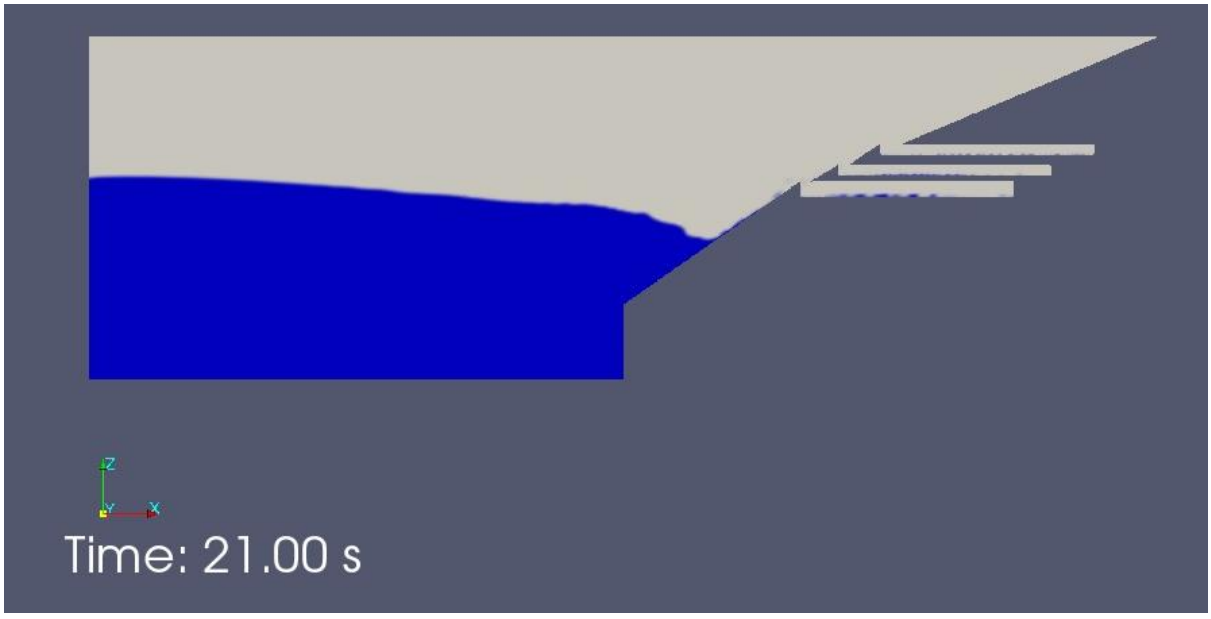

Figure E 4 - Simulation at 21.00 s (run-down of the wave)

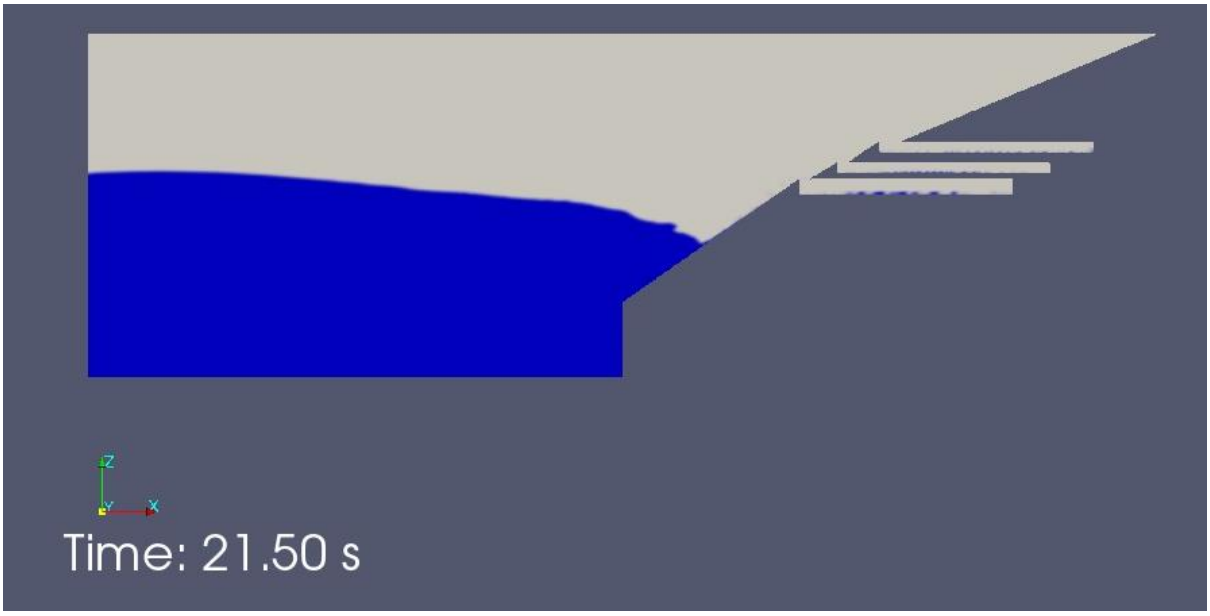

Figure E 5 - Simulation at 21.50 s (water in the lower height on the slope)

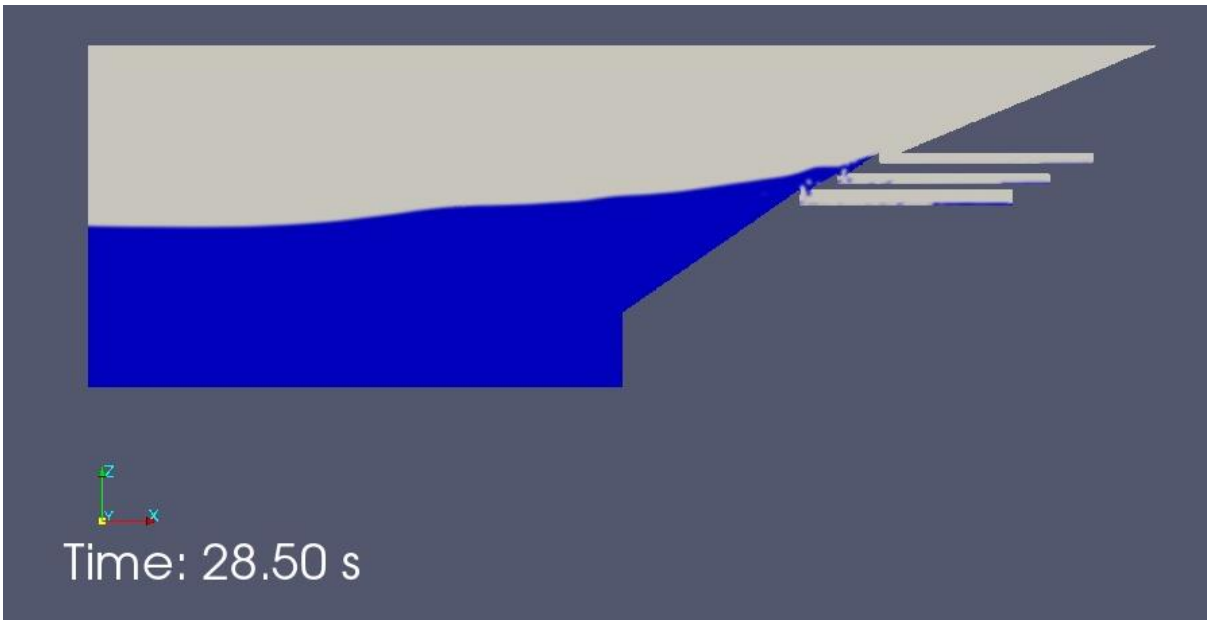

Figure E 6 - Simulation at 28.50 s (maximum run-up of the second wave)

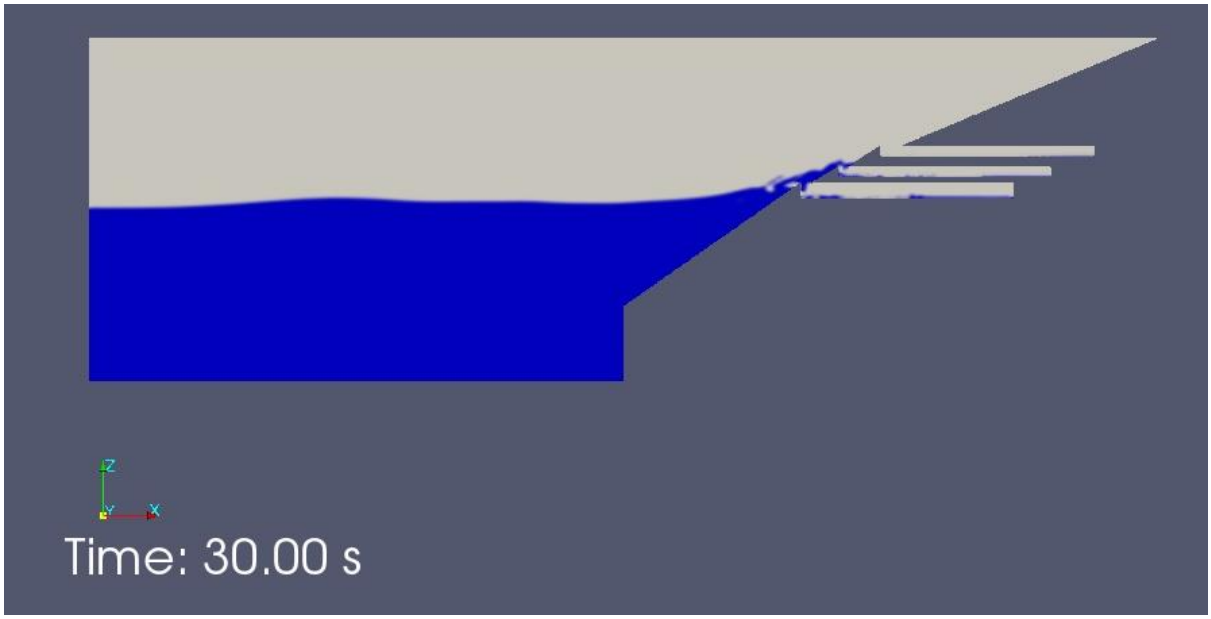

Figure E 7 – Simulation at 30.00 s (final instant of the simulation)

Appendix F – Kinetic turbulence and Velocity variation

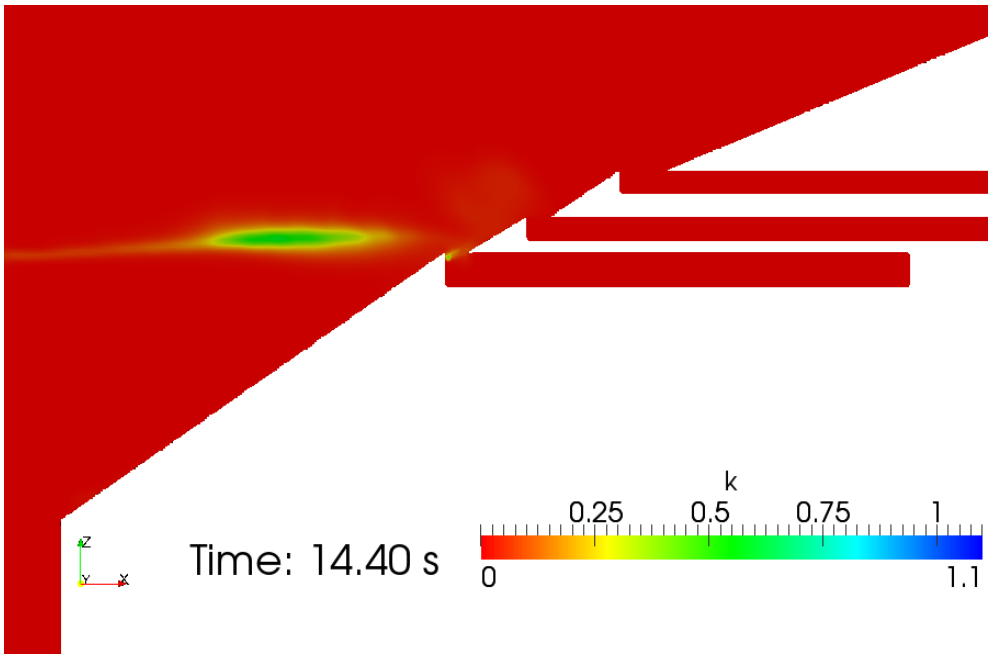

Figure F 1 - Kinetic turbulence variation at 14.40 s at the entrance of the reservoirs (kinetic turbulence in m^2/s^2)

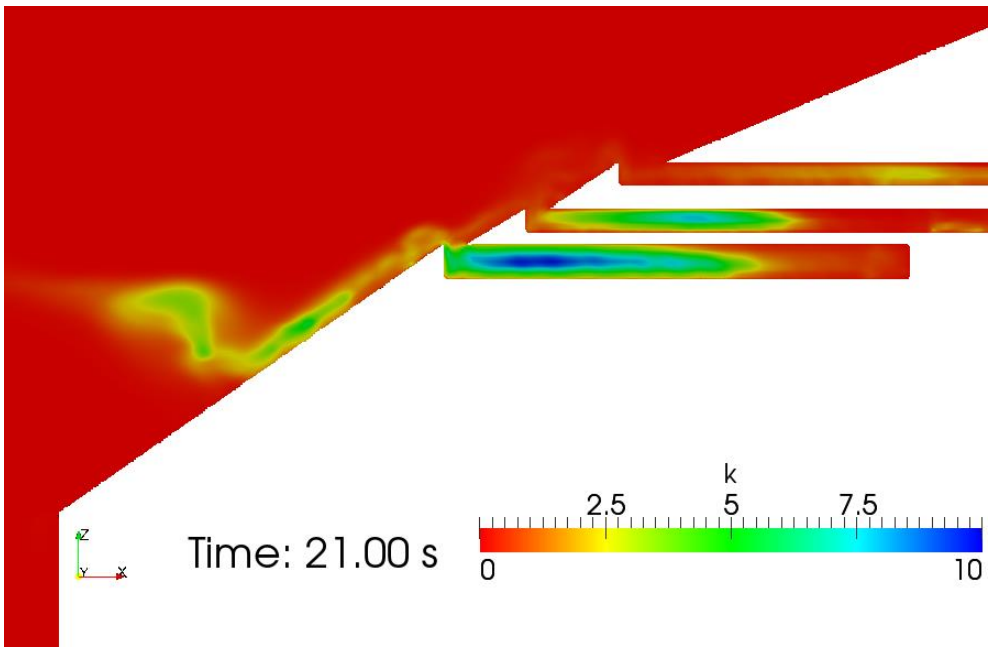

Figure F 2 - Kinetic turbulence variation at 21.00 s at the entrance of the reservoirs (kinetic turbulence in m^2/s^2)

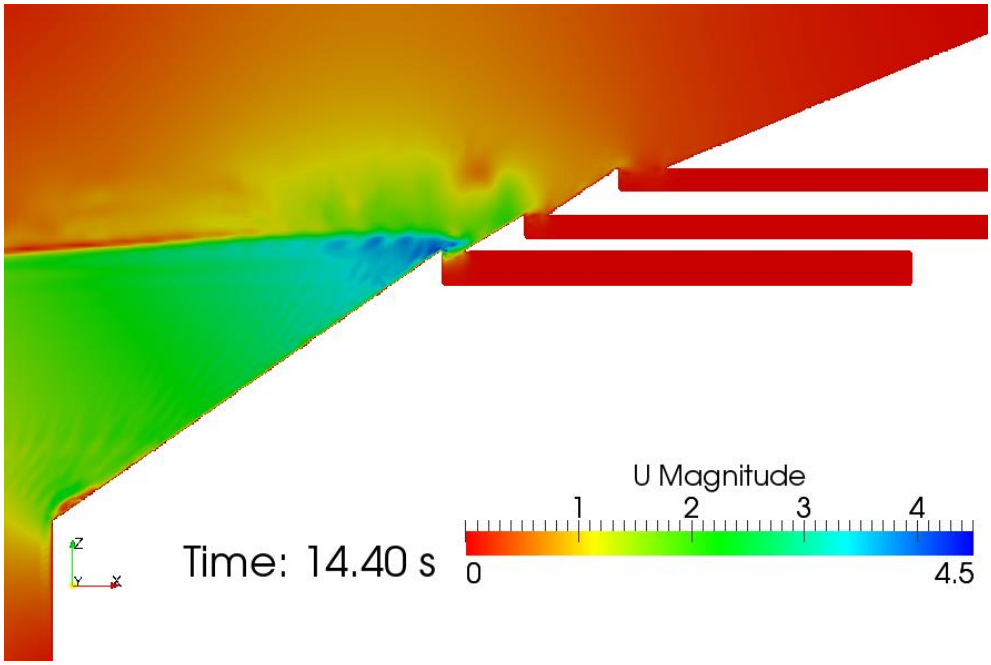

Figure F 3 - Velocity variation at 14.40 s at the entrance of the reservoirs (kinetic turbulence in m/s)

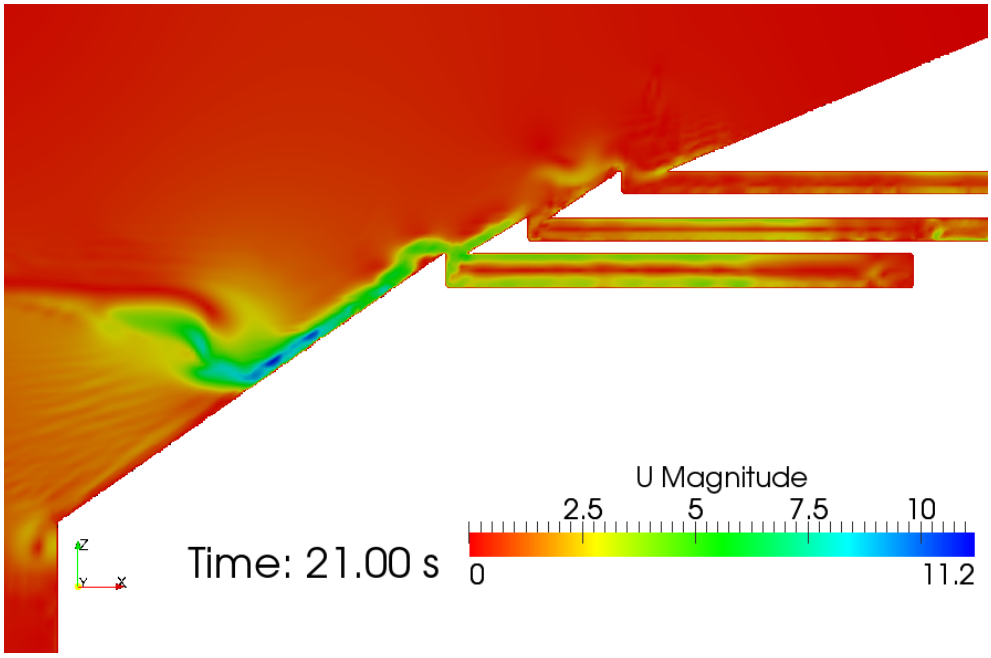

Figure F 4 - Velocity variation at 21.00 s at the entrance of the reservoirs (kinetic turbulence in m/s)